University of São Paulo
"Luiz de Queiroz" College of Agriculture

# High-resolution data for mapping the spatio-temporal variability of sugarcane fields

**Tatiana Fernanda Canata**

Thesis presented to obtain the degree of Doctor in Science. Area: Agricultural Systems Engineering

Piracicaba
2021

Tatiana Fernanda Canata
Biosystems Engineer

# High-resolution data for mapping the spatio-temporal variability of sugarcane fields

Advisor:
Prof. Dr. **JOSÉ PAULO MOLIN**

Thesis presented to obtain the degree of Doctor in Science. Area: Agricultural Systems Engineering

Piracicaba
2021

**Dados Internacionais de Catalogação na Publicação**
**DIVISÃO DE BIBLIOTECA – DIBD/ESALQ/USP**

Canata, Tatiana Fernanda

High-resolution data for mapping the spatio-temporal variability of sugarcane fields / Tatiana Fernanda Canata. - - Piracicaba, 2021.

102 p.

Tese (Doutorado) - USP / Escola Superior de Agricultura “Luiz de Queiroz”.

1. Agricultura de precisão 2. Índices de vegetação 3. Nuvem de pontos 4. Sensoriamento remoto I. Título

*I dedicate to* ***my*** *grandmother, Maria Apparecida Nunes*

# ACKNOWLEDGEMENTS

To God for blessing me every day.

To my family, Ivana, Marcos, Marcus for their indispensable support and love.

To the professor Dr. José Paulo Molin for guidance and dedication to sharing knowledge.

To the members of the Precision Agriculture Laboratory (LAP) Precision Agriculture and Mechanization group (gMAP) from ESALQ/USP that were essential to assist in the activities of this study.

To the employees from the Biosystems Engineering Department for the academic support.

To the Coordination for the Improvement of Higher Education Personnel (CAPES) for the scholarship provided during the graduate program.

To Solinftec, São Manoel sugar mill, and SAI Brasil for the operational support in the field activities.

I am grateful for the opportunity to work and shared moments with all of you

**SUMMARY**

RESUMO....6
ABSTRACT....7
LIST OF ABBREVIATIONS AND ACRONYMS....8
1. INTRODUCTION....9
References....11
2. LITERATURE REVIEW....13
2.1. Introduction....13
2.2. Precision agriculture practices for sugarcane....13
2.3. 3D sensing techniques....17
2.4. Satellite imagery for agriculture....23
References....26
3. SITE-SPECIFIC ASSESSMENT OF THE SPATIAL VARIABILITY OF SUGARCANE FIELDS USING 3D SENSING TECHNIQUES....37
ABSTRACT....37
3.1. Introduction....37
3.2. Material and Methods....38
3.3. Results and discussion....48
3.4. Conclusion....65
References....
4. INTEGRATING IMAGERY DATA AND MACHINE LEARNING TECHNIQUE FOR SUGARCANE YIELD MAPPING....71
ABSTRACT....71
4.1. Introduction....71
4.2. Material and Methods....73
4.3. Results and discussion....77
References....
5. FINAL CONSIDERATIONS....91
APPENDICES....93

## RESUMO

**Dados de alta resolução para o mapeamento da variabilidade espaço-temporal de talhões de cana-de-açúcar**

As soluções direcionadas por dados têm sido mais comuns na agricultura, principalmente, com o avanço da tecnologia para otimizar as operações no campo. As técnicas de agricultura de precisão e sensoriamento remoto tem permitido a aquisição de dados de variáveis agronômicas e diagnósticos mais precisos do que por meio dos métodos tradicionais. O monitoramento de áreas de cana-de-açúcar é comumente associado à escala regional ou a classificação de áreas de cana-de-açúcar baseada em imagens de satélite. Algumas técnicas podem apoiar a avaliação da variabilidade espaço-temporal dos talhões utilizando dados tridimensionais (3D) a partir da tecnologia LiDAR (*Light Detection and Ranging*), a qual tem contribuído no manejo específico da cultura considerando a variação da altura ou volume de plantas. Os pesquisadores têm aplicado os dados LiDAR e imagens aéreas em pequenas áreas, o que indica a necessidade de se compreender melhor a aquisição e o processamento de dados para as aplicações em larga escala, como nas áreas de cana-de-açúcar no Brasil. Este estudo tem como objetivo investigar o potencial dos dados 3D e imagens de satélite para mapear a variabilidade espaço-temporal dos talhões de cana-de-açúcar previamente a colheita. Os Capítulos 1 e 2 introduzem o tema da tese e destacam o estado da arte dos conceitos utilizados na pesquisa. No Capítulo 3 são descritos os métodos aplicados no processamento de dados 3D e imagens aéreas para avaliar a variabilidade espaço-temporal de uma área comercial de cana-de-açúcar. O mapa de produtividade foi gerado por um sistema-sensor que mede o fluxo de massa de acordo com a diferença da pressão hidráulica do picador na colhedora. A altura de plantas foi obtida com ALS (*Airborne Laser Scanning*) no ciclo final de produção da cultura por duas safras consecutivas. A nuvem de pontos gerada, seguida da filtragem de dados, possibilitou a obtenção do modelo de altura do dossel (CHM) como uma informação para investigar a associação entre a variação espacial da altura de plantas e o mapa de produtividade. Foi encontrada uma relação moderada entre o CHM e o mapa de produtividade, o que demonstrou o potencial dos dados de alta resolução para identificar a variabilidade espacial ao nível de talhão. O Capítulo 4 explora o uso de imagens orbitais para o mapeamento da produtividade de cana-de-açúcar usando dados de refletância e índices de vegetação ao longo do ciclo da cultura por três safras consecutivas. Os modelos de predição de produtividade foram desenvolvidos integrando imagens de satélite, aprendizado de máquina e regressão linear múltipla. A regressão utilizando Random Forest (RF) apresentou maior acurácia, uma vez que foi observada a não-linearidade do conjunto de dados, e as bandas espectrais apresentaram um menor erro na estimativa de produtividade. O mapeamento do vigor da cultura por meio da análise de séries temporais de imagens de satélite auxiliaram na identificação da variabilidade espacial dos talhões de cana-de-açúcar. Os resultados desta pesquisa demonstram o potencial de aplicação dos dados de alta resolução para orientar diagnósticos complementares e intervenções locais nos sistemas agrícolas, uma vez que indicam a variação do porte e vigor de plantas em larga escala antes da colheita.


Palavras-chave: Agricultura de precisão, Índices de vegetação, Nuvem de pontos, Sensoriamento remoto

## ABSTRACT

### High-resolution data for mapping the spatio-temporal variability of sugarcane fields

Data-driven solutions have been more common in agriculture, mainly, with the progress of technology to optimize the operations at the field. Precision agriculture and remote sensing techniques have enabled the data acquisition of agronomical variables and more accurate diagnostics than using traditional methods. The crop monitoring for sugarcane area is commonly associated with regional scale or classification of sugarcane areas based on satellite imagery. Some alternative techniques can support the assessment of the spatio-temporal variability of the fields using three-dimensional (3D) sensing data provided by LiDAR (Light Detection and Ranging) technology, which have contributed to the site-specific crop management considering the canopy height or volume variation. Researchers have applied LiDAR data and aerial images in small areas, which indicated the requirement of understanding better the data acquisition and processing for large-scale applications, such as sugarcane areas in Brazil. This study aims to investigate the potential of 3D sensing data and satellite imagery to map the spatio-temporal variability of sugarcane fields before harvesting. Chapters 1 and 2 introduce the topic of the thesis and highlight the state of the art of the concepts used in the research. Chapter 3 describes the applied methods for data processing of 3D sensing data and aerial images in order to assess the spatio-temporal variability of a commercial sugarcane field. The sugarcane yield map was generated by a sensor-system that measures the mass flow based on the difference of hydraulic pressure of the chopper system in the harvester. The plant height of sugarcane fields was obtained with an ALS (Airborne Laser Scanning) in the final crop production cycle for two consecutive seasons. The point cloud generated, followed by the data filtering, enabled to obtain the canopy height model (CHM) as an information to investigate the association between the spatial variation of crop height and the yield map. A moderate relationship was found between the CHM and the yield map, which demonstrated the potential of high-resolution data to identify the spatial variability at the field level. Chapter 4 explores the use of orbital images for sugarcane yield mapping using reflectance data and vegetation index over the crop cycle for three consecutive crop seasons. The yield prediction models were developed by integrating satellite images, machine learning and multiple linear regression. The regression using Random Forest (RF) showed greater accuracy, since the non-linearity of the dataset was observed, and the spectral bands showed a lower error in estimation of yield. Crop vigor mapping using time-series analysis of satellite imagery supports the identification of the spatial variability of sugarcane fields. The results of this research demonstrated the potential applications of high-resolution data for guiding complementary diagnostics and local interventions in agricultural systems, since it indicates the crop height or vigor variation in large-scale before harvesting.


Keywords: Point cloud, Precision agriculture, Remote sensing, Vegetation Index

# LIST OF ABBREVIATIONS AND ACRONYMS

| | |
|---|---|
| 3D | Three-dimensional |
| ALS | Airborne Laser Scanning |
| ANN | Artificial Neural Network |
| CAN | Controller Area Network |
| CHM | Canopy Height Model |
| CV | Coefficient of Variation |
| DGPS | Differential Global Positioning System |
| DSM | Digital Surface Model |
| DTM | Digital Terrain Model |
| GCP | Ground Control Point |
| GIS | Geographic Information System |
| GNSS | Global Navigation Satellite Systems |
| GSD | Ground Sample Distance |
| IMU | Inertial Measurement Unit |
| ISPA | International Society of Precision Agriculture |
| LiDAR | Light Detection and Ranging |
| ML | Machine Learning |
| MLR | Multiple Linear Regression |
| MTLS | Mobile Terrestrial Laser Scanning |
| PA | Precision Agriculture |
| RF | Random Forest |
| RGB | Red-green-blue |
| RMSE | Root Mean Squared Error |
| RPA | Remotely Piloted Aircraft |
| RS | Remote Sensing |
| RTK | Real Time Kinematic |
| SD | Standard Deviation |
| SfM | Structure from Motion |
| TIN | Triangulated Irregular Network |
| TRS | Total Recoverable Sugar |
| VI | Vegetation Index |

## 1. INTRODUCTION

The competitiveness of the agricultural sector makes evident the need to obtain higher levels of production through innovative agricultural practices. The expansion of using Precision Agriculture (PA) technologies deals with a greater demand for equipment and resources to obtain data, especially those dedicated to the identification of spatial variability of the fields. Particularly, the PA concept proposes to develop more accurate diagnostics as a guide for the decision-making process for local interferences based on the spatio-temporal variability of the fields. The application of PA, generally, contributes to monitoring the production cycle of the crop to better take advantage of the inputs. However, for sugarcane production, some deficiencies regarding technical solutions are verified for assessing the spatial variability of the fields, and the generation of yield maps that express the crop's response to the wide range of factors.

Sugarcane (*Saccharum* spp.) is characterized as a perennial crop and cultivated as semi-perennial predominantly in tropical regions (SCARPARI and BEAUCLAIR, 2010). The high demand regarding domestic and foreign markets for products obtained from sugarcane have intensified the need to obtain previous information directly associated with the crop yield. In Brazil, the cultivated area of sugarcane is about 9.0 million hectares with an average yield of 77.9 Mg $ha^{-1}$ for the 2020/2021 sugarcane growing season. Sugarcane production is expected to reach 586 million tons for the 2021/2022 season (COMPANHIA NACIONAL DO ABASTECIMENTO - CONAB, 2021), which 54% of the national production of sugarcane is allocated in São Paulo state. According to the FAO (2018), Brazil is the first global producer of sugarcane (about 25% of the global sugar production). In addition, the sugarcane biomass is responsible for 18% of the capacity of the country's electricity cogeneration (National Energy Balance, 2020 – database 2019). Few researches focus on PA strategies for sugarcane production. The main publications are related to the identification of the spatial variability of soil properties (JOHNSON and RICHARD, 2010), and pests and diseases (PEDROSA et al., 2017). Also, sugarcane yield predictions have been developed according to the meteorological data for regional scale. However, the identification of spatial variability allows other approaches, such as the site-specific crop management (BRAMLEY, 2009; MOLIN et al., 2015). Other PA practices are guided based on Remote Sensing (RS) techniques for crop monitoring using high-resolution data over large areas. Some examples are aerial imagery and ranging sensors (laser, radar, ultrasonic) with potential of using in agricultural tasks due to their capacity to obtain data when the size of the plants limits the access of machines into fields (MOLIN et al., 2015). Different sensors have been used in agricultural systems to support the management regarding crop, soil, and environment. The classification of the sensors is associated with the object, and the type of sensing (proximal or remote). Crop monitoring, detection of crop sanity, and yield mapping are some examples of sensor applications for optimizing the use of resources in agriculture.

Sensors based in spectroscopy is the most available technique to the farmers to plan site-specific management due to the different commercial solutions, and the focus of research areas for improving the profitability of the fields considering local interventions. In this case, some Vegetation Indexes (VIs) are commonly associated with the crop vigor that allows to generate diagnostics and recommendations by means of the spatial patterns identification. Traditional studies of sugarcane yield prediction involved satellite imagery for block or regional scales, comparing the VIs with the average yield of sugarcane plots (low spatial resolution). The introduction of 3D sensing data in agriculture occurred through photogrammetry technique for gathering data of the crop geometry and its structural components (height, volume, etc.), which are associated with the crop yield and its quality aspects. Also, 3D modeling of the crop canopy structures started to be measured more accurately. This kind of data

allowed to obtain more representative data in comparison to the traditional measurements (low-scale and labour-intensive).

The level of detail provided by 3D sensing data from ranging sensors enabled other agricultural applications, such as phenotyping studies for improving the assessment of the fields at larger scales. Spatio-temporal variability detection and the variable rate technology guided by the volume of the plants are some examples that the information from 3D sensing data contributes to the operational improvements of the tasks. The agricultural applications considering laser sensors, a LiDAR (Light Detection and Ranging) technology, started in silviculture during the 1960s to estimate forest biomass, such as eucalyptus, by means of aerial platforms named as ALS (Airborne Laser Scanning) (ROSS, 2013). Buelvas and Adamchuk (2017) indicated that the main advantage of using LiDAR is the capability to determine the growth vegetation dynamics, which allows, to enhance logistical aspects of harvest planning. The research perspective is to integrate the spectroscopy technique (multispectral data), ranging sensors, and crop/soil data to establish management zones within the field. Despite the economic importance of sugarcane for Brazilian agribusiness, the unique study found involving LiDAR for sugarcane fields was described by Lopes et al. (2010) to characterize the aerosol emissions from crop burning in the state of São Paulo. Shendryk et al. (2020) predicted biomass and leaf nitrogen content of sugarcane based on LiDAR data and multispectral imagery using RPA (Remotely Piloted Aircraft) for low-scale fields - plots of 2.0 m x 2.0 m. Therefore, there are no scientific researches found for us that reported the use of high-resolution data to map sugarcane fields closer to the harvest to characterize the spatial variability of the fields.

Due to the limited alternatives to monitoring sugarcane yield, previously of harvesting, this study proposes a methodology to assess the spatial patterns of sugarcane fields based on high-resolution data. The data processing and 3D modeling also were explored to collaborate with the research area and users to carry out sensing data, as an additional information for the site-specific crop management. The study aims to investigate alternative techniques for mapping the spatial variability of fields, and its relationship with sugarcane yield at the field level, based on crop canopy maps – height or vigor. The study contributes to the progress of developing accurate diagnostics for PA practices, and data-driven solutions for crop mapping, as long as data availability and technologies advance. The perspective is to perform it for local interventions, and real-time calibration of the agricultural machinery to optimize the operational performance of harvesting. The hypothesis of this study is that the variation of crop canopy obtained from high-resolution data, in the final crop production cycle, is spatially associated with the variation of sugarcane yield. The purpose of using RS techniques for mapping sugarcane fields elucidate its adoption to infer about the potential of agricultural production locally. The specific objectives of the study are i) investigate the potential of 3D sensing data to map the spatial variability of sugarcane fields; ii) verify if there is an association among canopy height model and sugarcane yield maps; iii) map the spatio-temporal variability of sugarcane fields by satellite imagery along the crop cycle; iv) integrate statistical techniques and satellite imagery to modeling sugarcane yield prediction at the field level.

The study is divided into three sections: a literature review, reporting the state of the art of the technologies involved in this study; the second section describes the methodology of data acquisition and processing of 3D sensing data to obtain the canopy height model and comparing it with the sugarcane yield map. The third section presents the spatio-temporal analysis of satellite imagery based on spectral bands and derived-VIs for developing sugarcane yield prediction models at the field level.

## References


BRAMLEY, R. G. V. 2009. Lessons from nearly 20 years of Precision Agriculture research, development, and adoption as a guide to its appropriate application. **Crop & Pasture Science**, 60(3):197-217. doi: 10.1071/CP08304.

BUELVAS, R.; ADAMCHUK, V. 2017. Crop canopy measurement using laser and ultrasonic sensing integration. **Proceedings...** ASABE Annual International Meeting. Washington, 16 a 19 de julho de 2017. p. 1-17. doi: 10.13031/aim.201701002.

CONAB. Companhia Nacional De Abastecimento. **Boletim da safra de cana-de-açúcar**. 2021. Brasília. Available at: < https://www.conab.gov.br/info-agro/safras/cana>. Acessed: 04/23/2021.

FAO. Food and Agriculture Organization of the United Nations. 2018. Available at: <http://www.fao.org/faostat/en/#data/QC>. Accessed: 09/14/2020.

JOHNSON, R. M.; RICHARD, E. P. 2010. Sugarcane Yield, Sugarcane Quality, and Soil Variability in Louisiana. **Agronomy Journal**, 97(3):760-771. doi: 10.2134/agronj2004.0184.

LOPES, F. J. S. da; HELD, G.; NAKAEMA, W. M.; RODRIGUES, P. F.; BASSAN, J. M.; LANDULFO, E. 2010. Initial analysis from a Lidar observation campaign of sugar cane fires in the Central and Western portion of the São Paulo State – Brazil. **Proc. of SPIE**, 8182:1-10. doi: 10.1117/12.898119.

MOLIN, J. P.; COLAÇO, A. F.; AMARAL, L. R. do. 2015. **Agricultura de Precisão**. 1 ed. Piracicaba: Oficina de Textos, 224 p., 2015.

NATIONAL ENERGY BALANCE. **Matriz Energética Nacional**. 2020. Brasília. Available at: https://www.epe.gov.br/pt/publicacoes-dados-abertos/publicacoes/balanco-energetico-nacional-2020. Accessed: 09/14/2020.

PEDROSA, E. M. R.; SILVA, L. M. A. da; VICENTE, T. F. S. da; CARDOSO, M. S. O. de; CASTRO, D. B.; ROLIM, M. M. 2017. Seasonal variation of plant-parasitic nematodes and relationship with nutritional and growth properties of sugarcane plantations. **Tropical Plant Pathology**, 42(2):132-136. doi: 10.1007/s40858-017-0129-5.

ROSS, F. N. 2013. How did we get here? An early history of forestry lidar. **Canadian Journal of Remote Sensing**, 39(1):6-17. doi: 10.5589/m13-011.

SCARPARI, M. S.; BEAUCLAIR, E. G. F. 2010. **Anatomia e botânica**. In: Dinardo-Miranda LL, Vasconcelos ACM, Landell MGA. (Ed.). Cana-de-açúcar. Campinas: Instituto Agronômico, 882p., 2010.

SHENDRYK, Y.; SOFONIA, J.; GARRARD, R.; RIST, Y.; SKOCAJ, D.; THORBURN, P. 2020. Fine-scale prediction of biomass and leaf nitrogen content in sugarcane using UAV LiDAR and multispectral imaging. **International Journal of Applied Earth Observation and Geoinformation**, 92:102177. doi: 10.1016/j.jag.2020.102177.

# 2. LITERATURE REVIEW

## 2.1. Introduction

The diversity of RS techniques and its applications allows that high-resolution data compose the required information layers for agricultural management based on geoprocessing. In the context of PA, it could assist to identify the factors associated with the spatio-temporal variability of the fields. In addition, these technologies combined with the mechanization of agricultural operations have potential to advance on developing the automation and control of the processes. The study involves the main areas of agricultural science, mainly PA, focusing on understanding the benefits of high-resolution data to provide diagnostics of the crop status at the field level. The aim of this literature review is to describe the technical-scientific scope of the main techniques involved in this study.

## 2.2. Precision agriculture practices for sugarcane

Crop data management is a key element to support growers on decision-making; when efficiently managed, it enables to optimize crop yield, costs related to the inputs, and reduces the negative impact of agricultural production on the environment. For that, PA tools are implemented using site-specific crop management to maximize the profitability of the farm while minimizing the environmental impact. According to the International Society of Precision Agriculture (ISPA) "PA is a management strategy that gathers, processes and analyzes temporal, spatial and individual data and combines it with other information to support management decisions according to estimated variability for improved resource use efficiency, productivity, quality, profitability, and sustainability of agricultural production" (ISPA, 2019).

Sugarcane crop demands large investments for implementation, maintenance, and harvesting, especially with machinery and agricultural inputs (SANTOS et al. 2014). The crop is conducted as semi-perennial with a growth cycle of approximately 12 or 18 months (SOUZA et al. 2017). Crop yield tends to decline after each cycle of harvesting, therefore, the data acquisition of agronomical variables over the season is important to maintain the yield records over the years, allowing the growers to increase the economic return (MANHÃES et al. 2014). The adoption of mechanized sugarcane harvesting made evident the limitations related to the identification of the row gaps, tillering density of plants, and assessment of losses in agricultural production (SANTOS et al., 2014; SERAFIM et al., 2013). Ma et al. (2014) reported that the main advantage of mechanizing operations in sugarcane corresponds to the regulation of mechanisms (cutting and cleaning on harvesting) according to the operational conditions, which enables to enhance the fuel consumption, the maintenance, among others.

The main criterion for planning sugarcane harvesting is the planting schedule, however the decision to harvest depends on the growth and vegetative development of the plants, which are differentiated by the environmental conditions of each region. According to Bocca et al. (2015) sugarcane yield estimation supports the systematization of the harvesting planning, and the decision making for replating the sugarcane fields, which usually occurs every five consecutive cuts. The main models for sugarcane yield prediction are developed based on historical production data (PIEWTHONGNGAM et al., 2009; HAMMER et al., 2020), and climatological database (EVERINGHAM et al., 2007) for regional scale, both considering the average demand of sugarcane processing by the mill (OLIVEIRA et al., 2017). On the other hand, the potential of PA techniques to associate sugarcane yield

prediction to the spatial variability of the fields, at the field level, is little explored in the literature, in part, due to the scarce commercial solutions that allow such monitoring with proper calibration of equipment and frequency of data acquisition. For Bramley et al. (2018) yield maps from several sugarcane growing seasons support relevant information to recommend N application.

The generation of sugarcane yield maps started in the studies conducted by Pierossi and Hassuani (1997) for harvesting of chopped sugarcane in Brazil, and by Cox et al. (1997) with the development of instrumentation for sugarcane harvesters in Australia. Magalhães and Cerri (2007) developed a data acquisition system using a mass flow sensor coupled to the sugarcane harvester elevator. Other devices have been proposed for yield mapping, through direct or indirect measurements (MOLIN and MENEGATTI, 2004; PRICE et al., 2011), with the characteristic limitations of the production environment. Yield maps are the key to managing crops in terms of spatial variation through the identification of the higher and lower yield patterns, which is an important component to implement PA (COLAÇO et al., 2020; MOMIN et al., 2019; BRAMLEY and TRENGOVE, 2013). For that, sensors have been increasingly used in agriculture to obtain georeferenced data (BRAMLEY et al., 2018; BRAMLEY and OUZMAN, 2019) to guide the PA practices for increasing crop yield and improving the product quality of sugarcane industry within agricultural sector (SILVA et al., 2011; NAWI et al., 2014; DRIEMEIER et al., 2016; SANCHES et al., 2019).

Particularly, crop yield and quality components are the basis of the payment system to the sugarcane growers (RODRIGUES et al., 2013). The Brazilian sugarcane industry pays for the total recoverable sugar (TRS), or in Australia, as a function of the commercial cane sugar (CCS). Sugarcane harvesters have a high level of instrumentation, as sensors generate real-time data to monitor machinery parameters related to the harvest operation. Nevertheless, sugarcane yield and quality data are still not fully available (CORRÊDO et al., 2020). Some reasons for this shortcoming are lack of user knowledge to deal with this kind of data, the requirement of data processing to remove outliers (MALDANER and MOLIN, 2020), sample contamination in the harvester elevator (quality aspect), and because data processing protocols for guiding agronomic decisions are limited. Corrêdo et al. (2021) described sampling strategies for predicting sugarcane quality by proximal sensing as an alternative to measure sugarcane quality on-board. The adoption of the solutions should be cost-effective, and it needs to focus on the improvement of crop management and automation of the harvesters (NAWI et al., 2014).

Traditionally, spatialized crop yield is generated by sensors that, directly or indirectly, measure the amount of harvested product together with the location provided by a GNSS (Global Navigation Satellite System) receiver. The direct measurement techniques are related to the mass flow data. Indirect techniques involve sensors and the use of data generated by the harvester (KIN et al., 2011). According to Cox et al. (2002), there are four customs to measure the mass flow of sugarcane: (1) chopper hydraulic pressure, which assumes that the power required to chop sugarcane into billets is proportional to the mass (XIE et al., 2019); (2) elevator power, which assumes that the power required moving the elevator is proportional to the sugarcane mass; (3) volumetric measurement, which uses the separation distance between the feed rollers as a volumetric indicator; (4) or direct mass involving the load cell on the elevator floor to measure the mass. The main components installed on the harvester for measuring sugarcane mass flow are shown in Figure 1.

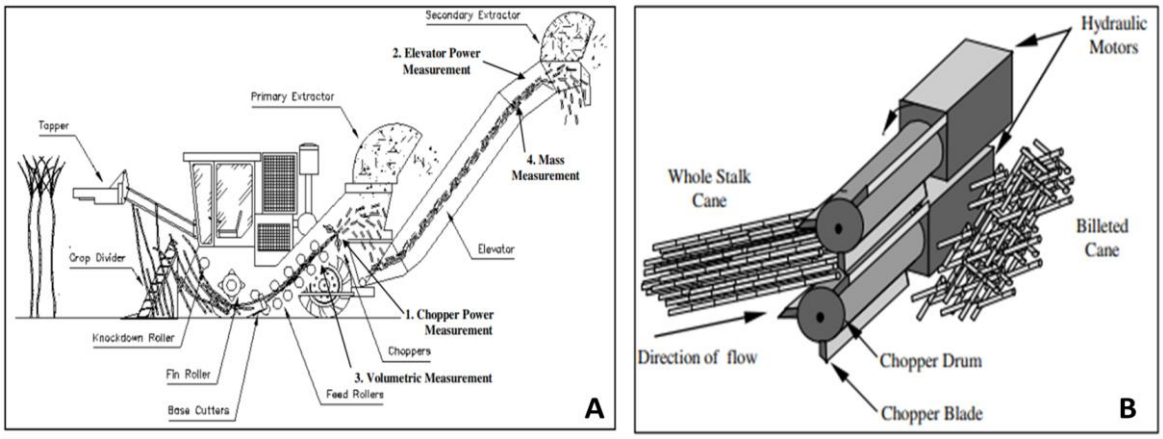


**Figure 1.** Measurement-systems of sugarcane mass flow (A); chopper system (B) – adapted from Cox et al. (2002)

The main factors that influence the accuracy of yield monitors are i) the frequency of data acquisition; ii) the feed rate of the harvester; iii) the measurement principle; iv) the adopted row spacing (MAILANDER et al. 2010). The yield monitor calibration is essential and is performed to transform the digital number generated by the sensors into a value equivalent to the actual amount of harvested mass. Calibration is normally performed by weighing a sequence of in-field wagons and it is recommended to repeat the calibration periodically during the harvest or, if possible, every time that changes the sugarcane varieties over the fields. According to Jensen et al. (2010), most of the commercially available mass flow sensors are based on the chopper hydraulic pressure, feed train roller displacement, and elevator power. Bramley (2009) proposed that sugarcane yield monitoring require to meet some requirements, such as georeferencing sugarcane production with a minimum accuracy of DGPS (Differential Global Positioning System), calibration of the mass flow sensors by event basis, and recording data at intervals of 3 seconds or less. The computational processing of such data is required to provide some additional information about the capacity of sugarcane production at the field level. The load cell on the elevator floor is the sugarcane yield monitor most studied because it does not require the use of empirical equations to measure the mass flow (CORRÊDO et al., 2020). The main sensor-based techniques to measure sugarcane yield are shown in Table 1. The accuracy of the yield monitor using the load cells in the elevator floor ranges from 89% (BENJAMIN et al. 2001; MAILANDER et al. 2010) to 96% (MOLIN and MENEGATTI 2004). The greater variation between its accuracy may be due to different densities of the harvested material, the different sugarcane varieties (BENJAMIN et al. 2001), the changing tare caused by the soil, the sediments, and the elevator vibration affected data readings from the load cell.

**Table 1.** Sensor-based techniques to measure sugarcane yield (adapted from CORRÊDO et al., 2020)

| Sensors | Local | $R^2$ | Accuracy (%) | References | Patent number |
|---|---|---|---|---|---|
| Load cell | Elevator | 0.95 | 90.0 | Cox et al. (1997, 1998) and Cox (2002) | Australian Patent 744047 |
| | | 0.97 | 89.0 | Benjamin et al. (2001) | NA |
| | | 0.50 | 96.5 | Molin and Menegatti (2004) | NA |
| | | 0.66 | 93.6 | Cerri and Magalhães, (2005); Magalhães and Cerri (2007) | Brazilian Patent PI0502658-0 |
| | | 0.97 | 89.0 | Mailander et al. (2010) | NA |
| Deflection plat; hydraulic pressure | Elevator | NA | NA | Wendte et al. (2001) | U.S. Patent 6272819 B1 |
| Fiber optic | Elevator | 0.93 | 93.8 | Price et al. (2007) | U.S. Patent 2010/0269470 A1 |
| Laser distance | Elevator | 0.98 | 92.5 | Price et al. (2011) | NA |
| | | 0.74 | NA | Price et al. (2017) | NA |
| Deflection plate | Back of the chopper | NA | NA | Quaderer and Cash (2015) | U.S. Patent 2014/0208870 A1 |
| 3D sensor | Elevator | NA | NA | Darr et al. (2019) | U.S. Patent 2019/10371561 |

NA - Not Available

Wendte et al. (2001) developed a sugarcane yield monitor, which used a deflection plate installed after the secondary extractor (Patent number US 6,272,819 B1). The aim was to measure the amount of sugarcane that is dropped from the elevator to the in-field wagon. Its monitoring included an elevator pressure sensor coupled to the elevator motor to generate the signal in response to the hydraulic pressure applied to the elevator and a sensor for elevator driveshaft torque. However, there is no data related to its accuracy. Quaderer and Cash (2015) also used the deflection plate to indirectly measure the amount of sugarcane dropped in the chopper rollers before it entered the elevator conveyor. Another sensor-based approach was made in the harvester elevator with the optical sensors placed in the flooring of the conveyer (PRICE et al., 2007 - Patent number US 2010/0269470 A1). For that, the sensors self-clean during material flow, and when combined with the proper electronics, software, and GNSS, it outputs a number that is relative to the mass flow rate. The field tests reported successful identification of crop variances, and overall sugarcane mass varied by 6.20%. Price et al. (2017) and Price et al. (2011) tested a sugarcane yield monitor that utilized a duty-cycle type approach with three fiber optic sensors mounted in the elevator floor to estimate the height and length of the sugarcane stalks, which it was used to obtain a relationship among the volume and the mass of sugarcane. The average prediction error was about 7.50%. Field-testing indicated that the system was robust, maintenance-free, and self-cleaning; however, some obstruction of the fiber optic sensors did occur in wet conditions (muddy soils).

Equipment with different technological principles, whether in the initial research step or with consolidated implementation for field applications, have been used to advance the collection of indirect information related to the sugarcane yield. The use of embedded systems for the proximal sensing of crops would provide relevant support for high-resolution data (higher number of samples per unit area) to assess spatio-temporal analysis of the fields. Darr et al. (2019) developed a system based on an imagery sensor installed in the harvester elevator to determine the volume of sugarcane stalks. However, there are still no studies about which kind of sensors are used and its accuracy. Alternative methods have been explored for sugarcane yield mapping, such as the proposed by Momim et al. (2019) based on vehicle tracking and fill event distance per row width. The purpose was using machinery data (harvesters, tractors, and semi-trucks) to design management zones according to the estimated yield. Volume is also an indirect measurement of mass flow using stereo cameras on harvester elevator. The principle is to measure the density of material for estimating sugarcane yield, and impurities by means of a calibration factor. However, no study was found reporting the robustness, and the accuracy of this measurement-system. Maldaner et al. (2021) proposed to predict sugarcane yield using engine parameters of the harvester, mainly specific fuel consumption, with an average error of 7.0 Mg $ha^{-1}$ compared to the observed yield data from a scale yield monitor. Diversified and joint crop information can enable the assessment of the spatial variability of the fields to identify different levels of crop production within fields, which is related to the agronomical attributes that directly influence on inputs optimization and rentability of the fields. The spatial variability mapping provides a robust and valuable support to the decision-making process of the growers during the crop cycle development. From this perspective, sugarcane yield monitoring has received more attention regarding the development of embedded technologies. On the other hand, there is still great need to advance in these aspects for more accurate measurement-systems.

## 2.3. 3D sensing techniques

The use of RS techniques in agriculture has become an alternative for crop monitoring over large areas in a shorter period. Such techniques are classified according to the platform on which the sensors are coupled to capture the electromagnetic radiation emitted by the target object, named as proximal or remote sensing. From the measured radiation, different information can be related to the characteristics of the crop, soil and relief (MULLA, 2013). The main publications regarding RS in agriculture describe the determination of soil chemical parameters (ADAMCHUK et al., 2004), water stress of plants (COHEN et al., 2005), and predictive yield models based on VI from satellite imagery (MOREL et al., 2014) or proximal sensing (PORTZ et al., 2012). However, the main limitation of these techniques is the spatial-temporal resolution, making the site-specific crop management impracticable due to the heterogeneity of original data, and the saturation of the signal emitted by sensors during the maturation of crop stage (POVH et al., 2008).

Another technical alternative is to use ranging sensors for assessing the agronomical variables of the crop through the geometrical information provided by the data readings - regardless of the size or phenological stage of the crop. Usually, the geometrical features are associated with the crop yield variation and crop status, which can be evaluated spatially during the crop development cycle using non-destructive methods (ROSELL e SANZ, 2012; MÉNDEZ et al., 2013). Finkelshtain et al. (2017) conducted a research using different ranges of pulses repetition frequencies of an ultrasonic sensing system on laboratory and greenhouse environments for the crop yield assessment (fruit mass per pepper plant). Laser sensors, compared to other ranging sensors, have greater potential for application in agriculture due to their operational performance under field conditions (EHLERT et al., 2006). Its

principle is based on the time interval between the emission and reception of the light beams in the two-dimensional plane, which enables to calculate the distance from the sensor to the target object (Figure 2A). The historical development of the embedded LiDAR systems on aircraft started in 1995 with the single wavelength pulses emitted by the laser sensor using low pulse repetition frequency (< 5kHz) and two single pulses - first and last returns. The full waveform of laser scanning started in 2000 with a considerable increase in pulse repetition frequency (200 – 250 kHz) that enabled it to provide detailed information of the target object using multiple returns (Figure 2B). After that, the robustness of the technology enabled it to design accessible sensors regarding the size of the platform for data acquisition (~1 kg) using multispectral data at higher pulse repetition frequency (> 6 MHz). These advances have collaborated to generate high-quality spatial data for 3D mapping applications (USSYSHKIN and THERIAULT, 2011). The recent trends in ALS demonstrate a progress on sensor and aircraft technologies, mainly to higher point densities by the increased pulse repetition frequencies, online and offline data processing of the point cloud, synchronized acquisition and processing of laser sensor points and imagery sensors mounted on multi-rotor systems, such as RPA (GIM International, 2019).

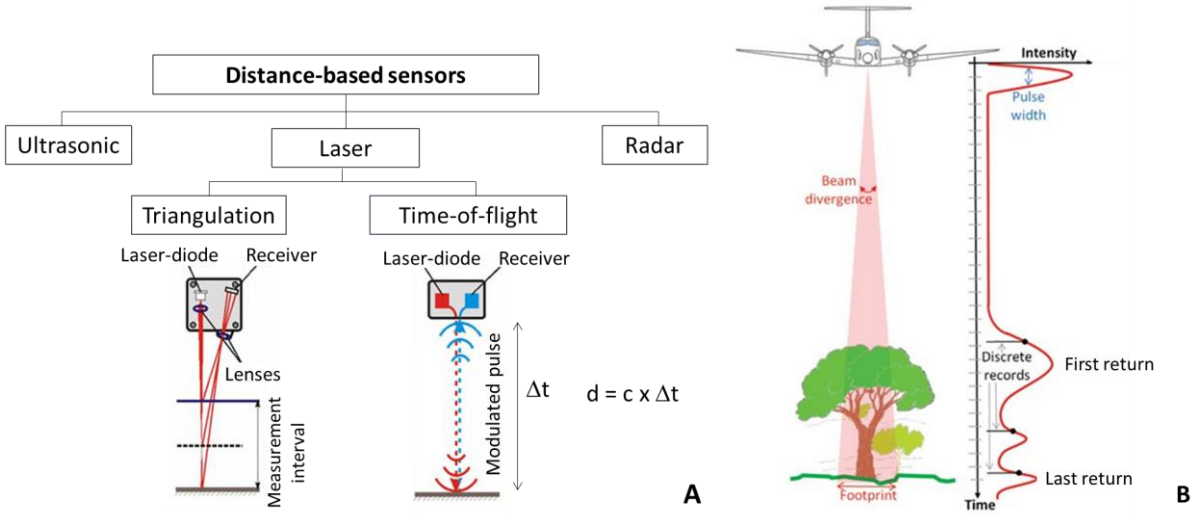


**Figure 2.** Principle of measurement of distance-based sensors – adapted from Ehlert et al. (2009) (A). Airborne laser scanning and multiple returns - adapted from Fernandez-Diaz (2011) (B)

Footprint is an important parameter in the high-precision geometric and radiometric calibration of LiDAR systems. It is defined as the spot area illuminated by a single laser beam, which varies with the beam direction, the flight altitude, and the regional terrain. The geometric size of the footprint is one of the most critical parameters of the laser sensor data because the distribution of pulse energy is not uniform over the extent of the footprint (ZHANG and SHEN, 2014). It decreases radially from the center and can be approximated by a two-dimensional Gaussian distribution. Due to the complexity of the vertical structure of vegetation, full waveform technology has been adopted for 3D mapping applications. More details of discret returns from LiDAR systems are described by Ussyshkin and Theriault (2011). The result of processing laser sensor data is the point cloud, characterized by the statistical distribution of the points from multiple returns on a dataset with the allocation of geographical coordinates for each point impacted by the laser beams (SANZ-CORTIELLA et al., 2011). Del-Moral-Martínez et al. (2015) described details regarding the integration of GNSS coordinates and laser sensor data. Laser sensors integrated with GNSS, cameras, odometers, also have been used for robotics systems in agriculture using

aerial and ground-based solutions to mapping weed distributions over the fields or measuring crop status (RUCKELSHAUSEN et al., 2009). The experimental platform suggested that both, autonomous navigation and environmental modeling capabilities, will enable to perform a robust dataset, from diagnostics to local interventions, and long-term registration of plant classification for selective weed-removal operations. 3D sensing data are commonly collected through aerial or mobile terrestrial platforms named as ALS and Mobile Terrestrial Laser Scanning (MTLS), respectively. Figure 3 demonstrates the most common platforms of LiDAR systems for research and commercial purposes, and an example of point cloud generation for assessing the height of maize crop over the fields. From the development of dedicated algorithms, it is possible to extract geometrical information of the crop canopy and digital elevation models with greater resolution (points per unit area).

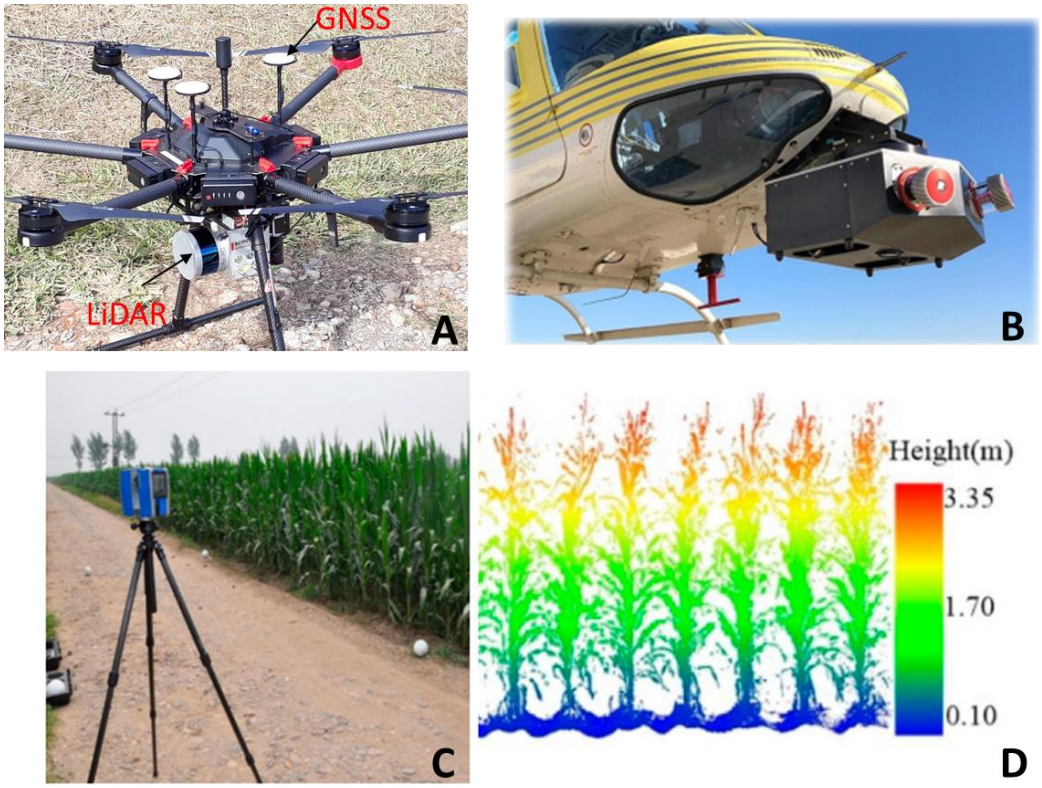


**Figure 3.** Aerial platforms for LiDAR data acquisition – remotely piloted aircraft (A); airborne laser scanning (B); mobile terrestrial laser scanning - adapted from Su et al. (2019) (C); point cloud of maize crop from laser sensor – adapted from Su et al. (2019) (D)

Point clouds have been used for the characterization of perennial crops in temperate regions (PALLEJÀ et al., 2010), the determination of the structure of perennial crops (JIANG et al., 2019; MURRAY et al., 2020); the modeling of orange orchards (COLAÇO et al., 2019); the estimation of barley, paddy rice, and wheat biomass (SCHAEFER and LAMB, 2016; BROCKS and BARETH et al., 2018; TILLY et al., 2014; WALTER et al., 2019); the assessment of wheat nitrogen status (EITEL et al., 2014); the measurement of dry matter of forage (GEBREMEDHIN et al., 2019); the analysis of plant growth within field (SUN et al., 2018); among others. Escolà et al. (2016) developed computational tools from the point cloud generated by MTLS to extracting usual metrics for horticulture, such as the identification of spatial variability of the plants through the volume of olive orchards, and

the determination of the crop growth between each evaluated period. Zhou et al. (2020) proposed to analyze changes in the vertical structure of maize plants with different degrees of lodging using LiDAR embedded in the RPA system as an alternative for monitoring crop lodging. The reconstruction of surfaces is another application of dense point cloud, which involves developing better solutions for autonomous navigation (GAO et al., 2018; HECHT, 2018), environmental monitoring (MALLET and BRETAR, 2009; ZHAO et al., 2017), and computer vision systems (HORAUD et al., 2016). Tachella et al. (2019) proposed a real-time algorithm for surfaces reconstruction using raw LiDAR data and a computational framework with greater performance (20 ms) than actual methods of data processing. This approach can collaborate to advance on data acquisition and processing of 3D sensing data for agricultural applications due to the complexity of the vegetation structure. An example is the canopy surface reconstruction of forestry developed by Leeuwen et al. (2010) to estimate tree growth and canopy volume over large areas. Yang et al. (2015) proposed a method for spatial-morphological analyses of trees based on point clouds from ALS as an effective modeling of the individual tree.

Other researches explored dense point clouds from aerial or ground-based laser sensors to extract agronomic parameters using 3D modeling, such as estimating leaf area index (JENSEN et al., 2008; ARNÓ et al., 2013; QU et al., 2018), and leaf area density (HOSOI et al., 2012; LI et al., 2017; KAMOSKE et al., 2019) for crops that have strong relationship among its geometry and productivity, mainly for perennial crops (SANZ et al., 2013; BLANQUART et al., 2020). Also, it can be a cost-effective alternative to the traditional measurements using labour-force for manual samplings (COMBA et al., 2020). In the context of PA, 3D modeling can be useful for the site-specific crop management of input applications (nutrients, pesticides, etc.) according to the detection of spatial patterns regarding the size and volume of the plants over the fields. Due to the potential of high-resolution data to assess the spatial variability of the fields, other studies reported some applications of distance-based sensors to detecting crop status variation in the pre-harvest period (SELBECK et al. 2010; CANATA et al. 2019). Also, the measurement of georeferenced plants height can be useful to estimate crop biomass (PORTZ et al. 2012) with embedded ranging sensors in sugarcane harvesters. In this case, topper instrumentation is required for sending the signal from the ultrasonic sensor to the CAN (Controller Area Network) of the harvester, which will provide the amount of sugarcane harvested at the row-level (CORRÊDO et al., 2020). This would enable some automatic adjustments to improve the operational speed and feed rate variables of the harvesters in real-time.

Shendryk et al. (2020) demonstrated an application of sensing technologies for detecting crop variations of sugarcane fields with different inputs of nitrogen. The crop growth was monitored measuring the plants height, density, and VIs by means of LiDAR technology and multispectral imagery sensors mounted on RPA. Different statistical models were performed to predict the leaf nitrogen content and crop biomass. The data fusion was not considered the best alternative for predicting biomass at the tillering phenological crop stage. The authors recommended using multispectral models for predicting sugarcane biomass early in the season (100-142 days after cutting), and laser sensor data for periods closer to the harvest. Both predictive models were able to guide strategies for the management of nutrients for a sustainable sugarcane production. Xu et al. (2020) reported the relationship among the height and the fresh weight of sugarcane plants using LiDAR embedded in RPA for sampling plots. Authors found that canopy cover and tillage methods have influence on fresh weight estimation. Although of different ranging and imagery sensors applications found in literature review, there is a lack of studies, mainly for sugarcane, focused on crop canopy mapping using geometric attributes, such as plant height, for the assessment of spatial variability at the field level. Most of the studies were conducted generating data without the georeferencing in experimental areas (small plots), which is impracticable for PA purposes.

The use of RPA has been a low-cost alternative, compared to the LiDAR systems, to monitoring crops based on photogrammetry. Despite obtaining a lower density of points, depending on field conditions, photogrammetry is an accurate reconstruction of the target object from overlapping images. The concept is to process the bidimensional data and establish the geometric relationship among images and objects through the Structure from Motion (SfM) imaging technique. This technique allows to extract digital surface or terrain models by means of orthophotos with greater demand of computational time, depending on the number of images. The main benefit of using RPA for low-altitude data acquisition is the higher spatial resolution (GSD – ground sample distance) compared to other RS technologies, such as satellite imagery. Also, images from RPA can be used when there is cloud cover limitation from satellite imagery. However, it is required to collect many overlapping images from different points of view of the entire field to construct the digital elevation models based on orthophotos, also named as orthomosaics. From the georeferenced images is possible to generate the 3D modeling of the crop through the point cloud (colour-enriched points), which enables to spatialize the structural characteristics of the vegetation.

Currently, the main challenge of using RPA systems for agricultural applications is the autonomy of data acquisition for large areas due to the payload of equipment. Also, the influence of luminosity on images requires the same field conditions during the data acquisition. On the other hand, there is a greater advance on development of proximal imaging systems, such as weed management strategies for local interventions (YANO et al., 2017; GÉE and DENIMAL, 2020), and indirect measurements of above-ground biomass at early phenological crop stages (LU et al., 2019; NIU et al., 2019). Other studies used digital cameras embedded in aerial platforms as an alternative to map crop diseases (MATTUPALLI et al., 2018), phenological features of the plants using time-series analysis (BURKART et al., 2018), classification of vegetation types (KOMÁREK et al., 2019), biomass estimation (BENDIG et al., 2014; ACORSI et al., 2019), rice protein content estimation (ONOYAMA et al., 2018), environmental monitoring (TMUŠIĆ et al., 2020), among others. Mesas-Carrascosa et al. (2020) developed a solution to the viticulture based on red-green-blue (RGB) cameras embedded in RPA to derive crop canopy information, such as the height of individual grapevines with an error of 0.07 m. Also, the use of images has advanced to monitoring crop in real-time through integrated sensors, such as digital cameras, inertial units, and GNSS receivers. Sumesh et al. (2021) proposed to map the spatial variability of plant height and stalk density of sugarcane fields based on object-based image analysis considering RGB-based data. The authors found an accuracy of 90% between the manual measurements of plant height and the estimated values. Souza et al. (2017) used an RPA for plant height estimation of sugarcane fields using imagery data based on the digital models of surface (DSM), of terrain (DTM), and canopy height model (CHM), as shown in Figure 4. The purpose was to map the plant height as an indicator of variation of the sugarcane yield, which it was measured using low-resolution data (stalk mass per plot).

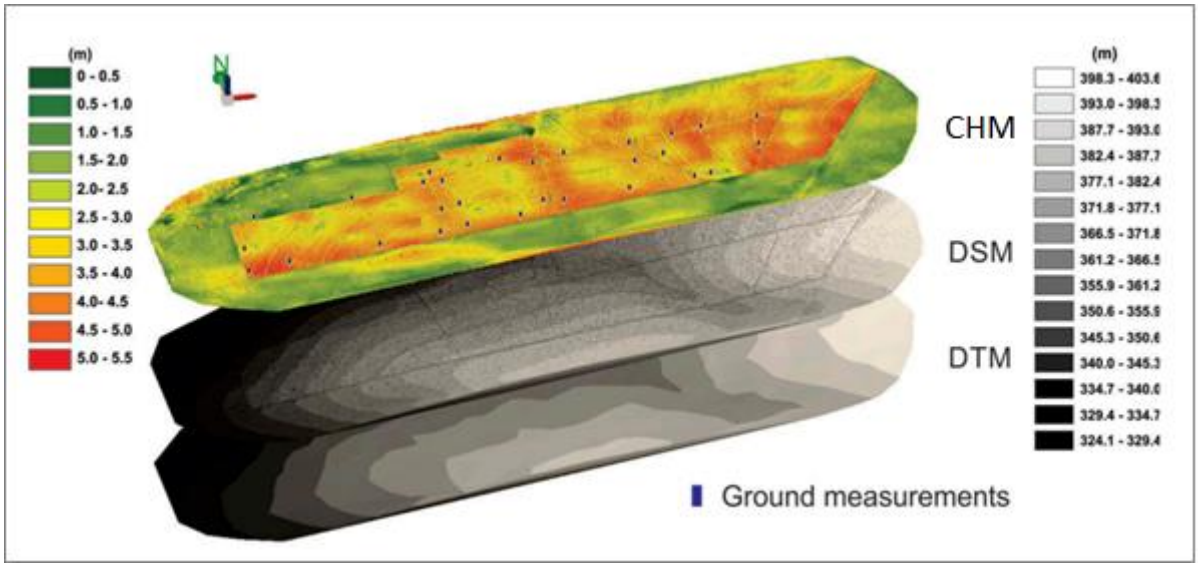


**Figure 4.** Digital elevation models obtained from RGB imagery of sugarcane fields - adapted from Souza et al. (2017)

García-Martínez et al. (2020) demonstrated the potential of predicting corn grain yield based on VIs for early stages of the crop (47-79 days after sowing) using multispectral sensors embedded on RPA and artificial neural networks. The estimated canopy cover demonstrated a moderate correlation with yield (r = 0.77). Maimaitijiang et al. (2020) developed a data fusion system for soybean monitoring based on satellite and RPA images to integrate spectral information with canopy structure features. The results, using machine learning technique, demonstrated better performance for above-ground biomass estimation for early crop stages considering both sources of data - the canopy structure information and spectral features. Maimaitijiang et al. (2017) developed a data acquisition system using multispectral and thermal sensors to estimate soybean grain yield based on plant height by means of RPA. The authors described the data fusion associated with supervised learning methods as an alternative for improving the yield prediction accuracy. Holman et al. (2016) proposed using field phenotyping of wheat based on RGB images to measure the crop growth under different nitrogen fertilizer rates. The main result was obtaining digital surface models as a novel spatial mapping of crop height variation within individual plots. The research perspectives for sensing technologies are to develop agricultural pattern identification due to the recent advancements on visual recognition tasks (CHIU et al., 2020). For that, the database of images should integrate computer vision systems and crop sciences applications, such as to detect anomaly patterns previously of crop damage (JAROLMASJED et al., 2019; KANJIR et al., 2018), for yield mapping in-field before harvesting (SCHUELLER, 2021; WEI and MOLIN, 2020), individual plant segmentation for phenotyping analyzes (JIN et al., 2018), among others. Additionally, integrated agricultural systems would benefit the growers and industry because it could assist the site-specific crop management for each growing season based on within field variability, plan the harvest schedules, and assist on-farm logistics.

## 2.4. Satellite imagery for agriculture

Data-driven solutions have been more incorporated in agricultural systems, mainly, because a diversity of tools has made it easier to gather agronomic data at the field. Even though it continues to become more sophisticated, the data interpretation to design the recommendations within field is the main current challenge for the PA cycle. For that, some modeling methods have been developed to improve the understanding of agronomical factors, such as supervised and non-supervised learning methods, deep learning, and artificial intelligence (BARBOSA et al., 2020; LIAKOS et al., 2018). According to Saifuzzaman et al. (2019) sensing data is becoming critical for assessing soil properties and the characterization of spatial variability, mainly through satellite imagery and proximal sensing tools. A survey carried out with 504 Brazilian farmers about the adoption of digital tools indicated that 84% of the interviewed farmers use at least one digital technology in their production system. At least 20% of the farmers indicated to use images for obtaining general information of the fields. Other applications required by the users were about using images for forecasting climatic risks, mapping land use, detection of disease, pests, weed, and water deficit. The main challenge pointed out for adopting technologies on long-term is the lack of knowledge of the farmers or managers to deal with different technological complexity (BOLFE et al., 2020).

The techniques for yield prediction and crop vigor mapping also have been explored considering multispectral and hyperspectral data from satellite imagery. The main advantage is to perform different methodologies using orbital images that, in some cases, are accessible to the users to assess the agricultural areas of interest. Traditionally, VIs are the most common information extracted from orbital images for mapping crop vigor variation considering multiple seasons. The principle of reflectance measurements assumes that the chlorophyll pigments in green leaves strongly absorb in the visible region of the spectrum (400–700 nm), especially in the blue and red wavelengths, where energy is captured for photosynthesis. Meanwhile in the near-infrared (NIR), from approximately 700 to 1300 nm, leaves exhibit high reflectance values and transmission, mostly related to its structural properties and biomass, and absorb less radiation in this spectral region (TUCKER, 1979; AVERY and BERLIN, 1992). Depending on the phenological crop stage and the level of interaction with the environment, the change in patterns of light reflectance by crop can be detected by satellite images. Some examples include monitoring plant stress indicators based on spectral reflectance properties (GITELSON and MERZLYAK, 1996; ZHANG et al., 2018). Shanahan et al. (2001) compared different VIs to assess the crop canopy variation and its influence on corn grain yield using aircraft imagery. The results indicated that Green Normalized Difference Vegetation Index (GNDVI) values were the most correlated with grain yield. The contributions of satellite imagery in agriculture are also related to the classification of agricultural surfaces (SONOBE et al., 2018), land use (WANG et al., 2019), spatial predictions of soil properties (SILVERO et al., 2021; SICRE et al., 2020), quantification of the available pasture biomass (REIS et al., 2020), to delimit management zones for annual crops (DAMIAN et al., 2020), monitor within-field yield variability for many crops, such as corn (KAYAD et al., 2019) and cotton (BAIO et al., 2018), mapping vineyard variability (KHALIQ et al., 2019) and grasslands biomass (CISNEROS et al., 2020), plan the wheat harvest (TAGHIZADEH et al., 2019), develop crop growth model (LEVITAN and GROSS, 2018), among others.

The identification of spatial and temporal variability of the fields is the main criterion for initial steps of adopting PA tools. For that, satellite imagery provides useful multi-temporal data for large areas with a greater frequency to design agricultural management (SEGARRA et al., 2020). Bramley (2009) proposed that the identification of spatial variability of the fields and the prediction of crop yield can be performed by indirect methods, such as RS techniques, to enhance the traditional methods of crop monitoring (RAHMAN and ROBSON,

2016; NAGY et al., 2018). Multi-temporal satellite imagery, combined with georeferenced agronomic data, also can be used to cluster information layers for designing management zones accurately (MULLA, 2013; BREUNIG et al., 2020). Blasch et al. (2020) detected crop yield patterns through RS tools to investigate the variation in production conditions, such as soil properties. Sibanda et al. (2015) demonstrated the potential of using spectral bands to quantify the above-ground biomass of grasses under different management practices on a regional scale. Baio et al. (2018) reported a positive correlation between Normalized Difference Vegetation Index (NDVI) and fiber cotton yield considering the spatial variability of nine growing seasons.

Considering the crop growth irregular over the fields, the assessment of satellite imagery over the crop development cycle, is useful to identify the factors associated with the cause of spatial variability of the fields. Sugarcane crop is an example of intensive variation of biomass over the seasons, assuming that crop yield tends to decline year-over-year, imagery data enables to measure the potential of crop production in-season indirectly. For this reason, orbital images have been an alternative to mapping crop vigor variation through the spectral response during the sugarcane development cycle (MOREL et al., 2014). Despite of the saturation effect from signal of spectral bands for advanced phenological crop stages, NDVI and NDRE (Normalized Difference Red-Edge Index) are the most common VIs to quantify sugarcane biomass (AMARAL et al, 2015; ROSA et al., 2015). In most researches, sugarcane yield prediction is based on meteorological data (FERNANDES et al., 2011; FERNANDES et al., 2017), on sugar mill database (HAMMER et al., 2019), and crop simulation models (MONTEIRO and SENTELHAS et al., 2018). Sugarcane yield prediction models have developed to monitor sugarcane crop by clustering analysis through multi-temporal satellite images of low spatial resolution for regional (GONÇALVES et al., 2018 – Figure 5A; DUBEY et al., 2018 – Figure 5B) or block level (RAHMAN and ROBSON, 2020). In this case, the main limitation is the comparison of the estimated yield values with the actual yield reported by the mill. It can influence on accuracy of modeling because average values of production are considered instead of high-resolution data (samples per ha) provided by agricultural machinery, given that it has been increasingly used as a data source by agricultural manufacturers and users (CORRÊDO et al., 2020).

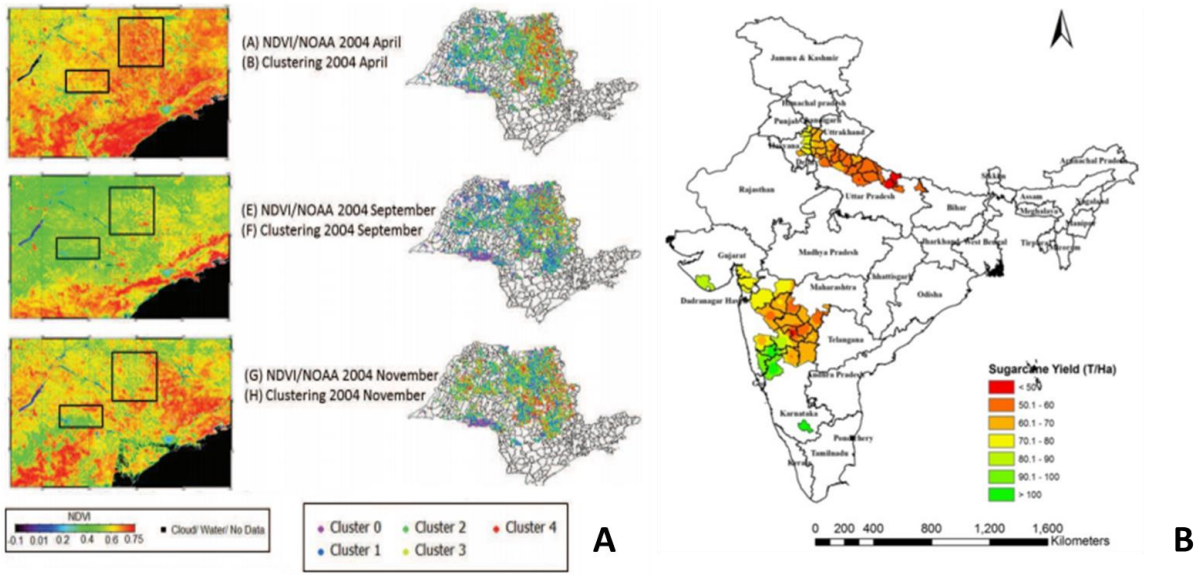


**Figure 5.** Regional scale of sugarcane yield estimation based on vegetation index – Gonçalves et al. (2018) (A), and for sugarcane growing districts of India - Dubey et al. (2018) (B)

The application of RS time-series approach has supported the crop yield modeling when integrated with statistical techniques. For example, it can guide innovative technologies based on modeling for local calibrations of the harvesters, and planning harvest logistics, since it requires many resources at the optimal period of the crop stage. For that, Machine Learning (ML) technique has become common in agricultural sciences involving large datasets, mainly for non-linear combination of the variables, when the Multiple Linear Regression (MLR) is not suitable. ML technique aims to learn, or choose from, a pool of candidate probability models that can best predict unobserved data (MOROTA et al., 2018). Usually, an individual example is described by a set of attributes, also known as features or variables (LIAKOS et al., 2018). The method involves a learning process from training data to perform a task, relating each input attribute to its associated target focusing to limit the error of prediction or forecasting (ELAVARASAN et al., 2018). ANN (Artificial Neural Network) and RF (Random Forest) are the most common ML methods for developing crop yield prediction models, whereas RF is the most suitable method for sugarcane yield prediction (MALDANER et al., 2021; ABDEL-RAHMAN et al., 2012). RF method is a combination of decision trees that each tree depends on the values of a random vector sampled independently from the input with the same distribution for all trees in the forest. RF differs from single decision tree models because it relies on the average result of many trees. For each tree, the data are recursively split into more homogenous units, which are commonly referred to as nodes (BLANCO et al., 2018). The RF process is to select the best combination of the number of trees (ntree) and the number of variables available for splitting the data at each tree node (mtry) (IP et al., 2018). Xu et al. (2020) reported data RF performs better than other regression methods, such as MLR, regarding the prediction accuracy of sugarcane fresh weight based on crop height. Leroux et al. (2019) and Sakamoto (2020) found better performance for estimating the spatial distribution of maize and soybean yield using RF regression. But, for sugarcane there is still a gap in knowledge for yield mapping integrating sensing data and ML techniques.

The ML techniques also have been explored to optimizing the site-specific crop management using on-farm experiments, as an approach to demonstrate the value of PA practices (SAIKAI et al., 2020). Khan et al. (2020) used orbital images (a combination of the spectral bands and VIs) and ANN to estimate Mentha crop biomass. They found a strong linear relationship ($r = 0.87$) among observed and predicted biomass values. Jeffries et al. (2020) combined crop simulation models, orbital images, and ML techniques for mapping sub-field maize yield, resulting in a relative error of 39% (comparing observed and predicted yield values). Fernandes et al. (2017) developed a methodology to anticipate the sugarcane yield prediction by three months before harvesting. The authors indicated the time-series analysis of NDVI and ANN for feature selection as a method to improve the performance of prediction for sixty selected municipalities in São Paulo State, Brazil. In this case, the limitation was to compare the predicted yield values with the national data survey. That is the main reason for exploring multi-temporal reflectance data and sugarcane yield mapping using high-resolution data. The perspective of using orbital images in agriculture include to obtain higher spatial and temporal resolution (pixel level) to map the spatial variability of crop yield response (TREVISAN et al., 2020), to perform sustainable solutions for agricultural operations based on artificial intelligence (SHEIKH et al., 2021), and monitoring plant physiological status based on solar induced chlorophyll fluorescence, as an alternative to measure top-of-canopy reflectance (SIEGMANN et al., 2019; VARGAS et al., 2020).

## References


ACORSI, M. G.; MIRANDA, F. D. A. das; MARTELLO, M.; SMANIOTTO, D. A.; SARTOR, L. R. 2019. Estimating Biomass of Black Oat Using UAV-Based RGB Imaging. **Agronomy**, 9(7): 344. doi: 10.3390/agronomy9070344.

AMARAL, L. R. do; MOLIN, J. P.; SCHEPERS, J. S. 2015. Algorithm for variable-rate nitrogen application in sugarcane based on active crop canopy sensor. **Agronomy Journal**, 107(4): 1513-1523. doi: 10.2134/agronj14.0494.

ARNÓ, J.; ESCOLÀ, A.; VALLÈS, J. M.; LLORENS, J.; SANZ, R.; MASIP, J.; PALACÍN, J.; ROSELL-POLO, J. R. 2013. Leaf area index estimation in vineyards using a ground-based LiDAR scanner. **Precision Agriculture** 14: 290–306. doi: 10.1007/s11119-012-9295-0.

AVERY, T. E.; BERLIN, G. L. 1992. **Fundamentals of Remote Sensing and Airphoto Interpretation**. Macmillan: London, UK.

BAIO, F. H. R.; NEVES, D. C.; CAMPOS, C. N. S.; TEODORO, P. E. 2018. Relationship between cotton productivity and variability of NDVI obtained by Landsat images. **Bioscience Journal**, 34(6):197–205. doi: 10.14393/BJ-v34n6a2018-39583.

BENDIG, J.; BOLTEN, A.; BENNERTZ, S.; BROSCHEIT, J.; EICHFUSS, S.; BARETH, G. 2014. Estimating Biomass of Barley Using Crop Surface Models (CSMs) Derived from UAV-Based RGB Imaging. **Remote Sensing**, 6(11): 10395-10412. doi: 10.3390/rs61110395.

BENJAMIN, C. E.; MAILANDER, M. P.; PRICE, R. R. 2001. Sugar Cane Yield Monitoring System. **Applied Engineering in Agriculture** 26: 965–969. doi: 10.13031/2013.35905.

BLANCO, C. M. G.; GOMEZ, V. M. B.; CRESPO, P.; LIEß, M. 2018. Spatial prediction of soil water retention in a Páramo landscape: Methodological insight into machine learning using random forest. **Geoderma**, 316:100–114. doi: 10.1016/j.geoderma.2017.12.002.

BLANQUART, J-E.; SIRIGNANO, E.; LENAERTS, B.; SAEYS, W. 2020. Online crop height and density estimation in grain fields using LiDAR. **Biosystems Engineering**, 198:1-14. doi: 10.1016/j.biosystemseng.2020.06.014.

BLASCH, G.; LI, Z.; TAYLOR, J. A. 2020. Multi-temporal yield pattern analysis method for deriving yield zones in crop production systems. **Precision Agriculture**, 21:1263-1290. doi: 10.1007/s11119-020-09719-1.

BOLFE, E. L.; JORGE, L. A. C. de; SANCHES, I. D.; LUCHIARI, A. J.; COSTA, C. C. da; VICTORIA, D. C. de; INAMASU, R. Y.; GREGO, C. R.; FERREIRA, V. R.; RAMIREZ, A. R. 2020. Precision and Digital Agriculture: Adoption of Technologies and Perception of Brazilian Farmers. Agriculture, 10(12):653. doi: 10.3390/agriculture10120653.

BRAMLEY, R. G. V. 2009. Lessons from nearly 20 years of Precision Agriculture research, development, and adoption as a guide to its appropriate application. **Crop and Pasture Science** 60: 197–217. doi: 10.1071/CP08304.

BRAMLEY, R. G. V; TRENGOVE, S. 2013. Precision agriculture in australia: Present status and recent developments. **Engenharia Agricola** 33: 575–588. doi: 10.1590/S0100-69162013000300014.

BRAMLEY, R. G. V.; OUZMAN, J.; GOBBETT, D. L. 2018. Regional scale application of the precision agriculture thought process to promote improved fertilizer management in the Australian sugar industry. **Precision Agriculture**. Springer US: 1–17. doi: 10.1007/s11119-018-9571-8.

BRAMLEY, R. G. V.; OUZMAN, J. 2019. Farmer attitudes to the use of sensors and automation in fertilizer decision-making: nitrogen fertilization in the Australian grains sector. **Precision Agriculture** 20: 157–175. doi: 10.1007/s11119-018-9589-y.

BREUNIG, F. M.; GALVÃO, L. S.; DALAGNOL, R.; SANTI, A. L.; FLORA, D. P. D.; CHEN, S. 2020. Assessing the effect of spatial resolution on the delineation of management zones for smallholder farming in southern Brazil. **Remote Sensing Applications: Society and Environment**, 19:100325. doi: 10.1016/j.rsase.2020.100325.

BURKART, A.; HECHT, V. L.; KRASKA, T.; RASCHER, U. 2018. Phenological analysis of unmanned aerial vehicle-based time series of barley imagery with high temporal resolution. **Precision Agriculture** 19: 134–146. doi: 10.1007/s11119-017-9504-y.

CANATA, T. F.; MOLIN, J. P.; SOUSA, R. V. de. 2019. A measurement system based on lidar technology to characterize the canopy of sugarcane plants. **Engenharia Agricola** 39: 240–247. doi: 10.1590/1809-4430-Eng.Agric.v39n2p240-247/2019.

CISNEROS, A.; FIORIO, P.; MENEZES, P.; PASQUALOTTO, N.; WITTENBERGHE, V.S.; BAYMA, G.; FURLAN NOGUEIRA, S. 2020. Mapping Productivity and Essential Biophysical Parameters of Cultivated Tropical Grasslands from Sentinel-2 Imagery. **Agronomy**, 10(5):711. doi: 10.3390/agronomy10050711.

CHIU, M. T.; XU, X.; WEI, Y.; HUANG, Z.; SCHWING, A. G.; BRUNNER, R.; KHACHATRIAN, H.; KARAPETYAN, H.; DOZIER, I.; ROSE, G.; WILSON, D.; TUDOR, A.; HOVAKIMYAN, N.; HUANG, T. S.; SHI, H. 2020. Agriculture-Vision: A Large Aerial Image Database for Agricultural Pattern Analysis. **Proceedings of the IEEE/CVF Conference on Computer Vision and Pattern Recognition**, 2828-2838. arXiv:2001.01306.

COLAÇO, A. F.; BRAMLEY, R. 2019. Site–Year Characteristics Have a Critical Impact on Crop Sensor Calibrations for Nitrogen Recommendations. **Agronomy Journal**, 111(4):2047-2059. doi: 10.2134/agronj2018.11.0726.

COLAÇO, A. F.; TREVISAN, R. G.; KARP, F. H. S.; MOLIN, J. P. 2020. Yield mapping methods for manually harvested crops. Computers and Electronics in Agriculture, 177: 105693. doi: 10.1016/j.compag.2020.105693.

COMBA, L.; BIGLIA, A.; RICAUDA, D. A.; TORTIA, C.; MANIA, E.; GUIDONI, S.; GAY, P. 2020. Leaf Area Index evaluation in vineyards using 3D point clouds from UAV imagery. **Precision Agriculture** 21: 881–896. doi: 10.1007/s11119-019-09699-x.

CORRÊDO, L. P.; CANATA, T. F.; MALDANER, L. F.; LIMA, J. J. A.; MOLIN, J. P. 2020. Sugarcane Harvester for In-field Data Collection: State of the Art, Its Applicability and Future Perspectives. **Sugar Tech**, 5(8):327-345. doi: 10.1007/s12355-020-00874-3.

CORRÊDO, L. P.; MALDANER, L. F.; BAZAME, H. C.; MOLIN, J. P. 2021. Evaluation of Minimum Preparation Sampling Strategies for Sugarcane Quality Prediction by vis-NIR Spectroscopy. **Sensors**, 21(6): 2195. doi: 10.3390/s21062195.

COX, G. J. 2002. A Yield Mapping System for Sugar Cane Chopper Harvesters. University of Southern Queensland.

DAMIAN, J. M.; PIAS, O. H. de C.; CHERUBIN, M. R.; FONSECA, A. Z. da; FORNARI, E. Z.; SANTI, A. L. 2020. Applying the NDVI from satellite images in delimiting management zones for annual crops. **Scientia Agricola**, 77(1): e20180055. doi: 10.1590/1678-992x-2018-0055.

DARR, M. J.; CORBETT, D. J.; HERMAN, H.; VALLESPI-GONZALEZ, C.; DUGAS, B. E.; BADINO, H. 2019. Yield Measurement and Base Cutter Height Control Systems for a Harvester. Patent US20150124054A1.

DEL-MORAL-MARTINEZ, I.; ARNÓ, J.; ESCOLÀ, A.; SANZ, R.; MASIP-VILALTA, J.; COMPANY-MESSA, J.; ROSELL-POLO, J. R. 2015. Georeferenced scanning system to estimate the leaf wall area in tree crops. **Sensors** 15(4): 8382-8405. doi: 10.3390/s150408382.

DRIEMEIER, C.; LIU, Y. L.; SANCHES, G. M.; PONTES, A. O.; MAGALHÃES, P. S. G.; FERREIRA, J. E. 2016. A computational environment to support research in sugarcane agriculture. **Computers and Electronics in Agriculture** 130. Elsevier B.V.: 13–19. doi: 10.1016/j.compag.2016.10.002.

DUBEY, S. K; GAVLI, A. S.; YADAV, S. K.; SEHGAL, S.; RAY, S. S. 2018. Remote Sensing-Based Yield Forecasting for Sugarcane crop in India. **Journal of the Indian Society of Remote Sensing**, 46(11):1823-1833. doi: 10.1007/s12524-018-0839-2.

ELAVARASAN, D.; VINCENT, D. R.; SHARMA, V.; ZOMAYA, A. Y.; SRINIVASAN, K 2018. Forecasting yield by integrating agrarian factors and machine learning models: A survey. **Computers and Electronics in Agriculture**, 155:257-282. doi: 10.1016/j.compag.2018.10.024.

FERNANDES, J. L.; ROCHA, J. V.; LAMPARELLI, R. A. C. 2011. Sugarcane yield estimates using time series analysis of spot vegetation images. **Scientia Agricola**, 68(2): 139-146. doi: 10.1590/S0103-90162011000200002.

FERNANDES, J. L.; EBECKEN, N. F. F.; ESQUERDO, J. C. D. M. 2017. Sugarcane yield prediction in Brazil using NDVI time series and neural networks ensemble**. International Journal of Remote Sensing**, 38(16):4631-4644. doi: 10.1080/01431161.2017.1325531.

FINKELSHTAIN, R; BECHAR, A.; YOVEL, Y.; KÓSA, G. 2017. Investigation and analysis of an ultrasonic sensor for specific yield assessment and greenhouse features identification. **Precision Agriculture** 18: 916–931. doi: 10.1007/s11119-016-9479-0.

GAO, H.; CHENG, B.; WANG, J.; LI, K.; ZHAO, J.; LI, D. 2018. Object Classification Using CNN-Based Fusion of Vision and LIDAR in Autonomous Vehicle Environment. **IEEE Transactions on Industrial Informatics**, v. 14, n. 9, p. 4224-4231. doi: 10.1109/TII.2018.2822828.

GARCÍA-MARTÍNEZ, H.; FLORES-MAGDALENO, H.; ASCENCIO-HERNÁNDEZ, R.; KHALIL-GARDEZI, A.; TIJERINA-CHÁVEZ, L.; MANCILLA-VILLA, O. R.; VÁZQUEZ-PEÑA, M. A. 2020. Corn Grain Yield Estimation from Vegetation Indices, Canopy Cover, Plant Density, and a Neural Network Using Multispectral and RGB Images Acquired with Unmanned Aerial Vehicles. **Agriculture**, 10(7):277. doi: 10.3390/agriculture10070277.

GÉE, C.; DENIMAL, E. 2020. RGB Image-Derived Indicators for Spatial Assessment of the Impact of Broadleaf Weeds on Wheat Biomass. **Remote Sensing**, 12(18): 2982. doi: 10.3390/rs12182982.

GIM International. 2019. Available at: <https://www.gim-international.com/content/article/recent-developments-in-airborne-lidar-2>. Accessed: 11/06/2020.

GITELSON, A. A.; MERZLYAK, M. N. 1996. Signature analysis of leaf reflectance spectra: Algorithm development for remote sensing of chlorophyll. **Journal of Plant Physiology**, 148: 494–500.

GONÇALVES, R. R. V.; ZULLO, J. J.; AMARAL, B. F.; SOUSA, E. P. M.; ROMANI, L. A. S. 2018. Agricultural Monitoring in Regional Scale Using Clustering on Satellite Image Time Series. **Intech Open**, chapter 3. doi: 10.5772/intechopen.71148.

HAMMER, R. G.; SENTELHAS, P. C.; MARIANO, J. C. Q. 2020. Sugarcane Yield Prediction Through Data Mining and Crop Simulation Models. **Sugar Tech** 22: 216–225. doi: 10.1007/s12355-019-00776-z.

HECHT, J. Lidar for self-driving cars. **Opt. Photon**. News 29, 26–33 (2018).

HORAUD, R.; HANSARD, M.; EVANGELIDIS, G.; MÉNIER, C. 2016. An overview of depth cameras and range scanners based on time-of-flight technologies. **Mach. Vis. Appl**. 27, 1005–1020.

HOSOI, F.; OMASA, K. 2012. Estimation of vertical plant area density profiles in a rice canopy at different growth stages by high-resolution portable scanning lidar with a lightweight mirror. **ISPRS Journal of Photogrammetry and Remote Sensing** 74:11-19. doi: 10.1016/j.isprsjprs.2012.08.001.

IP, R. H.; ANG, L. M.; SENG, K. P.; BROSTER, J. C.; PRATLEY, J. E. 2018. Big data and machine learning for crop protection. **Computers and Electronics in Agriculture**, 151:376-383. doi: 10.1016/j.compag.2018.06.008.

JAROLMASJED, S.; SINDHUJA, S.; MARZOUGUI, A.; KOSTICK, S.; YONGSHENG, S.; QUIRÓS, J. J. V.; Evans, K. 2019. High-Throughput Phenotyping of Fire Blight Disease Symptoms Using Sensing Techniques in Apple. **Frontiers in Plant Science**, 10:576. doi: 10.3389/fpls.2019.00576.

JEFFRIES, G. R.; GRIFFIN, T. S.; FLEISHER, D. H.; NAUMOVA, E. N.; KOCH, M.; WARDLOW, B. D. 2020. Mapping sub-field maize yields in Nebraska, USA by combining remote sensing imagery, crop simulation models, and machine learning. **Precision Agriculture**, 21:678–694. doi: 10.1007/s11119-019-09689-z.

JENSEN, J. R. J.; HUMES, K. S.; VIERLING, L. A.; HUDAK, A. T. 2008. Discrete return lidar-based prediction of leaf area index in two conifer forests. **Remote Sensing of Environment** 112(10): 3947-3957. doi: 10.1016/j.rse.2008.07.001.

JENSEN, T.; BAILLIE, C.; BRAMLEY, R.; BELLA, L. D.; WHITEING, C.; DAVIS, R. 2010. Assessment of sugarcane yield monitoring technology for precision agriculture. In: **Proceedings Australian Society of Sugar Cane Technologies**, 32: 410–423.

JIN, S.; SU, Y.; GAO, S.; WU, F.; HU, T.; LIU, J.; LI, W.; WANG, D.; CHEN, S.; JIANG, Y.; PANG, S.; GUO, Q. 2018. Deep Learning: Individual Maize Segmentation From Terrestrial Lidar Data Using Faster R-CNN and Regional Growth Algorithms. **Frontiers in Plant Science**, 9:866. doi: 10.3389/fpls.2018.00866.

KAMOSKE, A. G.; DAHLIN, K. M.; STARK, S. C.; SERBIN, S. P. 2019. Leaf area density from airborne LiDAR: Comparing sensors and resolutions in a temperate broadleaf forest ecosystem. **Forest Ecology and Management** 433: 364-375. doi: 10.1016/j.foreco.2018.11.017.

KANJIR, U.; ĐURIĆ, N.; VELJANOVSKI, T. 2018. Sentinel-2 Based Temporal Detection of Agricultural Land Use Anomalies in Support of Common Agricultural Policy Monitoring. **ISPRS International Journal of Geo-Information**, 7, 405. doi:10.3390/ijgi7100405.

KAYAD, A.; SOZZI, M.; GATTO, S.; MARINELLO, F.; PIROTTI, F. 2019. Monitoring within-field variability of corn yield using Sentinel-2 and machine learning techniques. **Remote Sensing**, 11(23):2873. doi: 10.3390/rs11232873.

KHALIQ, A.; COMBA, L.; BIGLIA, A.; AIMONINO, D.R.; CHIABERGE, M.; GAY, P. 2019. Comparison of satellite and UAV-based multispectral imagery for vineyard variability assessment. **Remote Sensing**, 11(4):436. doi:10.3390/rs11040436.

KHAN, M. S.; SEMWAL, M.; SHARMA, A.; VERMA, R. K. 2020. An artificial neural network model for estimating Mentha crop biomass yield using Landsat 8 OLI. **Precision Agriculture**, 21(4):18-33. doi: 10.1007/s11119-019-09655-9.

KIN, Y. Y.; SUDHANSHU, S.; JAMUAR, A. Y. 2011. Combine harvester instrumentation system for use in precision agriculture. **Instrumentation Science and Technology** 39: 374–393. doi: 10.1080/10739149.2011.585195.

KOMÁREK, J.; KLOUČEK, T.; PROŠEK, J. 2019. The potential of Unmanned Aerial Systems: A tool towards precision classification of hard-to-distinguish vegetation types? **International Journal of Applied Earth Observation and Geoinformation**, 71: 9-19. doi: 10.1016/j.jag.2018.05.003.

LEEUWEN, M V.; COOPS, N. C.; WULDER, M. A. 2010. Canopy surface reconstruction from a LiDAR point cloud using Hough transform. **Journal Remote Sensing Letters** 1(3): 125-132. doi: 10.1080/01431161003649339.

LEROUX, L.; CASTETS, M.; BARON, C.; ESCORIHUELA, M.-J.; BÉGUÉ, A.; LO SEEN, D. 2019. Maize yield estimation in West Africa from crop process-induced combinations of multi-domain remote sensing indices. **European Journal of Agronomy**, 108:11–26. doi: 10.1016/j.eja.2019.04.007.

LEVITAN, N., GROSS, B. 2018. Utilizing collocated crop growth model simulations to train agronomic satellite retrieval algorithms. **Remote Sensing**, 10(12):1968. doi: 10.3390/rs10121968.

LI, S.; DAI, L.; WANG, H.; WANG, Y.; HE, Z.; LIN, S. 2017. Estimating Leaf Area Density of Individual Trees Using the Point Cloud Segmentation of Terrestrial LiDAR Data and a Voxel-Based Model. **Remote Sensing** 9(11): 1202. doi: 10.3390/rs9111202.

LIAKOS, K. G.; BUSATO, P.; MOSHOU, D.; PEARSON, S.; BOCHTIS, D. 2018. Machine Learning in Agriculture: A Review. **Sensors**, 18(8): 2674. doi: 10.3390/s18082674.

LOBELL, D. B. 2013. The use of satellite data for crop yield gap analysis. **Field Crops Research**, 143:56–64. doi: 10.1016/j.fcr.2012.08.008.

LU, N.; ZHOU, J.; HAN, Z.; LI, D.; CAO, Q.; YAO, X.; TIAN, Y.; ZHU, Y.; CAO, W.; CHENG, T. 2019. Improved estimation of aboveground biomass in wheat from RGB imagery and point cloud data acquired with a low-cost unmanned aerial vehicle system. **Plant Methods** 15(17). doi: 10.1186/s13007-019-0402-3.

MA, S.; KARKEE, M.; SCHARF, P. A.; ZHANG, Q. 2014. Sugarcane harvester technology: A critical overview. **Applied Engineering in Agriculture** 30: 727–739. doi: 10.13031/aea.30.10696.

MAILANDER, M.; BENJAMIN, R.; PRICE, C.; HALL, S. 2010. Sugar cane yield monitoring system. Applied Engineering in Agriculture 26. St. Joseph, MI: **American Society of Agricultural and Biological Engineers**: 965–970. doi: 10.13031/2013.35905.

MAIMAITIJIANG, M.; GHULAM, A.; SIDIKE, P.; HARTLING, S.; MAIMAITIYIMING, M.; PETERSON, K. T.; SHAVERS, E.; FISHMAN, J.; PETERSON, J. P.; KADAM, S.; BURKEN, J.; FRITSCHI, F. B. 2017. Unmanned Aerial System (UAS)-based phenotyping of soybean using multi-sensor data fusion and extreme learning machine. **ISPRS Journal of Photogrammetry and Remote Sensing**, 134:43-58. doi: 10.1016/j.isprsjprs.2017.10.011.

MAIMAITIJIANG, M.; SAGAN, V.; SIDIKE, P.; DALOYE, A. M.; ERKBOL, H.; FRITSCHI, F. B. 2020. Crop Monitoring Using Satellite/UAV Data Fusion and Machine Learning. **Remote Sensing**, 12(9):1357. doi: 10.3390/rs12091357.

MALDANER, L. F.; MOLIN, J. P. 2020. Data processing within rows for sugarcane yield mapping. **Scientia Agricola** 77(5): e20180391. doi: 10.1590/1678-992x-2018-0391.

MALDANER, L. F.; CORREDO, L. de P.; CANATA, T. F.; MOLIN, J. P. 2021. Predicting the sugarcane yield in real-time by harvester engine parameters and machine learning approaches. **Computers and Electronics in Agriculture**, 181:105945. doi: 10.1016/j.compag.2020.105945.

MALLET, C.; BRETAR, F. 2009. Full-waveform topographic lidar: State-of-the-art. **ISPRS Journal of Photogrammetry and Remote Sensing**, 64, 1–16.

MANHÃES, C. M. C.; GARCIA, R. F.; FRANCELINO, F. M. A.; CORREA JUNIOR, D.; SOLANO, C. S.; FRANCELINO, H. 2014. Visible Losses in Mechanized Harvesting of Sugarcane Using the Case IH A4000 Harvester. **American Journal of Plant Sciences** 05: 2734–2740. doi: 10.4236/ajps.2014.518289.

MATTUPALLI, C.; MOFFET, C. A.; SHAH, K. N.; YOUNG, C. A. 2018. Supervised Classification of RGB Aerial Imagery to Evaluate the Impact of a Root Rot Disease. **Remote Sensing**, 10(6): 917. doi: 10.3390/rs10060917.

MESAS-CARRASCOSA, F. J.; CASTRO, A. I. de; TORRES-SÁNCHEZ, J.; TRIVIÑO-TARRADAS, P.; JIMÉNEZ-BRENES, F. M.; GARCÍA-FERRER, A.; LÓPEZ-GRANADOS, F. 2020. Classification of 3D Point Clouds Using Color Vegetation Indices for Precision Viticulture and Digitizing Applications. **Remote Sensing**, 12(2): 317. doi: 10.3390/rs12020317.

MOLIN, J. P.; MENEGATTI, L. A. A. 2004. Field-testing of a sugar cane yield monitor in Brazil. **ASAE Annual International Meeting** 2004 0300: 733–744. doi: 10.13031/2013.16159.

MOMIN, M. A.; GRIFT, T. E.; VALENTE, D. S.; HANSEN, A. C. 2019. Sugarcane yield mapping based on vehicle tracking. **Precision Agriculture**, 20(5), 896-910. doi: 10.1007/s11119-018-9621-2.

MONTEIRO, L. A.; SENTELHAS, P. C. 2017. Sugarcane yield gap: can it be determined at national level with a simple agrometeorological model? **Crop and Pasture Science** 68:272-284. doi: 10.1071/CP16334.

MOREL, J.; TODOROFF, P.; BÉGUÉ, A.; BURY, A.; MARTINÉ, J. F.; PETIT, M. 2014. Toward a satellite-based system of sugarcane yield estimation and forecasting in smallholder farming conditions: a case study on Reunion Island. **Remote Sensing**, 6(7):6620-6635. doi: 10.3390/rs6076620.

MOROTA, G.; VENTURA, R.; SILVA, F. F.; KOYAMA, M.; FERNANDO, S. C. 2018. Machine learning and data mining advance predictive big data analysis in precision animal agriculture. **Journal of Animal Science**, 96(4):1540-1550. doi: 10.1093/jas/sky014.

MULLA, D. J. 2013. Twenty-five years of remote sensing in precision agriculture: key advances and remaining knowledge gaps. **Biosystems Engineering**, 114(4):358-371. doi: 10.1016/j.biosystemseng.2012.08.009.

NAGY, A.; FEHÉR, J.; TAMAS, J. 2018. Wheat and maize yield forecasting for the Tisza river catchment using MODIS NDVI time series and reported crop statistics. **Computers and Electronics in Agriculture**, 151:41-49. doi: 10.1016/j.compag.2018.05.035.

NAWI, N. M.; GUANGNAN, C.; JENSEN, T. 2014. In-field measurement and sampling technologies for monitoring quality in the sugarcane industry: a review. **Precision Agriculture** 15: 684–703. doi: 10.1007/s11119-014-9362-9.

NIU, Y.; ZHANG, L.; ZHANG, H.; HAN, W.; PENG, X. 2019. Estimating Above-Ground Biomass of Maize Using Features Derived from UAV-Based RGB Imagery. **Remote Sensing**, 11(11): 1261. doi: 10.3390/rs11111261.

ONOYAMA, H.; CHANSEOK, R.; MASAHIKO, S.; MICHIHISA, I. 2018. Estimation of rice protein content before harvest using ground-based hyperspectral imaging and region of interest analysis. **Precision Agriculture** 19: 721–734. doi: 10.1007/s11119-017-9552-3.

PORTZ, G; MOLIN, J. P.; JASPER, J. 2012. Active crop sensor to detect variability of nitrogen supply and biomass on sugarcane fields. **Precision Agriculture** 13: 33–44. doi: 10.1007/s11119-011-9243-4.

PRICE, R. R.; LARSEN, J.; PETERS, A. 2007. Development of an optical yield monitor for sugar cane harvesting. In 2007 ASABE Annual International Meeting, Technical Papers. Vol. 1 BOOK. St. Joseph, MI: **American Society of Agricultural and Biological Engineers**. doi: 10.13031/2013.23546.

PRICE, R. R.; JOHNSON, R. M.; VIATOR, R. P.; LARSEN, J.; PETERS, A. 2011. Fiber optic yield monitor for a sugarcane harvester. **Transactions of the ASABE** 54: 31–39.

PRICE, R. R.; JOHNSON, R. M.; VIATOR, R. P. 2017. An overhead optical yield monitor for a sugarcane harvester based on two optical distance sensors mounted above the loading elevator. **Applied Engineering in Agriculture** 33: 687–693.

QUADERER, J. G.; CASH, M. F. 2015. Sugar cane yield mapping. doi: 10.1111/j.1540-4781.1969.tb04998.x.

QU, Y.; SHAKER, A.; SILVA, C. A.; KLAUBERG, C.; PINAGÉ, E. R. Remote Sensing of Leaf Area Index from LiDAR Height Percentile Metrics and Comparison with MODIS Product in a Selectively Logged Tropical Forest Area in Eastern Amazonia. **Remote Sensing** 10(6): 970, 2018. doi: 10.3390/rs10060970.

RAHMAN, M. M.; ROBSON, A. J. 2016. A Novel Approach for sugarcane yield prediction using Landsat time series imagery: a case study on Bundaberg region. **Advances in Remote Sensing**, 5(2):93-102. doi: 10.4236/ars.2016.52008.

RAHMAN, M. M.; ROBSON, A. J. 2020. Integrating Landsat-8 and Sentinel-2 Time Series Data for Yield Prediction of Sugarcane Crops at the Block Level. **Remote Sensing**, 12(8): 1313. doi: 10.3390/rs12081313.

REIS, A. A. dos; WERNER, J. P. S.; SILVA, B. C.; FIGUEIREDO, G. K. D. A.; ANTUNES, J. F. G.; ESQUERDO, J. C. D. M.; COUTINHO, A. C.; LAMPARELLI, R. A. C.; ROCHA, J. V.; MAGALHÃES, P. S. G. 2020. Monitoring Pasture Aboveground Biomass and Canopy Height in an Integrated Crop–Livestock System Using Textural Information from PlanetScope Imagery. **Remote Sensing**, 12(16): 2534. doi: 10.3390/rs12162534.

RODRIGUES, F. A.; MAGALHÃES, P. S. G.; FRANCO, H. C. J. 2013. Soil attributes and leaf nitrogen estimating sugar cane quality parameters: Brix, pol and fibre. **Precision Agriculture** 14: 270–289. doi: 10.1007/s11119-012-9294-1.

ROSA, H. J. A.; AMARAL, L. R. do; MOLIN, J. P.; CANTARELLA, H. 2015. Sugarcane response to nitrogen rates, measured by a canopy reflectance sensor. **Pesquisa Agropecuária Brasileira**, 50(9): 840-848. doi: 10.1590/S0100-204X2015000900013.

RUCKELSHAUSEN, A.; BIBER, P.; DORNA, M.; GREMMES, H.; KLOSE, R.; LINZ, A.; RAHE, R.; RESCH, R.; THIEL, M.; TRAUTZ, D.; WEISS, U. 2009. BoniRob: An autonomous field robot platform for individual plant phenotyping. **Precision Agriculture**, 9: 841-847.

SAIKAI, Y.; PATEL, V.; MITCHELL, P. D. 2020. Machine learning for optimizing complex site-specific management. **Computers and Electronics in Agriculture**, 174: 105381. doi: 10.1016/j.compag.2020.105381.

SANCHES, G. M.; MAGALHÃES, P. S. G.; FRANCO, H. C. J. 2019. Site-specific assessment of spatial and temporal variability of sugarcane yield related to soil attributes. **Geoderma**, 334: 90–98. doi: 10.1016/j.geoderma.2018.07.051.

SANTOS, N. B. dos; ROUVERSON, P. S.; CASIMIRO, D. G. JUNIOR. 2014. Economic analysis for sizing of sugarcane (Saccharum spp.) mechanized harvesting. **Engenharia Agrícola**, 34: 945–954. doi: 10.1590/s0100-69162014000500013.

SANZ, R.; ROSELL, J. R.; CALVERAS, L.; JORDI, G., E.; MARTÍ, S. P. de. 2013. Relationship between tree row LIDAR-volume and leaf area density for fruit orchards and vineyards obtained with a LIDAR 3D Dynamic Measurement System. **Agricultural and Forest Meteorology**, 171–172:153–162. doi: 10.1016/j.agrformet.2012.11.013.

SAKAMOTO, T. 2020. Incorporating environmental variables into a MODIS-based crop yield estimation method for United States corn and soybeans through the use of a random forest regression algorithm. **ISPRS Journal of Photogrammetry and Remote Sensing**, 160: 208–228. doi: 10.1016/j.isprsjprs.2019.12.012.

SCHWALBERT, R. A.; AMADO, T. J. C.; NIETO, L.; VARELA, S.; CORASSA, G. M.; HORBE, T. A. N.; RICE, C. W.; PERALTA, N. R.; CIAMPITTI, I. A. 2018. Forecasting maize yield at field scale based on high-resolution satellite imagery. **Biosystems Engineering**, 171: 179–192. doi: 10.1016/j.biosystemseng.2018.04.020.

SCHUELLER, J. K. 2021. Opinion: Opportunities and Limitations of Machine Vision for Yield Mapping. **Frontiers in Robotics and AI**, 8:627280. doi: 10.3389/frobt.2021.627280.

SEGARRA, J.; BUCHAILLOT, M. L.; ARAUS, J. L.; KEFAUVER, S. C. 2020. Remote Sensing for Precision Agriculture: Sentinel-2 Improved Features and Applications. **Agronomy**, 10(5): 641. doi: 10.3390/agronomy10050641.

SELBECK, J.; DWORAK, V.; EHLERT, D. 2010. Testing a vehicle-based scanning lidar sensor for crop detection. **Canadian Journal of Remote Sensing** 36: 24–35. doi: 10.5589/m10-022.

SHANAHAN, J. F.; SCHEPERS, J. S.; FRANCIS, D. D.; VARVEL, G. E.; WHILHELM, W. W.; TRINGE, J. M.; SCHLEMMER, M. R.; MAJOR, D. J. 2001. Use of remote-sensing imagery to estimate corn grain yield. **Agronomy Journal**, 93(3): 583-589. doi: 10.2134/agronj2001.933583x.

SHEIKH, J. A.; CHEEMA, S. M.; ALI, M.; AMJAD, Z.; TARIQ, J. Z.; NAZ, A. 2021. IoT and AI in Precision Agriculture: Designing Smart System to Support Illiterate Farmers. In: Ahram T. (eds) Advances in Artificial Intelligence, Software and Systems Engineering. AHFE 2020. **Advances in Intelligent Systems and Computing**, 1213: 490-496. Springer, Cham. doi: 10.1007/978-3-030-51328-3_67.

SHENDRYK, Y.; SOFONIA, J.; GARRARD, R.; RIST, Y.; SKOCAJ, D.; THORBURN, P. 2020. Fine-scale prediction of biomass and leaf nitrogen content in sugarcane using UAV LiDAR and multispectral imaging. **International Journal of Applied Earth Observation and Geoinformation**, 92: 102177. doi: 10.1016/j.jag.2020.102177.

SIBANDA, M.; MUTANGA, O.; ROUGET, M. 2015. Examining the potential of Sentinel-2 MSI spectral resolution in quantifying above ground biomass across different fertilizer treatments. **ISPRS Journal of Photogrammetry and Remote Sensing**, 110:55-65. doi: 10.1016/j.isprsjprs.2015.10.005.

SICRE, C. M.; FIEUZAL, R.; BAUP, P. 2020. Contribution of multispectral (optical and radar) satellite images to the classification of agricultural surfaces. **International Journal of Applied Earth Observation and Geoinformation**, 84:101972. doi: 10.1016/j.jag.2019.101972.

SIEGMANN, B.; ALONSO, L.; CELESTI, M.; COGLIATI, S.; COLOMBO, R.; DAMM, A.; DOUGLAS, S.; GUANTER, L.; HANUŠ, J.; KATAJA, K.; KRASKA, T.; MATVEEVA, M.; MORENO, J.; MULLER, O.; PIKL, M.; PINTO, F.; QUIRÓS VARGAS, J.; RADEMSKE, P.; RODRIGUEZ-MORENE, F.; SABATER, N.; SCHICKLING, A.; SCHÜTTEMEYER, D.; ZEMEK, F.; RASCHER, U. 2019. The High-Performance Airborne Imaging Spectrometer HyPlant—From Raw Images to Top-of-Canopy Reflectance and Fluorescence Products: Introduction of an Automatized Processing Chain. **Remote Sensing**, 11(23): 2760. doi: 10.3390/rs11232760.

SILVA, C. B.; MORAES, M. A. F. D. de; MOLIN, J. P. 2011. Adoption and use of precision agriculture technologies in the sugarcane industry of São Paulo state, Brazil. **Precision Agriculture**, 12: 67–81. doi: 10.1007/s11119-009-9155-8.

SILVA, R. P.; CORRÊA, C. F.; CORTEZ, J. W.; FURLANI, C. E A. 2008. Controle estatístico aplicado ao processo de colheita mecanizada diurna e noturna de cana-de-açúcar. **Engenharia Agrícola**, 28: 292–304. doi: 10.1590/S0006-87052011000400028.

SILVERO, N. E. Q.; DEMATTÊ, J. A. M.; AMORIM, M. T. A.; SANTOS, N. V. dos; RIZZO, R.; SAFANELLI, J. L.; POPPIEL, R. R.; MENDES, W. S. de; BONFATTI, B. R. 2021. Soil variability and quantification based on Sentinel-2 and Landsat-8 bare soil images: A comparison. **Remote Sensing of Environment**, 252:112117. doi: 10.1016/j.rse.2020.112117.

SONOBE, R.; YAMAYA, Y.; TANI, H.; WANG, X.; KOBAYASHI, N.; MOCHIZUKI, K. 2018. Crop classification from Sentinel-2-derived vegetation indices using ensemble learning. **Journal of Applied Remote Sensing**, 12(2): 026019 doi: 10.1117/1.JRS.12.026019.

SOUZA, C. H. W. de; LAMPARELLI, R. A. C.; ROCHA, J. V.; MAGALHÃES, P. S. G. 2017. Height estimation of sugarcane using an unmanned aerial system (UAS) based on structure from motion (SfM) point clouds. **International Journal of Remote Sensing** 38: 2218–2230. doi: 10.1080/01431161.2017.1285082.

SUMESH, K. C.; NINSAWAT, S.; SOM-ARD, J. 2021. Integration of RGB-based vegetation index, crop surface model and object-based image analysis approach for sugarcane yield estimation using unmanned aerial vehicle. **Computers and Electronics in Agriculture**, 180: 105903. doi: 10.1016/j.compag.2020.105903.

SPEKKEN, M.; MOLIN, J. P.; ROMANELLI, T. L. 2015. Cost of boundary manoeuvres in sugarcane production. **Biosystems Engineering** 129. Academic Press: 112–126. doi: 10.1016/j.biosystemseng.2014.09.007.

SU, W.; HUANG, J.; LIU, D.; ZHANG, M. 2019. Retrieving Corn Canopy Leaf Area Index from Multitemporal Landsat Imagery and Terrestrial LiDAR Data. **Remote Sensing**, 11(5): 572. doi: 10.3390/rs11050572.

TACHELLA, J.; ALTMANN, Y.; MELLADO, N.; MCCARTHY, A.; TOBIN, R.; BULLER, G. S.; TOURNERET, J. Y.; MCLAUGHLIN, S. 2019. Real-time 3D reconstruction from single-photon lidar data using plug-and-play point cloud denoisers. **Nature Communications** 10: 4984. doi: 10.1038/s41467-019-12943-7.

TAGHIZADEH, S.; NAVID, H.; ADIBAN, R.; MAGHSODI, Y. 2019. Harvest chronological planning using a method based on satellite-derived vegetation indices and artificial neural networks. **Spanish Journal of Agricultural Research**, 17(3):206. doi: 10.5424/sjar/2019173-14357.

TMUŠIĆ, G.; MANFREDA, S.; AASEN, H.; JAMES, M. R.; GONÇALVES, G.; BEN-DOR, E.; BROOK, A.; POLINOVA, M.; ARRANZ, J. J.; MÉSZÁROS, J.; ZHUANG, R.; JOHANSEN, K.; MALBETEAU, Y.; LIMA, I. P. de; DAVIDS, C.; HERBAN, S.; McCABE, M. F. 2020. Current Practices in UAS-based Environmental Monitoring. **Remote Sensing**, 12(6): 1001. doi: 10.3390/rs12061001.

TREVISAN, R. G.; BULLOCK, D. S.; MARTIN, N. F. 2020. Spatial variability of crop responses to agronomic inputs in on-farm precision experimentation. **Precision Agriculture**. doi: 10.1007/s11119-020-09720-8.

TUCKER, C. J. 1979. Red and photographic infrared linear combinations for monitoring vegetation. **Remote Sensing of Environment**, 8: 127–150.

USSYSHKIN, V.; THERIAULT, L. 2011. Airborne Lidar: Advances in Discrete Return Technology for 3D Vegetation Mapping. **Remote Sensing** 3: 416-434; doi: 10.3390/rs3030416.

VARGAS, J. Q.; BENDIG, J.; MAC ARTHUR, A.; BURKART, A.; JULITTA, T.; MASEYK, K.; THOMAS, R.; SIEGMANN, B.; ROSSINI, M.; CELESTI, M.; SCHÜTTEMEYER, D.; KRASKA, T.; MULLER, O.; RASCHER, U. 2020. Unmanned Aerial Systems (UAS)-Based Methods for Solar Induced Chlorophyll Fluorescence (SIF) Retrieval with Non-Imaging Spectrometers: State of the Art. **Remote Sensing**, 12(10): 1624. doi: 10.3390/rs12101624.

WANG, M.; LIU, Z.; ALI BAIG, M.H.; WANG, Y.; LI, Y.; CHEN, Y. 2019. Mapping sugarcane in complex landscapes by integrating multi-temporal Sentinel-2 images and machine learning algorithms. **Land Use Policy**, 88: 104190.

WEI, M. C. F.; MOLIN, J. P. 2020. Soybean Yield Estimation and Its Components: A Linear Regression Approach. **Agriculture**, 10(8), 348. doi: 10.3390/agriculture10080348.

WENDTE, L. K. W.; SKOTNIKOV, B. R. A.; THOMAS, O. P. K. K. 2001. Sugar cane yield monitor. United States.

XIE, L.; WANG, J.; CHENG, S.; ZENG, B.; YANG, Z. 2019. Performance Evaluation of a Chopper System for Sugarcane Harvester. **Sugar Tech** 21: 825–837. doi: 10.1007/s12355-019-00714-z.

XU, J.-X.; MA, J.; TANG, Y.-N.; WU, W.-X.; SHAO, J.-H.; WU, W.-B.; WEI, S.-Y.; LIU, Y.-F.; WANG, Y.-C.; GUO, H.-Q. 2020. Estimation of Sugarcane Yield Using a Machine Learning Approach Based on UAV-LiDAR Data. **Remote Sensing**, 12(17): 2823. doi: 10.3390/rs12172823.

YANG, H.; CHEN, W.; QIAN, T.; SHEN, D.; WANG, J. 2015. The Extraction of Vegetation Points from LiDAR Using 3D Fractal Dimension Analyses. **Remote Sensing**, 7(8): 10815-10831. doi: 10.3390/rs70810815.

YANO, I. H.; MESA, N. F. O.; SANTIAGO, W. E.; AGUIAR, R. H.; TERUEL, B. 2017. Weed Identification in Sugarcane Plantation Through Images Taken from Remotely Piloted Aircraft (RPA) and kNN Classifier. **Journal of Food and Nutrition Sciences**, 5(6): 211-216. doi: 10.11648/j.jfns.20170506.11.

ZHANG, Y.; SHEN, X. 2014. Quantitative Analysis on Geometric Size of LiDAR Footprint. **IEEE Geoscience and Remote Sensing Letters**, 11(3): 701-705. doi: 10.1109/LGRS.2013.2276126.

ZHANG, Z.; LIU, M.; LIU, X.; ZHOU, G. 2018. A New Vegetation Index Based on Multitemporal Sentinel-2 Images for Discriminating Heavy Metal Stress Levels in Rice. **Sensors**, 18(7): 2172. doi: 10.3390/s18072172.

ZHAO, G.; LIAN, M.; LI, Y.; DUAN, Z.; ZHU, S.; MEI, L.; SVANBERG, S. 2017. Mobile lidar system for environmental monitoring. **Applied Optics**, 56(5): 1506-1516. doi: 10.1364/AO.56.001506.

ZHOU, L.; GU, X.; CHENG, S.; YANG, G.; SHU, M.; SUN, Q. 2020. Analysis of Plant Height Changes of Lodged Maize Using UAV-LiDAR Data. **Agriculture**, 10(5): 146. doi: 10.3390/agriculture10050146.

# 3. SITE-SPECIFIC ASSESSMENT OF THE SPATIAL VARIABILITY OF SUGARCANE FIELDS USING 3D SENSING TECHNIQUES


## ABSTRACT

LiDAR (Light Detection and Ranging) technology is a high-resolution remote sensing tool that allows to assist in harvest planning. No research was found exploring the characterization of the spatial variability of sugarcane fields using this technology yet. The objective of the study was to describe the use of three-dimensional (3D) sensing techniques to characterize the spatial variability of sugarcane fields in the pre-harvest period. An ALS (Airborne Laser Scanning) was used for the data acquisition 10 days before sugarcane harvesting for two consecutive sugarcane growing seasons. The platform consists of a laser sensor, an inertial unit, and a GNSS (Global Navigation Satellite Systems) receiver. RGB images also were obtained 15 days before harvesting. From the point clouds, digital surface model (DSM), digital terrain model (DTM), and canopy height model (CHM) were generated to spatialize the crop canopy height at the field level. The LiDAR-derived metrics extracted were the percentiles, with the highest coefficient of variation observed for $P50^{th}$ (59%), indicating a very high spatial variability of the crop canopy height. The RMSE (Root Mean Squared Error) of the sugarcane stalk height estimation based on CHM was 0.47 m. The relationship among the CHM and the yield map showed moderate correlation (r=0.49). This study demonstrates that 3D sensing data can provide relevant information for the assessment of plant height and, potentially, to consider it as an indicator of the field regions with distinct levels of production.


## 3.1. Introduction

The application of Remote Sensing (RS) techniques in agriculture allows to collect high-resolution data (spatial and temporal) for mapping and monitoring crops, which are essential to the PA practices. RS also enables identifying agronomic factors associated with the inherent variability of the fields (MOLIN et al., 2015). The aerial imagery and scanning sensors (laser, ultrasonic, and radar) have been adopted to detect the spatial variability of the fields. The main reason is the capacity of the embedded sensors on terrestrial or aerial platforms to obtain high sample density, in short time, and large-scale, compared with the traditional measurements that are labour-intensive (BUELVAS et al., 2019). Maes and Steppe (2019) reported the progress of applying RS tools to the PA scenario as a solution to provide essential spatial information to the agronomic diagnostics. Some examples are regarding the potential of the image-based aerial platforms to assess drought stress in early stages of the crops, to develop site-specific weed detection, to detect growth vigor, crop nutrient status, and yield prediction. They also highlighted the integration of different datasets to improve the applicability of the developed models. The perspective is to optimize the agricultural practices with an increase of knowledge systems due to the availability of larger amounts of crop data (SAIZ-RUBIO and ROVIRA-MÁS, 2020).

Different measuring techniques have been introduced in agriculture using LiDAR for crop analysis to advance on the automated extraction of the attributes related to the crop yield from point clouds (PAULUS, 2019). Silva et al. (2020) demonstrated the potential of modeling forest plantations using LiDAR and manual measurements (stem volume) to assess forestry conditions remotely. Paulus et al. (2014) verified the response of the volumetric shape of sugar beet subject to drought conditions based on laser sensors as a potential technique for plant phenotyping. Another approach is the integration of laser and multispectral sensors to infer crop biomass (OKHRIMENKO et al., 2019; TILLY et al., 2015). Jimenez-berni et al. (2018) described LiDAR as a direct measurement of the crop canopy height that allows a multi-temporal and non-destructive assessment of ground cover and above-ground biomass of wheat. Other agricultural applications have been supported by 3D sensing data, such as fruit detection for apple orchards with an accuracy of more than 80% (GENÉ-MOLA et al., 2020). Both

platforms have been used to provide crop canopy models along its development cycle and integrated to calibrate structural attributes of the plants (BAZEZEW et al., 2018; HOPKINSON et al., 2013). Li et al. (2017) investigated the potential of point clouds generated from ALS to characterize the structural complexity of the maize canopy. The leaf area index was estimated with relative error of 5.63%. Also, these studies showed the benefits of ALS, and MTLS to obtain high-resolution data to guide site-specific practices. Data fusion is another alternative to advance on integration of multiple sources of data, Maimaitijiang et al. (2020) proposed modeling methods to soybean yield prediction using LiDAR and RGB imagery as an alternative for the site-specific crop management. The main limitation was the reduced payload of the RPA and sensors able to deal with the spectral saturation effect, independence of the ambient light conditions, and signal penetration on the dense crop canopy previous to the harvest (POLEY and McDERMID, 2020; DEERY et al., 2014). Shendryk et al. (2020) used multirotor RPA with LiDAR and imaging sensors embedded for predicting biomass and leaf nitrogen content in sugarcane. They found a moderate relationship ($R^2 \leq 0.52$) to estimate sugarcane biomass based on 3D modeling and multispectral images.

Mapping sugarcane areas using multi-temporal data has been used to monitor the spatial variability of the fields based on orbital images (WANG et al., 2019; LUCIANO et al., 2018). Also, the spectral bands (reflectance data and vegetation indices) have been investigated for sugarcane yield forecasting (LUCIANO et al., 2021; RAHMAN and ROBSON, 2020; BÉGUÉ et al, 2010). Despite the potential to explore the data from low-cost imagery, the saturation effect previous harvesting, and the most appropriate phenological period to determine crop yield are the main challenges to implement it for crops with high volume of biomass, such as maize, sugarcane, and wheat. Molijn et al. (2018) proposed a methodology for estimating sugarcane biomass from soil reference data and orbital imagery, associating biometric measurements, to monitor the dynamics of sugarcane production. Canata et al. (2019) developed a measurement system based on MTLS as a spatial assessment of crop canopy height in the pre-harvest period of sugarcane. To advance on the understanding and use of 3D sensing data in sugarcane, the objective of this study is to demonstrate the potential of LiDAR and RGB images for mapping the spatial variability of sugarcane fields and to explore the relationship among crop height variation and sugarcane yield at the field level. A validation of the measurements indicated by the ALS platform also is described.

## 3.2. Material and Methods

### 3.2.1. Field characteristics

The study was conducted in a commercial area of 200 ha of Argisol located around Botucatu municipality, São Paulo, Brazil (22°41'42.8" S; 48°16'54.0" W; elevation 480 m) for 2018/2019 and 2019/2020 sugarcane growing seasons. The climate in the study region is mesothermal, Cwa - humid subtropical (Köppen climate classification), which includes drought in the winter from June to September and wet conditions from November to April. The average annual rainfall is about 1433 mm (Figure 1). The air relative humidity is 71% with an annual average temperature of 23ºC (CUNHA et al., 2009). The sugarcane variety SP83-2847 was planted with a row spacing of 1.50 m ($4^{th}$ ratoon). All fields were mechanically green harvested in late season (wet time of the year - November).

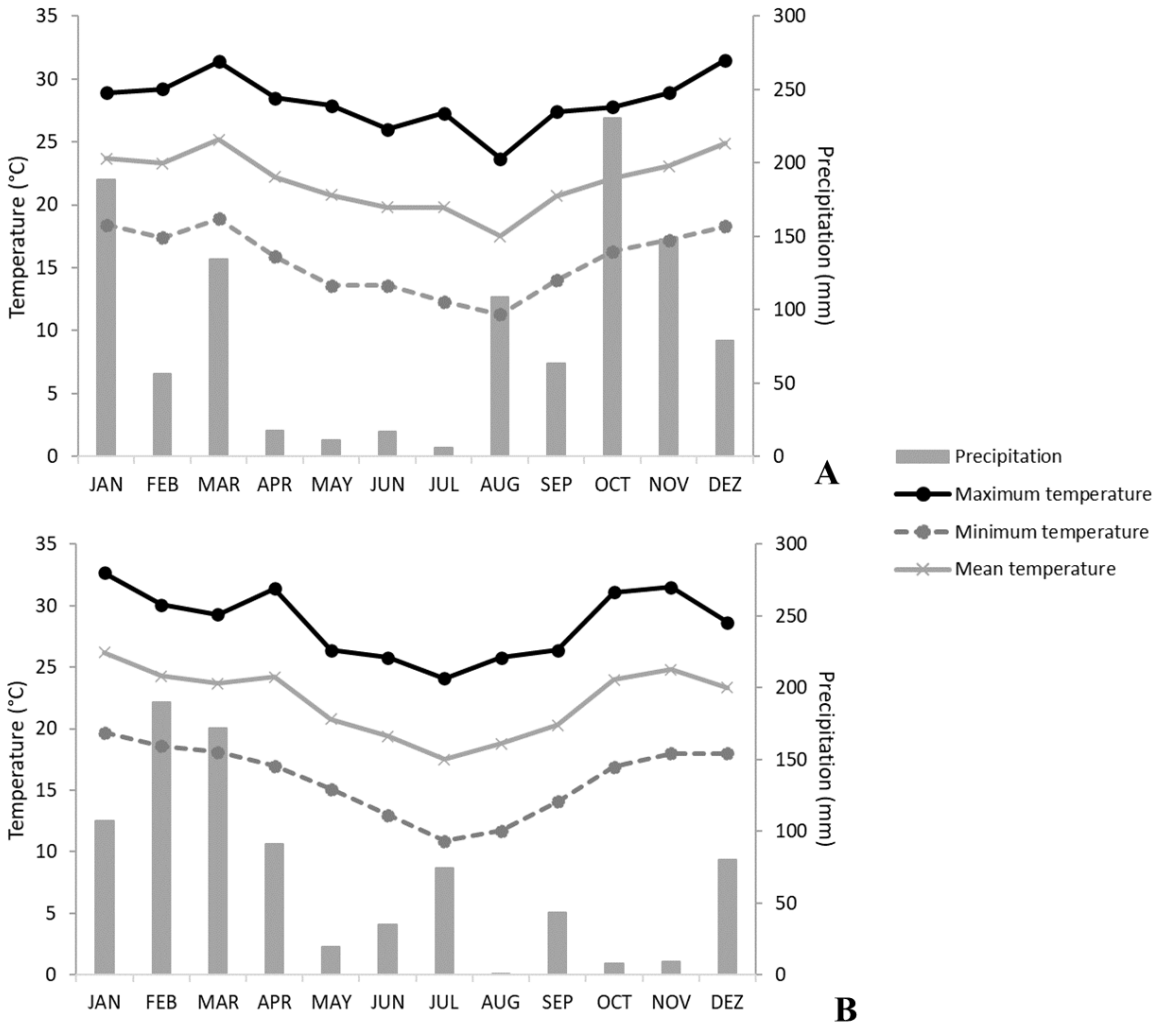


**Figure 1.** Mean annual precipitation and monthly temperature of the study site for 2018/2019 (A); 2019/2020 sugarcane growing seasons (B). Source: CIIAGRO (2021)

Manual measurements were collected in the 2018/2019 season across three selected fields (Field 1 – 18.07 ha; Field 2 – 12.67 ha; Field 3 – 5.31 ha) as the harvesting front advanced. 89 validation points were allocated on the study site (Figure 2A) and the geographical coordinates for each one was recorded using a GNSS receiver with satellite differential correction – TerraStar C (Novatel Inc., Canada) (Figure 2B). The sugarcane stalk and the crop canopy height (the highest leaf of the plant) were measured and georeferenced using a ruler (Figure 2C), according to the methodology described by Portz et al. (2012).

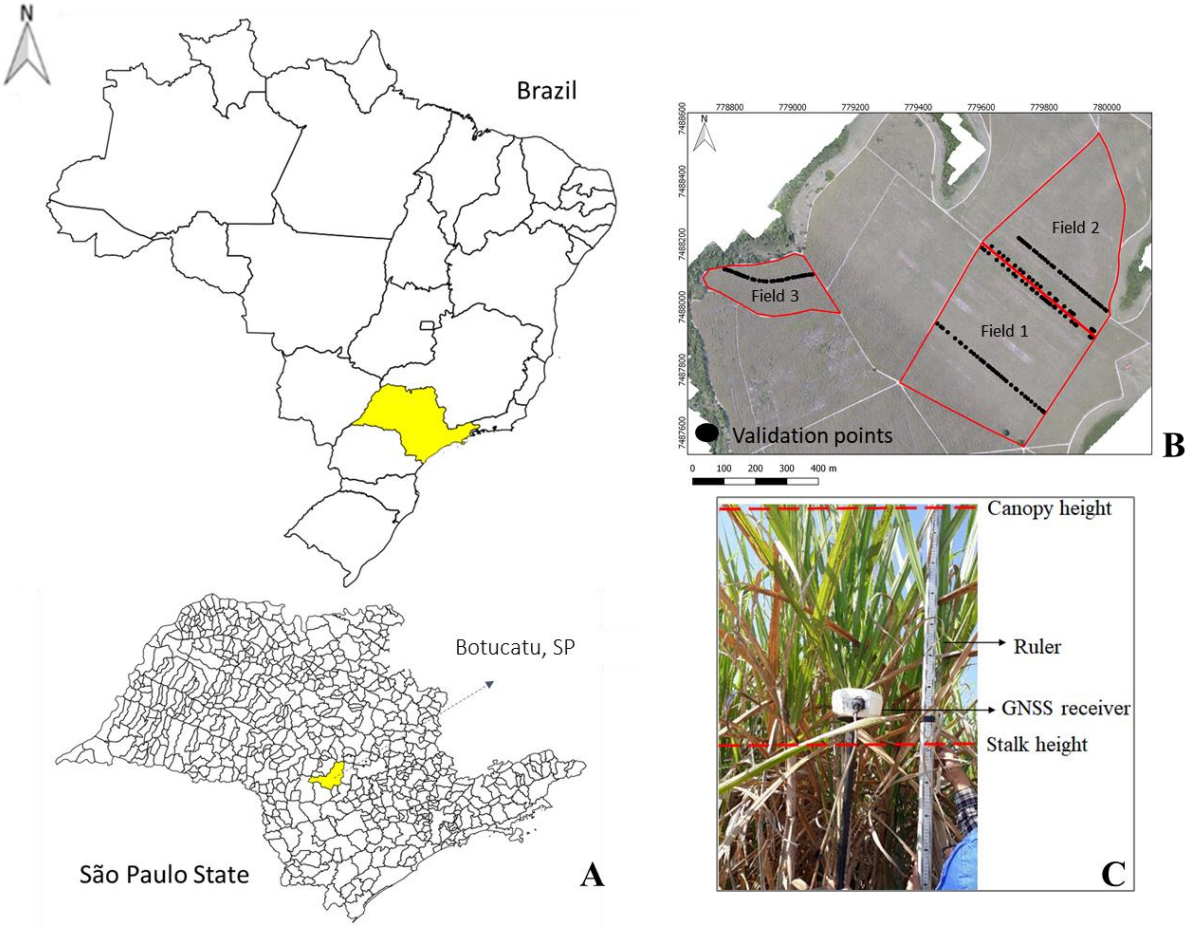


**Figure 2.** Sugarcane study site (A); validation points over the selected fields (B); manual measurements of plant height (C)

### 3.2.2. Data acquisition and processing

The embedded and integrated equipment were used: a laser sensor ALTM Gemini 56100 (Optech) for 2018/2019 sugarcane growing season, and Orion H300 (Optech) for the subsequent season; an inertial measurement unit (IMU), and a Global Navigation Satellite System (GNSS) receiver mounted on a helicopter. The sensors were mounted at a nadir angle with scans over the sugarcane fields. An IMU was integrated to correct the positioning error on the dataset according to the platform oscillation in the transversal (roll), lateral (pitch) and longitudinal (yaw). The data collected by the sensors were stored in a specific datalogger to ALS applications. The average flying altitude was 500 m above ground level.

The data acquisition occurred on two occasions, within each collection time, and manual measurements were taken after ALS data acquisition for the 2018/2019 sugarcane growing season. The first data acquisition (first flight) was carried out 10 days before harvesting for both seasons, and the second flight 10 days after harvesting with the same equipment. The purpose of the data acquisition after harvesting was to generate the DTM of reference. The main specifications for both data acquisition by ALS are shown in Table 1 and Figure 3A. A serial communication synchronized the data readings between the laser sensor and the GNSS receiver to reduce the source of error caused by the platform trajectory. Thus, the geographical coordinates were assigned to each point impacted by the light beam (Figure 3B) in the same reference system (DEL-MORAL-MARTINEZ et al., 2015).

**Table 1.** Specifications of the data acquisition from airborne laser scanning

| Parameters | ALTM Gemini 56100 | Orion H300 |
|---|---|---|
| Frequency | 70 kHz | 250 kHz |
| Number of returns | 4 | 4 |
| Laser wavelength | 1,064 nm | 1,064 nm |
| Scan angle | ±20º | ±20º |
| Vertical accuracy[1] | 0.20 m | 0.03-0.10 m |
| Footprint | 0.33 m | 0.33 m |

[1]According to the manufacturer

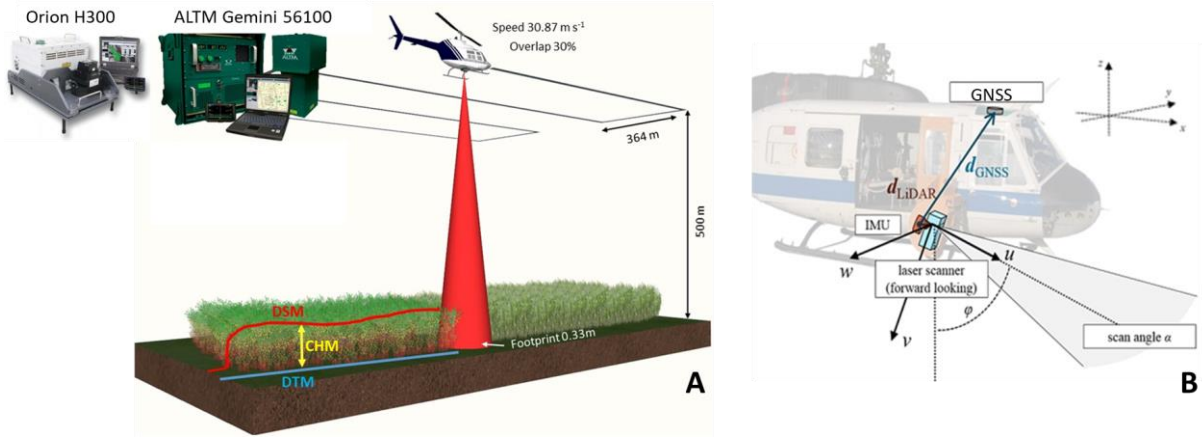


**Figure 3.** Overview of the data acquisition from airborne laser scanning (A), obtaining Cartesian coordinates – adapted from Hebel et al. (2013)

The Cartesian coordinates were calculated according to the Equations 1, 2, and 3 in R statistical software (R CORE TEAM, 2017) considering the average flying altitude above ground level (H), the distance indicated by the laser sensor ($d_{ij}$), and its scan angle ($\alpha_{ij}$).

$$X = d_{ij} \text{ sen } (\alpha_{ij}) \quad (1)$$

$$Y = y_{ij} \quad (2)$$

$$Z = H - d_{ij} \cos (\alpha_{ij}) \quad (3)$$

where X: Cartesian coordinate of the x-axis at the point ij (m); ij: registration of the points position reached by the light beam; $d_{ij}$: distance between the laser sensor and the object (m); $\alpha_{ij}$: scan angle of the laser sensor (°); Y: Cartesian coordinate of the y-axis at the point ij (m); $y_{ij}$: scanning direction by laser sensor; Z: Cartesian coordinate of the z-axis at the point ij (m); H: average flying altitude above ground level (m).

The planimetric coordinates (X and Y) and the ellipsoid height values (Z) were computed for all laser sensor data and georeferenced using the post-processing method. The original point clouds were stored in LAS

format and projected on WGS 84 (World Geodetic System 1984)/UTM zone 22S coordinate system. The preliminary analysis of the point clouds was done using CloudCompare 2.10.2 software (Girardeau-Montaut). All data allocated outside the field boundary and outliers, distance points out of range of maximum and minimum elevation values of the sugarcane fields, were manually excluded from point clouds.

The function *grid_metrics* of the lidR package (ROUSSEL et al., 2019) from R statistical software (R CORE TEAM, 2017) was used to create the DSM. This package is an interface for data manipulation and visualization of airborne LiDAR data. The *grid_metrics* function is an area-based approach. In the first data acquisition, the 3D data was used to calculate the DSM, which is the absolute height of sugarcane plants. The data processing steps to generate the DSM were i) to consider the maximum elevation parameter of the filtered point cloud generated before harvesting; ii) to rasterize the data with a pixel resolution of 0.50 m, due to the row spacing of sugarcane plants, and the indication of Mielcarek et al. (2020); iii) computing the metrics for each cell. The same function was used to generate the percentiles (P50$^{th}$; from P90$^{th}$ to P99$^{th}$) that are common LiDAR-derived metrics calculated in studies of 3D data (GORGENS et al., 2017; LI et al., 2020). 11 metrics were considered to support the identification of spatial variability in sugarcane fields.

The DTM can be obtained from a scan with bare soil, while the crop surface model is calculated from the top-most points of the point cloud, using a selection based on the top percentile (HÄMMERLE and HÖFLE, 2014; FRIEDLI et al., 2016). The DTM for both point clouds (before and after harvesting) were generated using the *grid_terrain* function of the lidR package (ROUSSEL et al., 2019) from R statistical software (R CORE TEAM, 2017) as demonstrated in Figure 4. Other algorithms of the same computational package were tested to generate DTM using the *lasground* function, which implements a progressive morphological filter for segmentation of ground points, and *lasfilter* function that returns the points from the dataset considering the last returns.

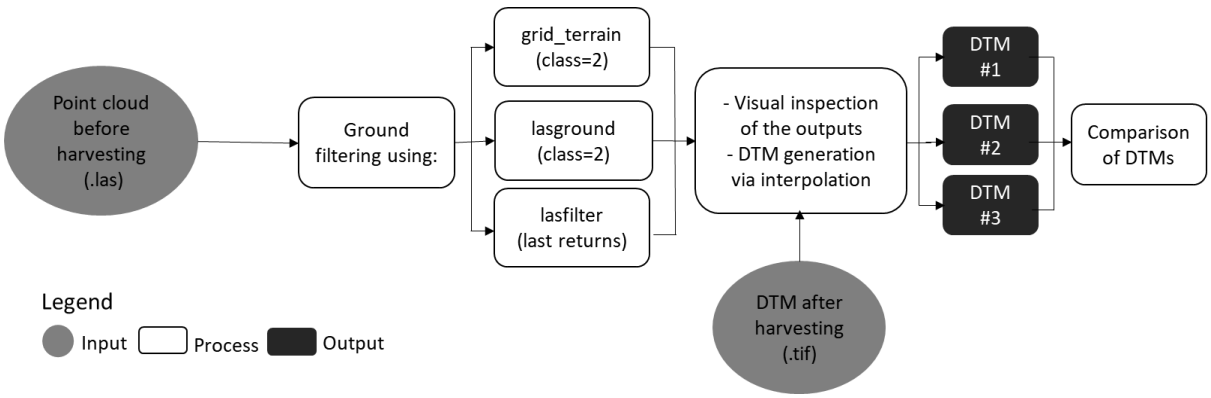


**Figure 4.** Workflow of generating digital terrain model based on LiDAR data

Only the points from ALS classified as ground (classification=2 - LAS file format) were interpolated using triangulated irregular network (TIN), Delaunay triangulation method, with the same pixel resolution of the DSM (0.50 m x 0.50 m). The contour lines of the fields were obtained from LiDAR data processing using the raster of DTM considering an elevation interval of 5.0 m between the contour lines in QGIS 2.18.26 software (QGIS DEVELOPMENT TEAM, 2018). The relationship among the elevation values from both DTMs was evaluated by calculating the RMSE according to Equation 4.

$$RMSE = \sqrt{\frac{1}{n}\sum_{i=1}^{n}(z_i - z)^2} \quad (4)$$

where n: number of the sample, $z_i$: predicted height (m), and z: observed height (m).

The resulting DTM maps from each algorithm were compared using fuzzy similarity index in Map Comparison Kit 3.2.3 software (Research Institute for Knowledge Systems, Netherlands). This analysis tool is considered a map-comparison technique that allows to measure the similarity at each pixel. For this study, the fuzzy numerical cell-by-cell comparison algorithm was used with the DTM generated from after harvesting as reference. The calculation is based on the fuzzy representation of a cell that depends on the cell itself and the cells in its neighborhood. The extent to which the local cells influence the fuzzy representation, where the value 1 represents total similarity and 0 total dissimilarity (VISSER and NIJS, 2006).

Aerial images were obtained 15 days before sugarcane harvesting for the 2018/2019 sugarcane growing season to characterize the crop canopy. The flight plan of RPA was defined using DroneDeploy® flight app (San Francisco, CA) with 32 Ground Control Points (GCP) distributed across the study site (Figure 5A). All GCP were georeferenced using a GNSS receiver (GPS L1/L2 + Glonass) with differential correction (Novatel Inc., Canada) on ground level (Figure 5B). The accuracy of the GNSS receiver is described by Maldaner et al. (2021). All RGB images were captured with a nadir view perspective. The equipment Advanced Phantom 4 (SZ DJI Technology Co., Ltd., Shenzhen, Guangdong, China) and an on-board RGB camera (DJI - FC6310A) were used with the specifications listed in Table 2. The flight mission was performed at a flight altitude of 100 m, speed of 10 m $s^{-1}$, overlap and sidelap of 70%. The Ground Sample Distance (GSD) of the imagery data was 0.03 m $pixel^{-1}$. The flight performed before harvesting generated 2,257 images covering all study site locations. All images were stored at the internal SD card of the platform, and manually transferred to the computer after the data acquisition. The orthomosaic was generated using Agisoft PhotoScan 1.2.0 software (Agisoft LLC, St. Petersburg, Russia) considering the parameters listed in Table 3. The point cloud (n = 8,269,130 points) was exported into LAS file format and projected in WGS 84/UTM zone 22S.

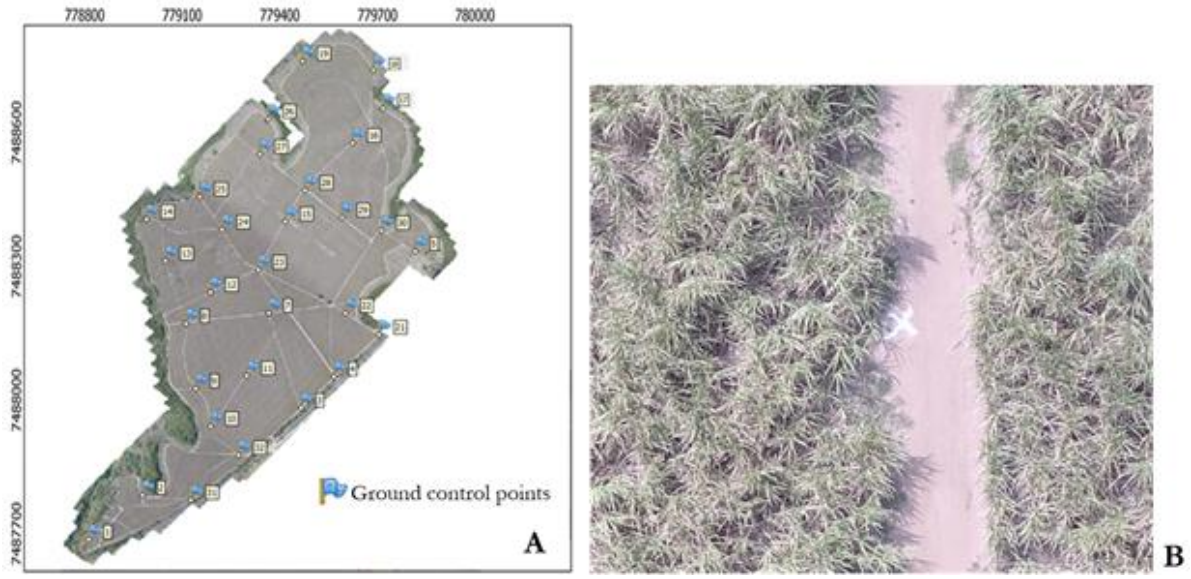


**Figure 5.** Ground control points allocated over the fields (A); before harvesting (B)

**Table 2.** Specifications of the on-board RGB camera

| Parameters | Values |
|---|---|
| Image sensor | CMOS[1] |
| Platform weight | 1.38 kg |
| ISO | 100 |
| Sensor resolution (pixels) | 4864 x 3648 pixels |
| Image density | 72 dpi |
| Intensity | 24 bits |
| Exposure time | 1/320 s |
| Focal length | 24 mm |
| Output image format | TIF |

[1]Complementary Metal Oxide Semiconductor

**Table 3.** Parameters of data processing from aerial images

| Steps | Parameters | Settings |
|---|---|---|
| Alignment of images | Accuracy | High |
| | Adaptive model | Yes |
| Point cloud | Quality | Highest |
| | Filtering | Medium |
| Texture | Mapping mode | Adaptative |
| | Mesh mode | Orthomosaic |
| Orthomosaic | Source of data | Point cloud |
| | Size | 2048 |

These parameters were chosen according to the literature regarding the data processing of aerial imagery (HOLMAN et al., 2016; MIELCAREK et al., 2020) and considered ideal for the field conditions. The orthomosaic

was analyzed using Structure from Motion (SfM) technique by the following steps: i) to align all selected images; ii) to georeference each ground control point with the coordinates from GNSS receiver; iii) to build a dense point cloud; iv) to create the orthomosaic at the same resolution of the digital models (0.50 m x 0.50 m). The use of SfM allows that the camera parameters and the positions are approximated from overlapping images. The creation of the mesh, in which the calculation algorithm must be chosen, the *arbitrary* type of surface was selected, according to the recommendations (HARKEL et al., 2020; MARÍN-BUZÓN et al., 2020). The main steps for processing aerial images from RPA are indicated in Figure 6. Visual analysis of the orthomosaic was performed to characterize the spatial variability of the crop canopy height.

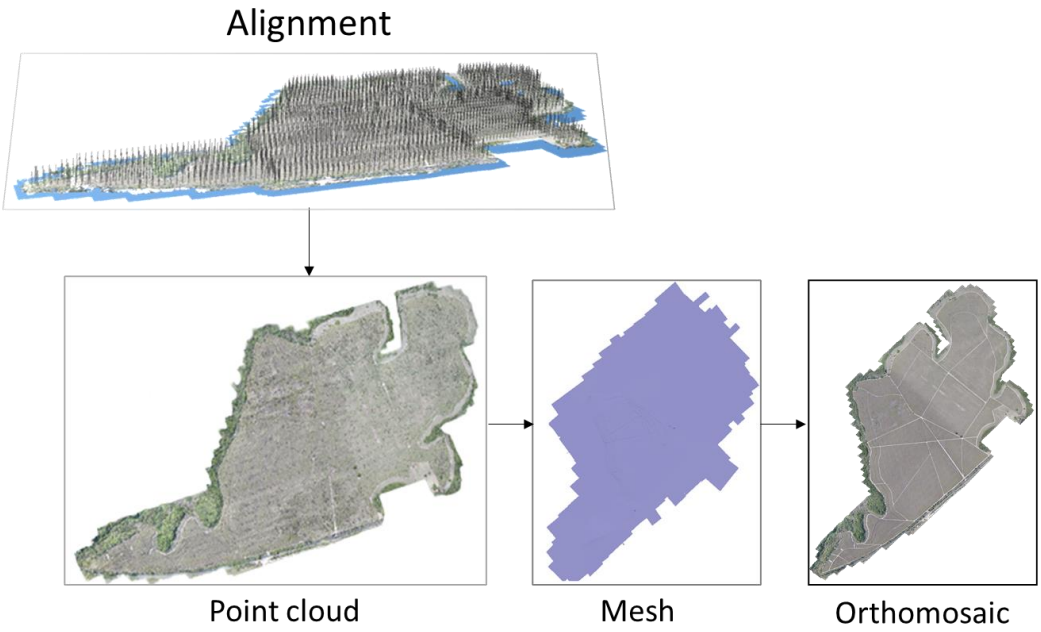


**Figure 6.** Workflow for the orthomosaic generation of the study site location based on aerial images

### 3.2.3. Spatial variability of crop canopy height

Determining the crop canopy height with LiDAR data requires the ground level estimation and subtracting it from the absolute height of the elevation (Equation 5, LOUDERMILK et al., 2009; JIMENEZ-BERNI et al., 2018). The CHM and the percentiles from point cloud were converted to vector layers on QGIS 2.18.26 (QGIS DEVELOPMENT TEAM, 2018) and compared with the georeferenced manual measurements.

$$CHM = DSM - DTM \quad (5)$$

where CHM: canopy height model (m); DSM: digital surface model (m); DTM: digital terrain model (m).

The relationship among LiDAR data and manual measurements is commonly used to verify the relative error of measuring plant height (HARKEL et al., 2020; BORRA-SERRANO et al., 2019), considering it an indicator

of the yield and highly influenced by soil, temperature, and light intensity (CHOLULA et al., 2020). The main steps and the computational tools for processing 3D sensing data from ALS are shown in Figure 7.

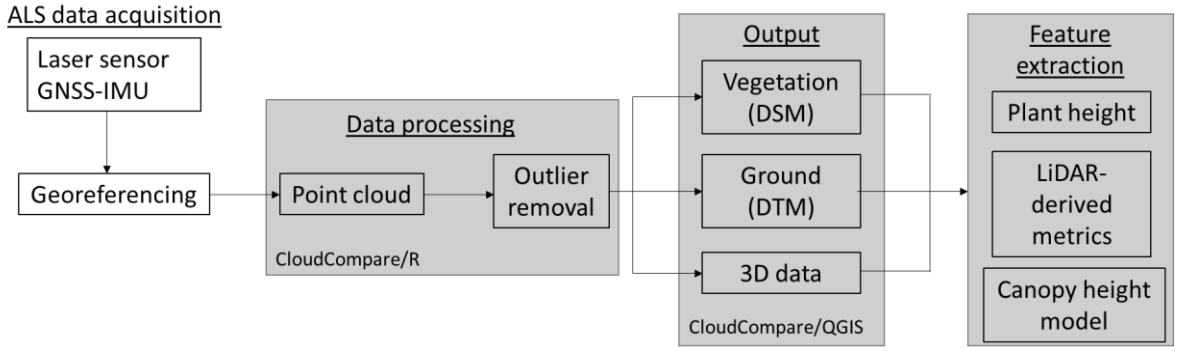


**Figure 7.** Workflow from ALS data acquisition to feature extraction based on digital models

The spatial variability of the sugarcane fields was determined according to the descriptive statistics of the dataset. The coefficient of variation (CV – Equation 6) was considered a useful criterion for PA concept to perform an initial analysis to identify the within field regions with a distinct potential of production (MOLIN et al., 2015).

$$CV = 100 \times \frac{\sigma}{\mu} \quad (6)$$

where CV: coefficient of variation (%); $\sigma$: standard deviation (m or Mg ha$^{-1}$); $\mu$: average value (m or Mg ha$^{-1}$).

An internal buffer of 5 m was applied to each field boundary for both maps using QGIS 2.18.26 (QGIS DEVELOPMENT TEAM, 2018). The spatial variability of the sugarcane fields also were identified based on visual analysis of the yield maps and CHM using QGIS 2.18.26 (QGIS DEVELOPMENT TEAM, 2018). The accuracy of the crop height measurements was assessed by calculating the RMSE between the observed and the predicted values of stalk and canopy heights. In addition, the linear regression was used to describe the relationship among these variables, and between CHM and yield map. The coefficient of determination ($R^2$) was calculated as a measure of the goodness of fit from the prediction model. The linear regression also was used to develop equations that relate the LiDAR data with the manual measurements, and with sugarcane yield (MIELCAREK et al., 2018). The pixel-based correlation was carried out among the manual measurements, yield map and CHM using Pearson's correlation coefficient (r). The built-in function *summary* of R statistical software (R CORE TEAM, 2017) was used to find the p-value of the results.

### 3.2.4. Sugarcane yield measurement

The sugarcane yield maps used as reference for comparing to digital models were generated for both sugarcane growing seasons by an on-board commercial sensor-system (Solinftec, Araçatuba, São Paulo, Brazil) that measures the difference in hydraulic pressure of the harvester chopper (Figure 8A) calibrated to the real total yield. A Global Navigation Satellite System (GNSS) receiver with Real-Time Kinematic (RTK) differential correction signal (GPS L1/L2 + Glonass) was installed on the harvesters for georeferencing the data every five seconds (0.20 Hz). The base station was fixed in a georeferenced point at the sugar mill, which is commonly used for other agricultural operations. Two harvesters generated the data for each season with an average speed of 1.60 m $s^{-1}$. The machine cuts each row at a time following an auto-steering file previously available from mechanical planting.

The data from harvesters were transferred to the local server of the sugar mill via telemetry and converted to yield values according to the linear regression ($R^2$ = 0.92, RMSE = 0.30 Mg $ha^{-1}$), as demonstrated in Figure 8B. The original data were converted to sugarcane yield based on the weight distribution of the haulage and spatially filtered using MapFilter 2.0 software according to the methodology described by Maldaner and Molin (2020). The removal of a significant number of points is expected due to the associated error on the yield data due to the sugarcane flow stabilization time and elevator time (MALDANER and MOLIN, 2020; VEGA et al., 2019). Although filtering yield data is a common practice in PA for any crop, issues related with high spatial density and data noise make the adequate filtering of yield monitor data especially important for sugarcane, with a significant amount of raw data being possibly deleted as a result. The input parameters were general filtering of 40%; local filtering of 10%, and spatial dependence of 20 m. The semivariogram was generated using Vesper 1.6 software (MINASNY et al., 2006) with the input parameters: 30 lags, 50% lag tolerance, and 200 m of maximum distance, and 200 iterations. These parameters were considered the best adjustment for semivariogram calculation based on exponential model (lower RMSE). The interpolation of the yield data was carried out in the same software using ordinary kriging method with the same spatial resolution of the digital models (0.50 m x 0.50 m). The validation points from manual measurements and from CHM were overlapped to the raster layer of the yield data to provide the spatial correlation analysis using the plugin *Point Sampling Tool* of QGIS 2.18.26 (QGIS DEVELOPMENT TEAM, 2018).

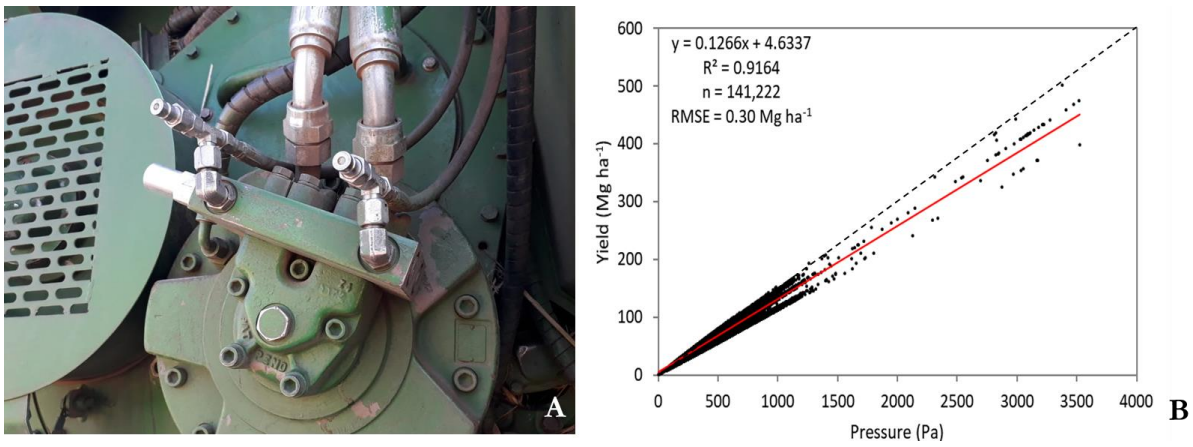


**Figure 8.** Chopper hydraulic pressure sensor installed on sugarcane harvester (A); relationship among the chopper hydraulic pressure and yield data (B); dashed line represents the 1:1 line and the solid line represents the fitted linear function

A local validation was carried out in commercial areas of sugarcane (186 ha) located in Quatá municipality, São Paulo, Brazil to assess the accuracy of the yield maps generated by the commercial sensor-system, previously described. The sugarcane variety was RB98769 of the first ratoon with double row spacing (1.50 m x 0.90 m). Four repetitions for each harvester were done using a scale (Líder, LD 2052, Araçatuba, São Paulo, Brazil) installed at the field (Figure 9A, Figure 9C). The load cells (Exacta Balanças - EX5000, Rancharia, São Paulo, Brazil) and the GNSS receiver with C/A signal were installed on in-field wagon, total capacity of 8 Mg, to provide the georeferenced sugarcane weight by a frequency of 1 Hz (Figure 9B). The resolution of the load cells was 10 kg. The original data from load cells and from sugarcane harvesters were removed at the beginning and at the end of each repetition. Also, the time delay of the synchronization between the harvester and the in-field wagon was removed. The yield data were transformed into weight considering the displacement of the harvester, and its cut width of 2.40 m. The interval time of 7 s (offset) was considered between the plant cutting and the chopper pressure signal of the harvester. The data from the in-field wagon was manually transferred via USB to the computer, and the yield data from harvesters were transferred to the server of the service provider via telemetry.


**Figure 9.** Scale installed at the field to measure the weight of in-field wagon (A), interface of the load cells to measure the weight of sugarcane in-field wagon over the fields (B), and its electronic component (C)

## 3.3. Results and discussion

### 3.3.1. Point cloud and digital models

The descriptive statistics, considering the preliminary data filtering, for both point clouds from ALS (I and II), and point cloud from RGB images (III) is shown in Table 4. 3D sensing data demonstrates the common

characteristic of high-resolution data for the point clouds generated before and after harvesting for the selected fields. An average point density of 12 points $m^{-2}$ was obtained for LiDAR data and 4 points $m^{-2}$ for RGB images for 2018/2019 crop season and about 50 points $m^{-2}$ considering LiDAR data for the subsequent season.

**Table 4.** Descriptive statistics of the point clouds considering the entire experimental area

| Season | Point clouds | Number of samples | Min | Max | Mean | SD | CV (%) |
|---|---|---|---|---|---|---|---|
| | | | | elevation (m) | | | |
| 2018/2019 | I | 23,656,655 | 409.32 | 506.12 | 474.88 | 4.62 | 0.97 |
| | II | 21,451,475 | 409.09 | 482.27 | 454.29 | 4.20 | 0.88 |
| | III | 8,269,130 | 409.93 | 495.68 | 474.19 | 6.35 | 1.34 |
| 2019/2020 | I | 133,109,189 | 452.11 | 539.45 | 496.10 | 4.11 | 0.83 |

LiDAR - I: before harvesting; II: after harvesting; RGB - III: before harvesting; n: number of samples; Min: minimum; Max: maximum; SD: standard deviation; CV: coefficient of variation

The point cloud generated before harvesting is shown in Figure 10A and after harvesting on Figure 10B for 2018/2019 crop season. Each point represents the positioning (X, Y) and the elevation (Z) in the same coordinate system. 35% of the total points were classified as ground for the first data acquisition, which impacts on the performance of the algorithms to filter the ground points. The point cloud from after harvesting data acquisition was used to generate the DTM of reference. The point cloud generated before harvesting from RGB images is shown in Figure 10C. Figure 10D represents the point cloud from the 2019/2020 crop season before harvesting.

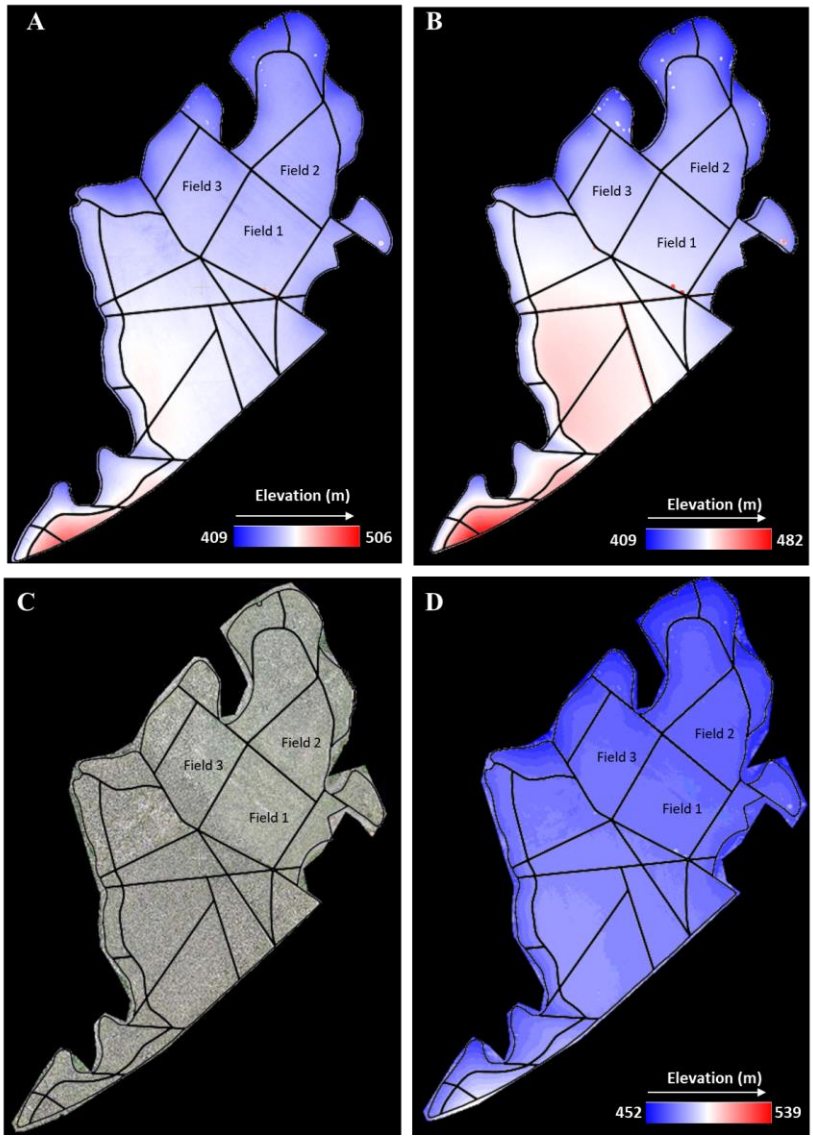


**Figure 10.** Point clouds generated from LiDAR data before harvesting (A); after harvesting (B); from RGB images before harvesting of the 2018/2019 season (C); point cloud generated from LiDAR data before harvesting of the 2019/2020 season (D)

As a representation of 3D modeling of the crop canopy, the point cloud generated before harvesting for the selected field (Field 1) is shown in Figure 11A in order to provide a visual assessment of the crop height variation at the field level. The 2D and 3D representations of the point cloud section also are demonstrated in Figure 11B and Figure 11C, respectively. It demonstrates the capacity of the settings adopted for the data acquisition from ALS to characterize the structural complexity of the crop, where the first returns represent the DSM, and the last returns represent the DTM.

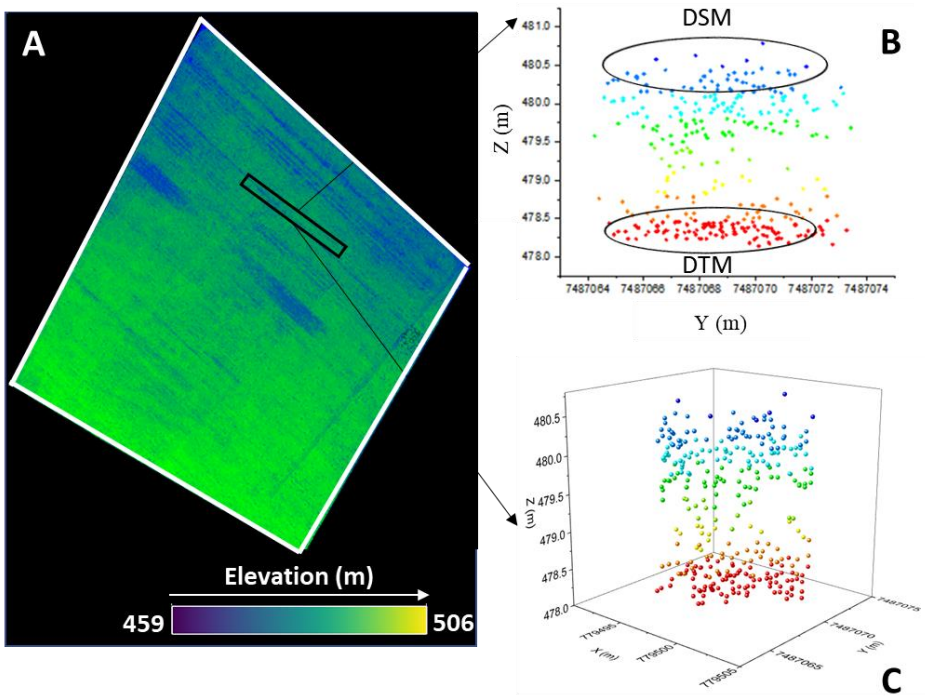


**Figure 11.** Point cloud generated before harvesting (A); a point cloud section: 2D (B); 3D for 2018/2019 season (C)

The overlap from ALS during the data acquisition influenced digital models due to the density points of the laser sensor, thus a normalization of the elevation values was performed. Crop mapping using ALS provides a more detailed characterization of the plant profile due to the multiple pulses emitted by the laser sensor. One of the main limitations of RGB images is the incapacity to detect the ground level of the field due to the high-density of the crop canopy in the pre-harvest period. That is the main reason for adopting LiDAR technology as an alternative method to detect crop canopy variation of sugarcane fields. These results encourage other applications of 3D modeling since previous researches focused on smaller fields. It is considered that the methodology of canopy height measuring based on aerial platforms is more effective than the traditional manual measurements. The proposed methodology applied to convert the raw data from ALS into raster files for input on GIS software was robust to generate canopy height maps. The developed script in R software used approximately 60 minutes to complete all data processing steps sequentially (from point cloud to maps visualization). For data processing of multiple fields this approach should be reviewed. The point density achieved from LiDAR data was sufficient to generate the DTM for the first data acquisition (Figure 12A), which had a similar distribution of the elevation values from DTM after harvesting (Figure 12B). The relationship among both DTM for Field 1 is shown in Figure 12C, demonstrating that the linear regression had an $R^2$ of 0.99 and an RMSE of 0.13 m.

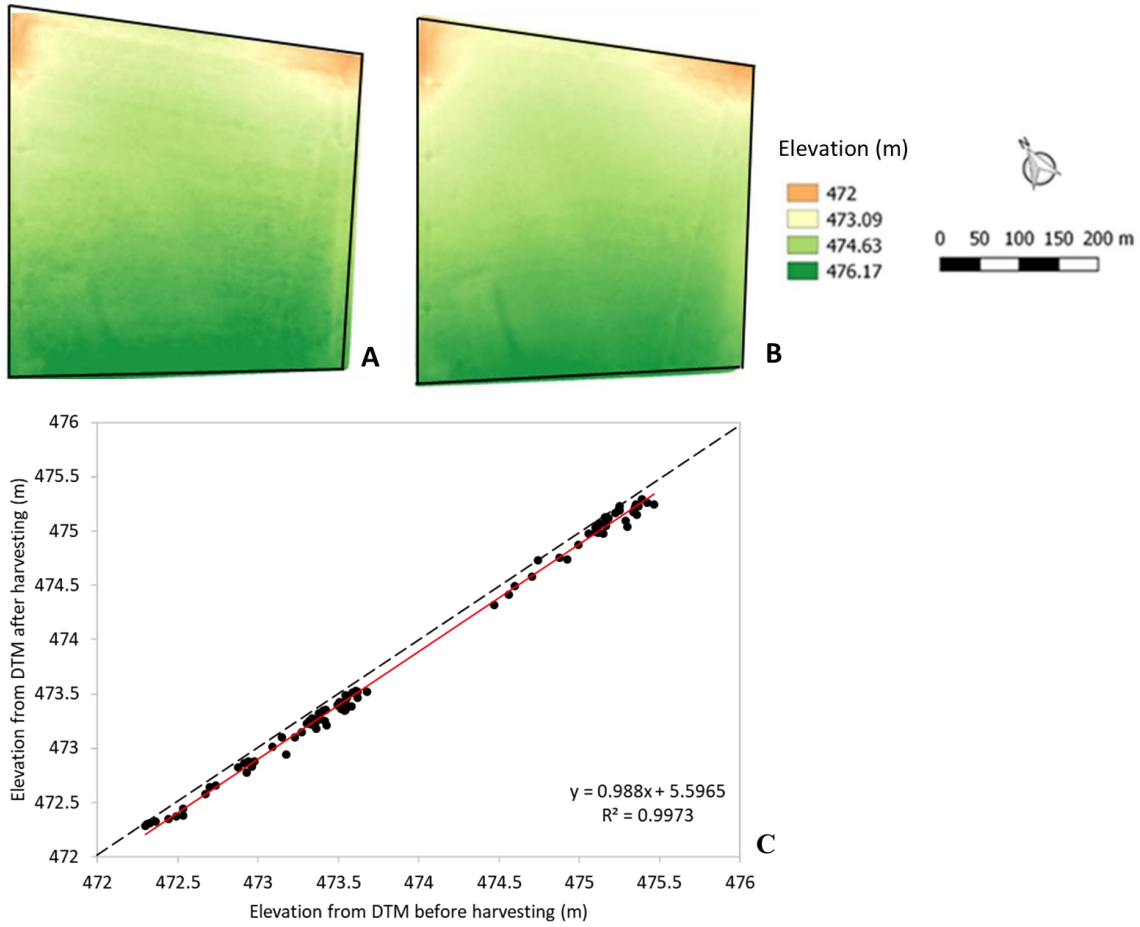


**Figure 12.** The digital terrain models of Field 1 before harvesting (A); after harvesting (B); relationship among both digital terrain models (C); the dashed line represents the 1:1 line and the solid line represents the fitted linear function

The settings adopted for the data acquisition using the ALS enabled the detection of the ground points on pre-harvest conditions (high-density distribution of the plants and overlapping of the leaves). This result was obtained for the specific field conditions found in this study and other field conditions should be investigated to verify if a single flight is sufficient to generate the DTM. Hämmerle and Höfle (2014) reported the effect of reduced point density of laser sensor data on generating digital models of the fields for grain crop. They found that the accurate measurement of the crop height did not always improve with increasing on point density. Other studies also related the effect of point density reduction on digital models as a parameter to decide about the settings of the data acquisition (SILVA et al., 2017; LUO et al., 2016). The comparison between the methods for generating DTM considering the Fuzzy similarity index is presented in Figure 13 for after harvesting – *grid_terrain* function (Figure 13A); lasfilter algorithm (Figure 13B); lasground algorithm (Figure 13C). The average value of similarity between the data from before and after harvesting was 1.0 for *grid_terrain* function; 0.79 for lasfilter algorithm; 0.90 for lasfilter algorithm. So, *grid_terrain* function is the most indicated filtering method to generate DTM from LiDAR data for similar field conditions found in this study.

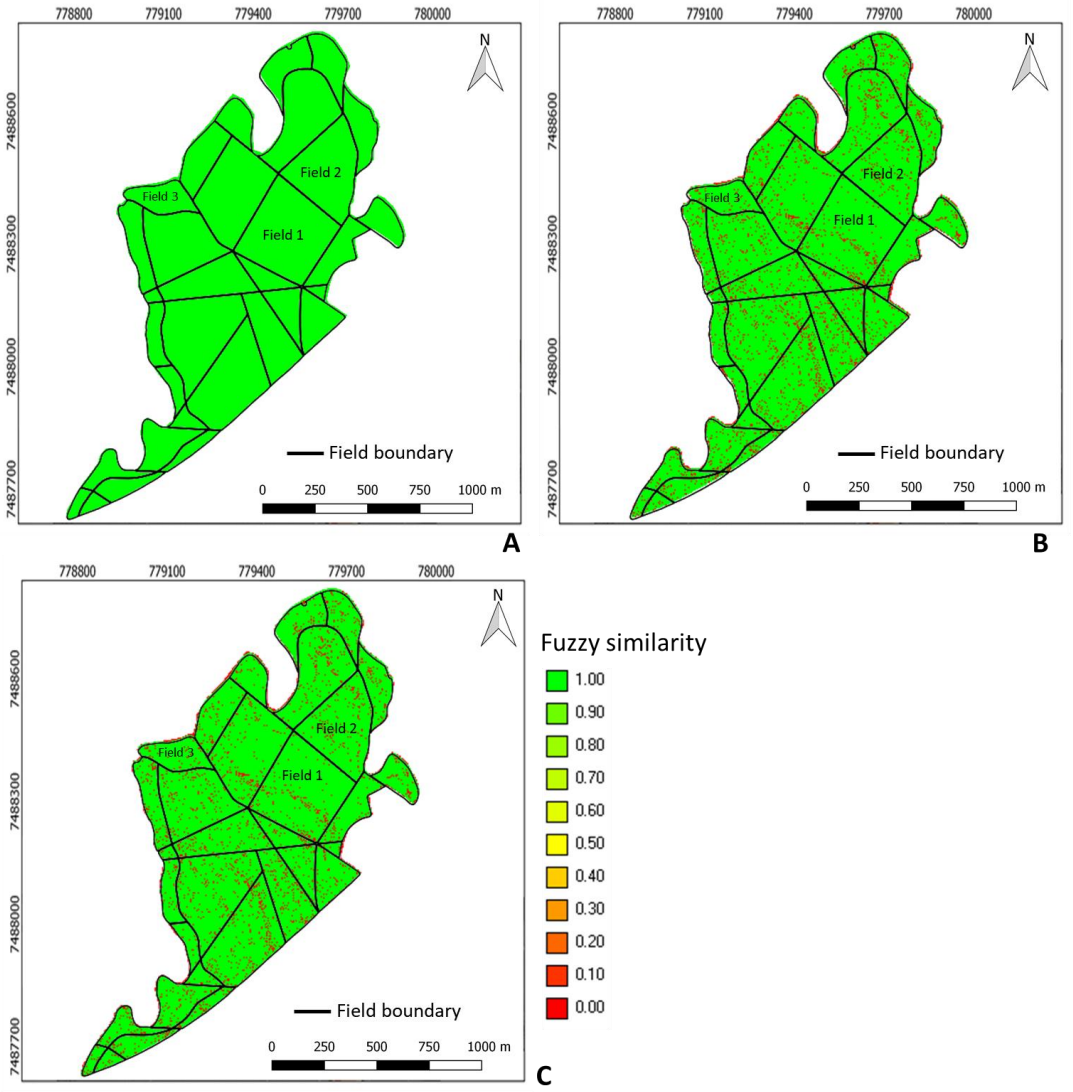


**Figure 13.** Fuzzy similarity of the digital terrain models for each function: grid_terrain (A); lasfilter (B); lasground (C)

The digital models of surface (Figures 14A) of terrain (Figure 14B) for 2018/2019 crop season, and the contour lines extracted (Figure 14C) from LiDAR data processing are shown as a characterization of the elevation values of the fields. These information are usually applied to support the systematization of the terrain (NASCIMENTO et al., 2017) with greater accuracy than traditional altimetric methods (CORSEUIL and ROBAINA, 2003). The orthomosaic of the study site location is shown in Figure 14D as a representation of an image-based mapping system for visual analysis of the spatial variability of sugarcane fields. The digital model of surface for the 2018/2019 crop season is demonstrated in Figure 14E. Brocks and Bareth (2018) used digital models as a non-destructive method for monitoring the vegetative development of barley and for predicting dry matter biomass with high accuracy ($R^2$=0.79). Schirrmann et al. (2016) elaborated crop surface models for monitoring agronomic parameters of winter wheat using RGB images from RPA platform, which enabled them to detect the spatial variations in early crop senescence and to model biophysical wheat parameters.

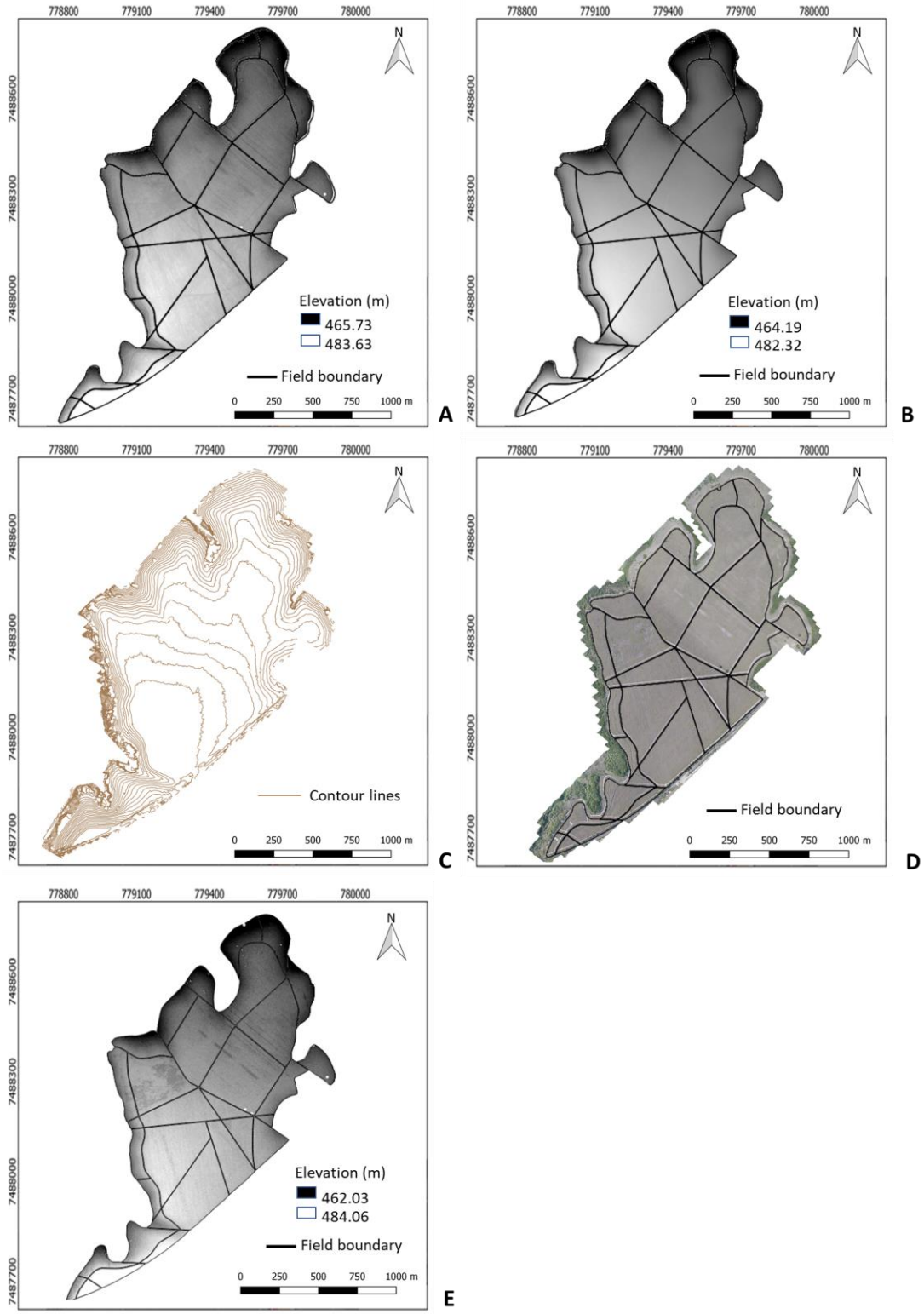


**Figure 14.** Digital models of surface (A); of terrain (B); contour lines (C); orthomosaic from the 2018/2019 season (D); digital model of surface from the 2019/2020 crop season (E)

### 3.3.2. Mapping of crop canopy height

The descriptive statistics of the validation points (Table 5), considering all fields, showed that the minimum sugarcane stalk height was 1.20 m and 2.44 m for crop canopy height. The maximum values were of 2.90 m and 4.30 m, respectively. The CV values indicated that there was a greater variability of the stalk height (19%) in relation to the crop canopy height (9%). Considering all fields, the RMSE values between the manual measurements and LiDAR data ranged from 0.47 m to 0.62 m for stalk height, and from 0.70 m to 0.81 m for canopy height. This error for estimating plant height is associated with the influence of several factors, such as the lodging plants effect that could compose a source of error for using high-resolution data. This condition is a common characteristic of pre-harvest conditions, mainly due to the environmental factors (CHOLULA et al., 2020; CANATA et al., 2019), and it was observed during the field measurements of the study. Also, the footprint diameter and the flight altitude of the data acquisition have a relevant impact on results. Considering the pre-harvest condition, the pulse spacing on the ground was shorter than the adopted footprint diameter, demonstrating that another approach using fine-tuning parameters of data acquisition should be considered in future studies for obtaining a more accurate method (lower RMSE) to measure sugarcane stalk height.

**Table 5.** Descriptive statistics of the validation points for each field

| | Field | n | Minimum | Maximum | Mean | Median | SD | RMSE | CV (%) |
|---|---|---|---|---|---|---|---|---|---|
| **Stalk height (m)** | 1 | 32 | 1.34 | 2.52 | 1.87 | 1.86 | 0.26 | 0.62 | 13.90 |
| | 2 | 31 | 1.20 | 2.90 | 2.07 | 2.09 | 0.41 | 0.51 | 19.80 |
| | 3 | 26 | 1.57 | 2.71 | 2.07 | 2.06 | 0.27 | 0.47 | 13.04 |
| **Canopy height (m)** | 1 | 32 | 2.59 | 4.10 | 3.22 | 3.12 | 0.34 | 0.81 | 10.56 |
| | 2 | 31 | 2.44 | 4.30 | 3.70 | 3.10 | 0.41 | 0.70 | 11.08 |
| | 3 | 26 | 2.61 | 3.90 | 3.17 | 3.20 | 0.29 | 0.72 | 9.14 |
| **CHM (m)** | 1 | 32 | 1.80 | 3.09 | 2.45 | 2.44 | 0.28 | - | 11.43 |
| | 2 | 31 | 1.57 | 3.23 | 2.47 | 2.57 | 0.37 | - | 14.98 |
| | 3 | 26 | 1.44 | 3.03 | 2.48 | 2.53 | 0.32 | - | 12.90 |

CHM: canopy height model; n: number of samples; SD: standard deviation; RMSE: Root Mean Squared Error; CV: coefficient of variation

The lower RMSE (0.47 m) obtained for crop canopy height from Field 3 can be explained by the field condition and also by the capacity of the laser sensor to emit multiple pulses of signal and detecting the returns associated with the crop canopy (the highest point from point cloud). Harkel et al. (2020) reported similar results for modeling different crops (potato, sugar beet, and winter wheat) based on plant height indicated by laser sensor, they found RMSE from 0.12 m to 0.34 m, comparing manual plant height and LiDAR data. The CHM generated to compare the accuracy of height estimation for the selected sugarcane fields is shown in Figure 15A. The relationship among the observed and the predicted crop height from CHM for each field (Field 1 - Figure 15B, Field 2 – Figure 15C, Field 3 – Figure 15D) showed that the accuracy of the method ranged from 0.31 to 0.38, with the highest accuracy ($R^2$ = 0.38) for Field 3 considering both variables (stalk and canopy height). This effect can be associated

with the maximum values considered for the interpolation used to generate DSM from the point cloud, and to the structural condition of the plants in the field.

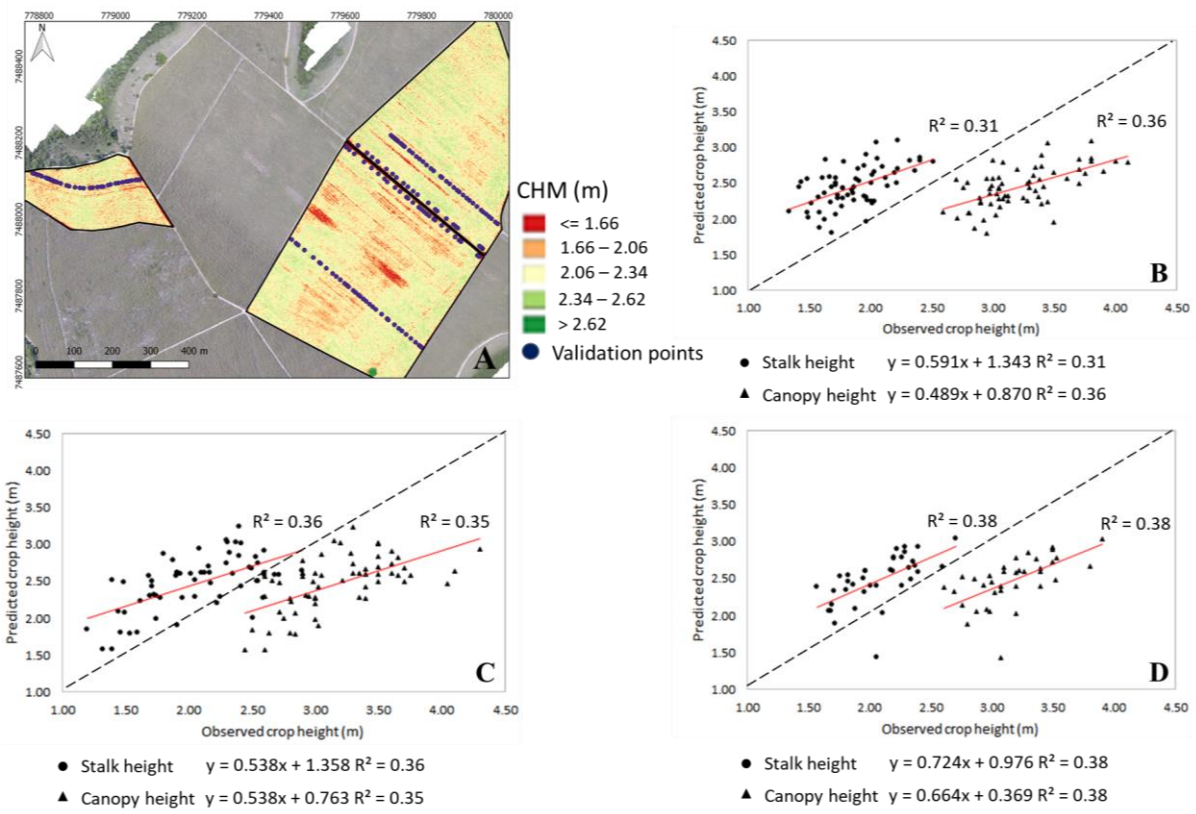


**Figure 15.** Canopy height model (A); Relationship among the validation points and predicted values from the CHM for Field 1 (B); Field 2 (C); Field 3 (D). The dashed line represents the 1:1 line and the solid line represents the fitted linear function

The descriptive statistics of LiDAR-derived metrics extracted from the point cloud is shown in Table 6 for the same validation points. These metrics can support preliminary filtering of the point cloud to eliminate signal noise and outliers from elevation data (WALTER et al., 2019). The CV values ranged from 42% to 69% considering all fields, and the highest value was verified for P50$^{th}$ (69% - Field 3). This variation indicated a very high spatial variability of the leaf height over the sugarcane fields. All maps of the percentiles from CHM for 2018/2019 and 2019/2020 seasons are shown in Appendix A and Appendix B, respectively.

**Table 6.** Descriptive statistics of the LiDAR-derived metrics for each field

| | Field | P50* | P90* | P91* | P92* | P93* | P94* | P95* | P96* | P97* | P98* | P99* |
|---|---|---|---|---|---|---|---|---|---|---|---|---|
| | | meters | | | | | | | | | | |
| **Minimum** | 1 | 0 | 0 | 0 | 0 | 0 | 0 | 0 | 0 | 0 | 0 | 0 |
| | 2 | 0 | 0 | 0 | 0 | 0 | 0 | 0 | 0 | 0 | 0 | 0 |
| | 3 | 0.08 | 0.08 | 0.08 | 0.08 | 0.08 | 0.08 | 0.08 | 0.08 | 0.08 | 0.08 | 0.08 |
| **Maximum** | 1 | 2.70 | 2.70 | 2.70 | 2.70 | 2.70 | 2.70 | 2.70 | 2.70 | 2.70 | 2.70 | 2.70 |
| | 2 | 2.51 | 2.70 | 2.70 | 2.71 | 2.71 | 2.72 | 2.72 | 2.73 | 2.75 | 2.78 | 2.81 |
| | 3 | 2.88 | 2.95 | 2.95 | 2.96 | 2.96 | 2.96 | 2.96 | 2.97 | 2.97 | 2.97 | 2.97 |
| **Mean** | 1 | 1.41 | 1.65 | 1.65 | 1.66 | 1.66 | 1.67 | 1.67 | 1.68 | 1.78 | 1.69 | 1.69 |
| | 2 | 1.27 | 1.50 | 1.50 | 1.51 | 1.52 | 1.52 | 1.53 | 1.53 | 1.54 | 1.54 | 1.55 |
| | 3 | 1.08 | 1.54 | 1.54 | 1.57 | 1.58 | 1.60 | 1.61 | 1.62 | 1.64 | 1.65 | 1.66 |
| **Median** | 1 | 1.54 | 1.73 | 1.73 | 1.74 | 1.75 | 1.75 | 1.76 | 1.76 | 1.68 | 1.78 | 1.78 |
| | 2 | 1.43 | 1.73 | 1.73 | 1.73 | 1.73 | 1.73 | 1.74 | 1.74 | 1.74 | 1.74 | 1.75 |
| | 3 | 1.07 | 1.72 | 1.72 | 1.72 | 1.72 | 1.72 | 1.72 | 1.73 | 1.73 | 1.73 | 1.73 |
| **SD** | 1 | 0.72 | 0.70 | 0.70 | 0.71 | 0.71 | 0.71 | 0.71 | 0.71 | 0.71 | 0.71 | 0.72 |
| | 2 | 0.78 | 0.80 | 0.80 | 0.80 | 0.80 | 0.80 | 0.81 | 0.81 | 0.81 | 0.81 | 0.81 |
| | 3 | 0.75 | 0.76 | 0.76 | 0.77 | 0.77 | 0.78 | 0.79 | 0.79 | 0.80 | 0.81 | 0.81 |
| **CV (%)** | 1 | 50.79 | 42.78 | 42.78 | 42.63 | 42.55 | 42.48 | 42.43 | 42.38 | 42.34 | 42.30 | 42.26 |
| | 2 | 61.41 | 53.06 | 53.06 | 52.92 | 52.85 | 52.79 | 52.73 | 52.68 | 52.62 | 52.57 | 52.53 |
| | 3 | 69.84 | 49.24 | 49.24 | 48.98 | 48.88 | 48.81 | 48.77 | 48.75 | 48.75 | 48.77 | 48.81 |

Pn*: percentile of the n percentage; SD: standard deviation; CV: coefficient of variation

The maximum values from percentiles P90$^{th}$ to P99$^{th}$ were similar to the maximum values of stalk height (2.70 m), indicating that extracting percentiles from point cloud would be a strategy to spatialize crop height without the influence of discrepant values. The percentiles demonstrated weak correlation with stalk height ($r = 0.35$), and RMSE values of about 1.0 m (Figure 16A). Overall, the CHM showed a systematic overestimation of the sugarcane stalk height (Figure 16B) considering the validation points. This effect is partly affected by the spatial resolution compared to the size of the objects (plants) and the capacity to reconstruct the canopy structure (BARETH et al., 2016; HOLMAN et al., 2016). Sumesh et al. (2021) found an average overestimation of 0.10 m considering RGB-based data of sugarcane fields using RPA data collection one month before harvesting.

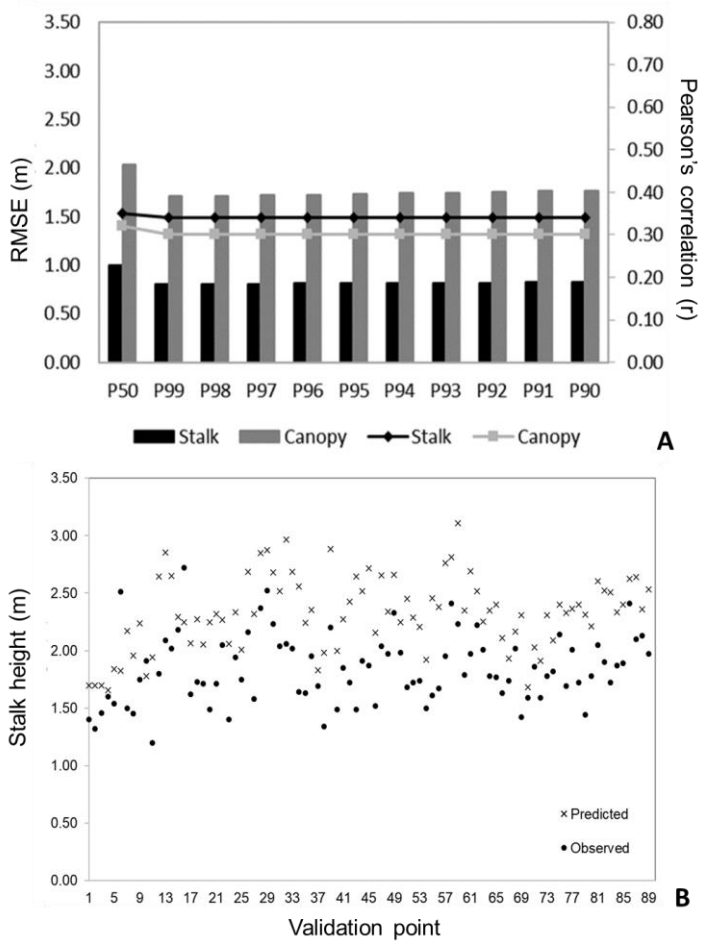


**Figure 16.** Pearson's correlation (r) and Root Mean Squared Error (RMSE) between the percentiles and the manual measurements (A); sugarcane stalk height of the observed and the predicted values for each validation point (B)

### 3.3.3. Relationship among canopy height model and yield map

The descriptive statistics of the dataset from original, filtered, interpolated yield, and CHM are presented in Table 7 for both crop seasons. The results highlighted that there is a requirement to exclude discrepant values from the original data to better understand the actual spatial variability of the fields (Figure 17). As a result of the filtering process, the CV value was reduced from 92.56% to 17.69% for the interpolated data of 2018/2019 season, and from 40.28% to 31.51% for the subsequent season, which indicated very high spatial variability of sugarcane yield for the fields. The CV value (54.54% and 32.51%) of CHM also indicated very high spatial variability of the crop canopy height for both seasons. The standard deviation (SD) values of interpolated yield data were 17.05 Mg $ha^{-1}$ and 16.56 Mg $ha^{-1}$ for each season. The prediction error of the sensor-system for measuring sugarcane yield was about 4.50% compared with the total mass indicated by the in-field wagon. The results regarding the accuracy of the sensor-system were explored in a submitted paper (Appendix C).

**Table 7.** Descriptive statistics of the dataset from yield data and canopy height model

| Season | Dataset | n | Minimum | Maximum | Mean | Median | SD | CV (%) |
|---|---|---|---|---|---|---|---|---|
| | | | yield (Mg ha$^{-1}$) | | | | | |
| 2018/2019 | Original | 215,603 | 0 | 498.21 | 76.94 | 76.20 | 71.22 | 92.56 |
| 2019/2020 | | 128,119 | 0.01 | 555.84 | 65.08 | 66.28 | 26.22 | 40.28 |
| 2018/2019 | Filtered | 190,201 | 38.53 | 89.86 | 66.78 | 62.07 | 11.82 | 17.69 |
| 2019/2020 | | 110,895 | 0.05 | 174.17 | 66.78 | 67.20 | 21.04 | 31.51 |
| 2018/2019 | Interpolated | 8,560,806 | 48.80 | 180.0 | 60.14 | 59.98 | 17.05 | 28.35 |
| 2019/2020 | | 8,567,341 | 35.18 | 103.61 | 69.41 | 70.12 | 16.56 | 23.86 |
| | | | height (m) | | | | | |
| 2018/2019 | CHM | 8,560,806 | 1.66 | 3.0 | 1.54 | 1.51 | 0.84 | 54.54 |
| 2019/2020 | | 8,567,341 | 1.73 | 3.13 | 2.43 | 2.39 | 0.79 | 32.51 |

n: number of samples; CHM: canopy height model; SD: standard deviation; CV: coefficient of variation

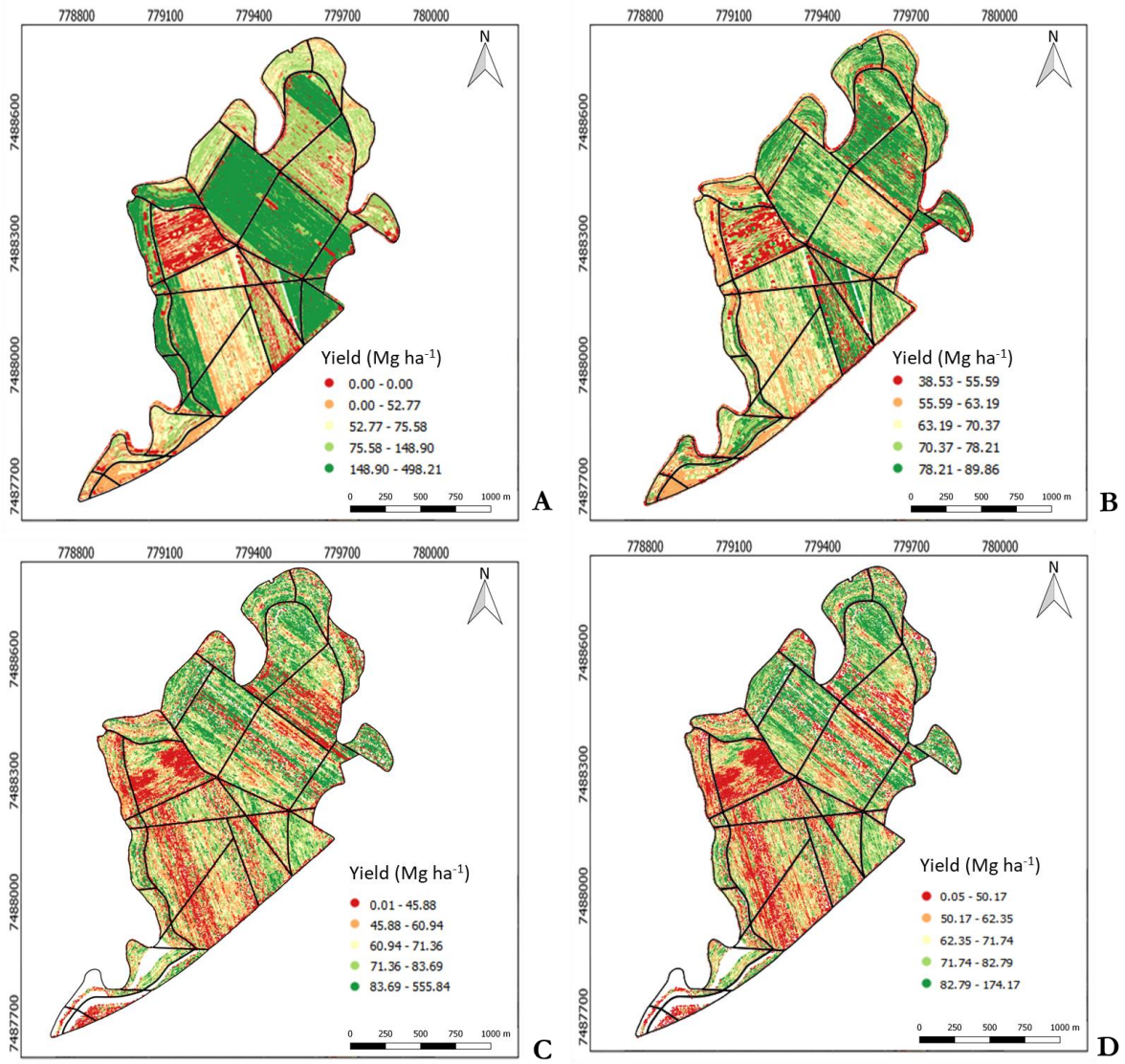


**Figure 17.** Sugarcane yield data from the 2018/2019 season (A); filtered data (B); sugarcane yield data from the 2019/2020 season (C); filtered data (D)

Table 8 summarizes the best-adjusted model used for interpolating sugarcane yield data with RMSE of 8.74 Mg ha$^{-1}$ for the dataset from 2018/2019 season, and of 2.67 Mg ha$^{-1}$ for the dataset from 2019/2020 crop season. The number of points per hectare met the requirements of at least 108 independent data per hectare according to the calculated grid (Table 8). The correlation matrix between the yield data and CHM for the same validation points is shown in Figure 19. Significative values at 0.01% were found with greater correlation for yield and crop canopy height (r = 0.51), followed by sugarcane yield and CHM (r = 0.49). A strong correlation was obtained between the CHM and the crop canopy height (r = 0.73) due to the greater association of the first returns from laser sensor points.

**Table 8.** Geostatistical analysis of the interpolation of yield data

| Season | n | Model | Range (m) | Sill | Nugget | RMSE (Mg ha$^{-1}$) | Calc. grid (samples ha$^{-1}$) |
|---|---|---|---|---|---|---|---|
| 2018/2019 | 8,560,806 | Exponential | 19.27 | 381.0 | 548.30 | 8.74 | 108 |
| 2019/2020 | 8,567,341 | Exponential | 31.02 | 239.90 | 109.20 | 2.67 | 42 |

n: number of samples; RMSE: Root Mean Squared Error; Calc. grid (Ripley, 1981): calculated grid = 10,000 (0.50 Range)$^{-2}$

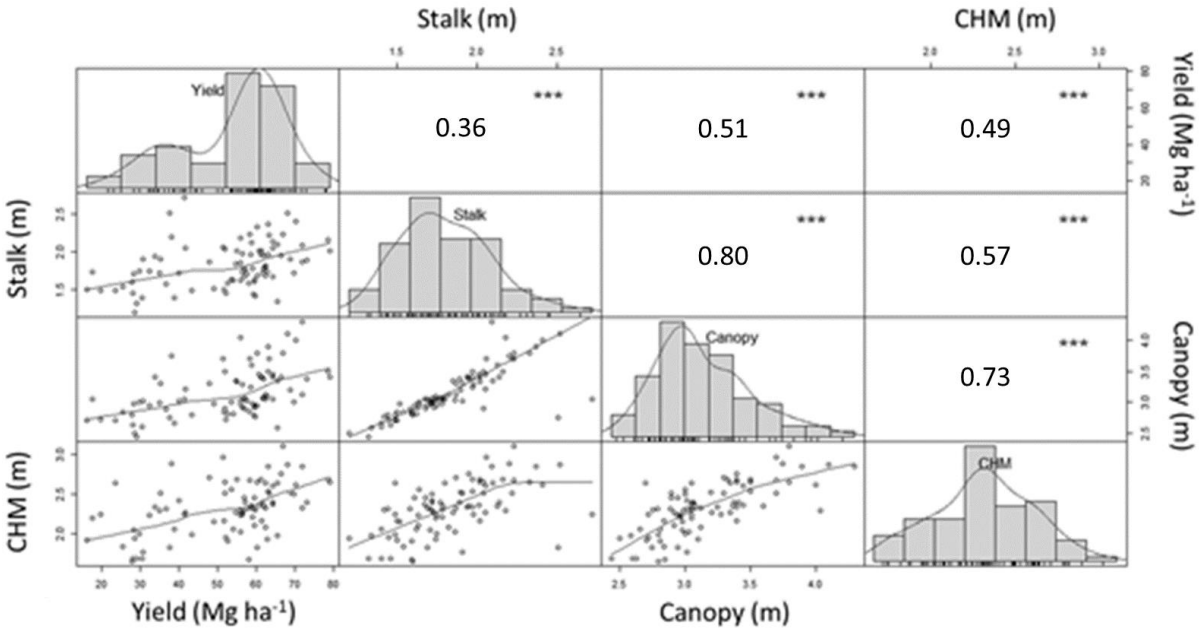


Significance codes: 0 '***' 0.001 '**' 0.01 '*' 0.05 '.' 0.1 'ns' 1

**Figure 18.** Correlation matrix of the validation points for manual measurements, yield map and canopy height model for the 2018/2019 sugarcane growing season

Five-color legend (natural breaks) was applied for visual analysis of the sugarcane yield map of 2018/2019 sugarcane growing season that ranged from 48.80 to 180.0 Mg ha$^{-1}$ (Figure 20A), and CHM that ranged from 1.66 m to 3.0 m (Figure 20B). The sugarcane yield map of 2019/2020 crop season (Figure 20C) indicated that the yield values ranged from 53.40 to 79.40 Mg ha$^{-1}$ and the correspondent CHM ranged from 2.06 m to 2.97 m (Figure 20D).

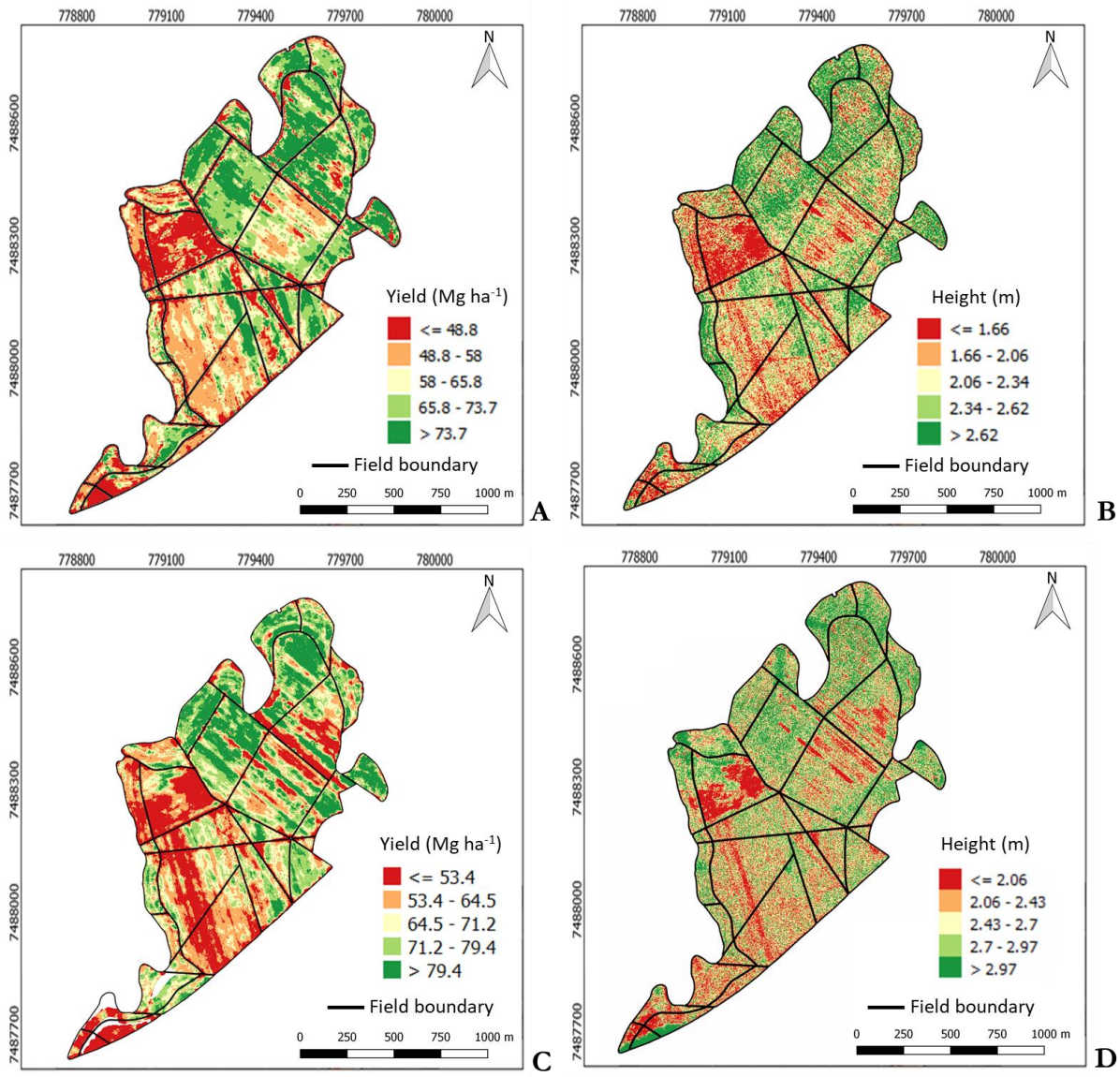


**Figure 19.** Interpolated sugarcane yield map for the 2018/2019 crop season (A); correspondent canopy height model (B); Interpolated sugarcane yield map for the 2019/2020 crop season (C); correspondent canopy height model (D)

The variation of the plant height indicated by the CHM would be a potential tool for detecting the spatial patterns over the fields, the different levels of sugarcane production and, consequently, to support better the harvest planning and the within field management. The moderate linear relationship among the CHM and the yield map indicated that there is no evidence of estimating sugarcane yield based on plant height, however the spatial distribution of the data from both 3D sensing techniques coincided with the yield variation at the field (Figure 21), which allows to infer about distinct levels of production before harvesting. Also, the CHM could be useful to mapping the field locations with and without sugarcane plants within rows, assisting on site-specific practices, such as to support the management zones delineation at the field level.

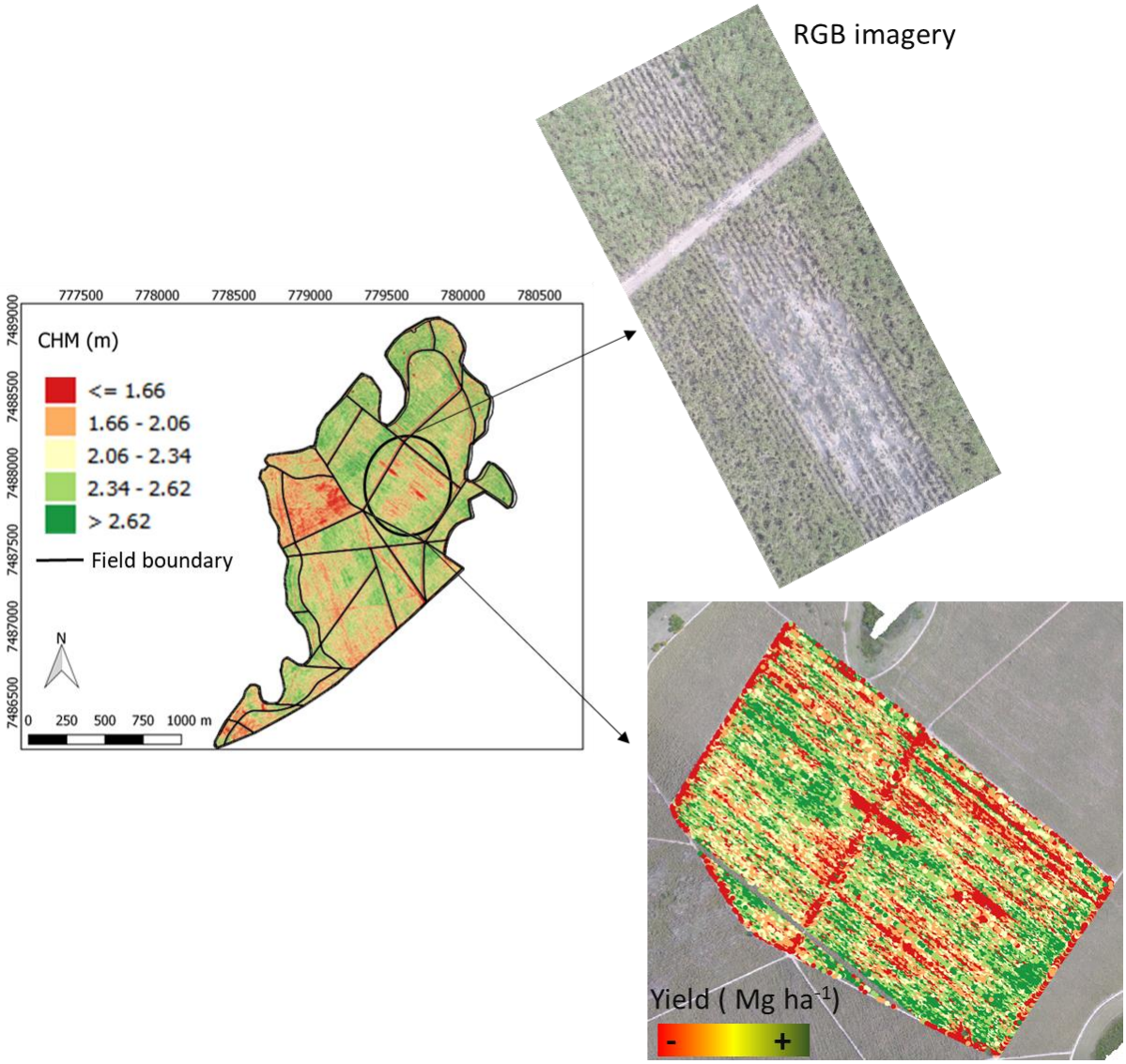


**Figure 20.** Visual analysis of the canopy height model, RGB imagery, and yield data for the same field location for the 2018/2019 sugarcane growing season

The study demonstrates the LiDAR data applications as a potential RS technique to identify the spatial variability of sugarcane fields through crop canopy mapping in the pre-harvest period using open-source software, available to any user. This approach can provide relevant information to support the site-specific crop management of sugarcane growers, and a suitable alternative to the multispectral information obtained during the crop maturation stage from aerial or terrestrial platforms. The economical and practical aspects also should be deeply discussed to enable the use of LiDAR-based platforms in agriculture, considering that it tends to make it feasible for the long-term.

## 3.4. Conclusion

The spatial distribution of canopy height was mapped based on a methodology involving high-resolution data that supports to identify spatial patterns over the sugarcane fields before harvesting. The DTMs generated before and after harvesting were numerically the same regarding the elevation values, indicating that a single flight would be required to generate the DTM of reference in similar field conditions of the current study. The plant height distribution within the field was mapped through the CHM obtained from a dense point cloud. The RMSE was 0.47 m considering the comparison between the manual measurements (sugarcane stalk height) and LiDAR data. The LiDAR-derived metrics associated with 3D sensing data provided the characterization of the spatial variability of commercial sugarcane fields, which was classified as very high (CV>30%) considering the high-resolution data from CHM, percentiles, and yield map. The visual analysis of the orthomosaic demonstrated the same pattern of spatial variability observed in the yield map and CHM. The relationship among CHM and sugarcane yield map was moderate according to the correlation values.

## References

BARETH, G.; BENDIG, J.; TILLY, N.; HOFFMEISTER, D.; AASEN, H.; BOLTEN, A. 2016. A Comparison of UAV and TLS-derived Plant Height for Crop Monitoring: Using Polygon Grids for the Analysis of Crop Surface Models (CSMs). **Photogrammetrie, Fernerkundung, Geoinformation.** 85–94. doi: 10.1127/pfg/2016/0289.

BAZEZEW, M. N.; HUSSIN, Y. A.; KLOOSTERMAN, E. H. 2018. Integrating Airborne LiDAR and Terrestrial Laser Scanner forest parameters for accurate above-ground biomass/carbon estimation in Ayer Hitam tropical forest, Malaysia. **International Journal of Applied Earth Observation and Geoinformation**, 73: 638-652. doi: 10.1016/j.jag.2018.07.026.

BÉGUÉ, A.; LEBOURGEOIS, V.; BAPPEL, E.; TODOROFF, P.; PELLEGRINO, A.; BAILARIN, F.; SIEGMUND, B. 2010. Spatio-temporal variability of sugarcane fields and recommendations for yield forecast using NDVI. **International Journal of Remote Sensing**, 31(20): 5391-5407. doi: 10.1080/01431160903349057.

BORRA-SERRANO, I.; SWAEF, T. de; MUYLLE, H.; NUYTTENS, D.; VANGEYTE, J.; MERTENS, K.; SAEYS, W.; SOMERS, B.; ROLDÁN-RUIZ, I.; LOOTENS, P. 2019. Canopy height measurements and non-destructive biomass estimation of Lolium perenne swards using UAV imagery. **Grass Forage Science**, 74: 356–369. doi: 10.1111/gfs.12439.

BROCKS, S.; BARETH, G. Estimating barley biomass with crop surface models from oblique RGB imagery. **Remote Sensing**. v.10, n.2, p.268, 2018.

BUELVAS, R. M.; ADAMCHUK, V. I.; LEKSONO, E.; TIKASZ, P.; LEFSRUD, M.; HOLOSZKIEWICZ, J. Biomass estimation from canopy measurements for leafy vegetables based on ultrasonic and laser sensors. **Computers and Electronics in Agriculture**, v.164, 104896, 2019.

CANATA, T. F.; MOLIN, J. P.; SOUSA, R. V. de. A measurement system based on LiDAR technology to characterize the canopy of sugarcane plants. **Engenharia Agrícola**, v.39, n.2, p.240-247, 2019.

CHOLULA, U.; SILVA, J. A. da; MARCONI, T.; THOMASSON, J. A.; SOLORZANO, J.; ENCISO, J. 2020. Forecasting Yield and Lignocellulosic Composition of Energy Cane Using Unmanned Aerial Systems. **Agronomy**, 10(5), 718. doi: 10.3390/agronomy10050718.

COLAÇO, A.F., MOLIN, J.P., ROSELL-POLO, J.R; ESCOLÀ, A. Application of light detection and ranging and ultrasonic sensors to high-throughput phenotyping and precision horticulture: current status and challenges. **Horticulture Research** 5, 35, 2018. doi: 10.1038/s41438-018-0043-0.

COLAÇO, A. F.; MOLIN, J. P.; ROSELL-POLO, J. R.; ESCOLÀ, A. Spatial variability in commercial orange groves. Part 1: canopy volume and height**. Precision Agriculture**, v.20, p.788-804, 2019.

CONAB. Companhia Nacional de Abastecimento. <https://www.conab.gov.br/info-agro/safras/cana/boletim-da-safra-de-cana-de-acucar>.

CORSEUIL, C. W.; ROBAINA, A. D. Altimetric determination thru the global positioning system. **Ciência Rural**, vol. 33, n. 4, p.673-678, 2003. doi: 10.1590/S0103-84782003000400014.

DEERY, D.; JIMENEZ-BERNI, J.; JONES, H.; SIRAULT, X.; FURBANK, R. 2014. Proximal remote sensing buggies and potential applications for field-based phenotyping. **Agronomy** 4(3): 349–379. doi: 10.3390/agronomy4030349.

EMBRAPA - Empresa Brasileira de Pesquisa Agropecuária. Sistema Brasileiro de Classificação de Solos. Brasília: CNPS, 1999. 412p.

ESCOLÀ, A.; MARTÍNEZ-CASASNOVAS, J. A.; RUFAT, J.; ARNÓ, J.; ARBONÉS, A.; SEBÉ, F.; PASCUAL, M.; GREGORIO, E.; ROSELL-POLO, J. R. 2016. Mobile terrestrial laser scanner applications in precision fruticulture/horticulture and tools to extract information from canopy point clouds. **Precision Agriculture**, 18(1): 111-132.

EITEL, J. U. H.; MAGNEY, T. S.; VIERLING, L. A.; BROWN, T. T.; HUGGINS, D. R. 2014. LiDAR based biomass and crop nitrogen estimates for rapid, non-destructive assessment of wheat nitrogen status. **Field Crops Research**, 159: 21–32. doi: 10.1016/j.fcr.2014.01.008.

FRIEDLI, M.; KIRCHGESSNER, N.; GRIEDER, C.; LIEBISCH, F.; MANNALE, M.; WALTER, A. 2016. Terrestrial 3D laser scanning to track the increase in canopy height of both monocot and dicot crop species under field conditions. **Plant Methods** 12(9). doi: 10.1186/s13007-016-0109-7.

GEBREMEDHIN, A.; BADENHORST, P. E.; WANG, J.; SPANGENBERG, G. C.; SMITH, K. F. 2019. Prospects for Measurement of Dry Matter Yield in Forage Breeding Programs Using Sensor Technologies. **Agronomy**, 9(2): 65. doi: 10.3390/agronomy9020065.

GENÉ-MOLA, J.; GREGORIO, E.; CHEEIN, F. A.; GUEVARA, J.; LLORENS, J.; SANZ-CORTIELLA, R.; ESCOLÀ, A.; ROSELL-POLO, J. R. 2020. Fruit detection, yield prediction and canopy geometric characterization using LiDAR with forced air flow. **Computers and Electronics in Agriculture**, 168, 105121, doi: 10.1016/j.compag.2019.105121.

GOMES, F.; GARCIA, C. H. **Estatística aplicada a experimentos agronômicos e florestais**. Piracicaba: FEALQ, 2002. 305p.

GORGENS, E. B.; VALBUENA, R.; RODRIGUEZ, L. C. E. A method for optimizing height threshold when computing airborne laser scanning metrics. **Photogrammetric Engineering & Remote Sensing**, v.83, n.5, p.343-350, 2017.

HÄMMERLE, M.; HÖFLE, B. 2014. Effects of Reduced Terrestrial LiDAR Point Density on High-Resolution Grain Crop Surface Models in Precision Agriculture. **Sensors**, 14(12): 24212-24230. doi: 10.3390/s141224212.

HARKEL, J. T.; BARTHOLOMEUS, H.; KOOISTRA, L. 2020. Biomass and crop height estimation of different crops using UAV-Based Lidar. **Remote Sensing**, 12(1): 17. doi: 10.3390/rs12010017.

HOLMAN, F. H.; RICHE, A. B.; MICHALSKI, A.; CASTLE, M.; WOOSTER, M. J.; HAWKESFORD, M. J. 2016. High Throughput Field Phenotyping of Wheat Plant Height and Growth Rate in Field Plot Trials Using UAV Based Remote Sensing. **Remote Sensing**, 8(12): 1031. doi: 10.3390/rs8121031.

HOPKINSON, C.; LOVELL, J.; CHASMER, L.; JUPP, D.; KLJUN, N.; GORSEL, E. V. 2013. Integrating terrestrial and airborne lidar to calibrate a 3D canopy model of effective leaf area index. **Remote Sensing of Environment**, 136: 301-314. doi: 10.1016/j.rse.2013.05.012.

JIANG, Y.; LI, C.; TAKEDA, F.; KRAMER, E. A.; ASHRAFI, H.; HUNTER, J. 3D point cloud data to quantitatively characterize size and shape of shrub crops. **Horticulture Research**, 6(43), 2019.

JIMENEZ-BERNI, J. A.; DEERY, D. M.; ROZAS-LARRAONDO, P.; CONDON, A. G.; REBETZKE, G. J.; JAMES, R. A.; BOVILL, W. D.; FURBANK, R. T.; SIRAULT, X. R. R. 2018. High Throughput Determination of Plant Height, Ground Cover, and Above-Ground Biomass in Wheat with LiDAR. **Frontiers in Plant Science**, 9:237. doi: 10.3389/fpls.2018.00237.

LEITE, R. V.; AMARAL, C. H.; PIRES, R. P.; SILVA, C. A.; SOARES, C. P. B.; MACEDO, R. P.; SILVA, A. A. L.; BROADBENT, E. N.; MOHAN, M.; LEITE, H. G. 2020. Estimating Stem Volume in Eucalyptus Plantations Using Airborne LiDAR: A Comparison of Area- and Individual Tree-Based Approaches. **Remote Sensing**, 12, 1513. doi: 10.3390/rs12091513.

LI, P.; ZHANG, X.; WANG, W.; ZHENG, H.; YAO, X.; TIAN, Y.; ZHU, Y.; CAO, W.; CHEN, Q.; CHENG, T. 2020. Estimating aboveground and organ biomass of plant canopies across the entire season of rice growth with terrestrial laser scanning. **International Journal of Applied Earth Observation and Geoinformation**, 91, 102132. doi: 10.1016/j.jag.2020.102132.

LI, W.; NIU, Z.; CHEN, H.; LI, D. 2017. Characterizing canopy structural complexity for the estimation of maize LAI based on ALS data and UAV stereo images. **International Journal of Remote Sensing**, 38(8): 2106-2116. doi: 10.1080/01431161.2016.1235300.

LOUDERMILK, L. E.; HIERS, J. K.; O'BRIEN, J. J.; MITCHELL, R. J.; SINGHANIA, A.; FERNANDEZ, J. C.; CROPPER, W. P. JR.; SLATTON, K. C. 2009. Ground-based LIDAR: a novel approach to quantify fine-scale fuelbed characteristics. **International Journal of Wildland Fire**, 18: 676–685. doi: 10.1071/WF07138.

LUCIANO, A. C. S. dos; PICOLI, M. C. A.; ROCHA, J. V.; FRANCO, H. C. J.; SANCHES, G. M.; LEAL, M. R. L. V.; MAIRE, G. L. 2018. Generalized space-time classifiers for monitoring sugarcane areas in Brazil**. Remote Sensing of Environment**, 215: 438-451. doi: 10.1016/j.rse.2018.06.017.

LUCIANO, A. C. S. dos; PICOLI, M. C. A.; DUFT, D. G.; ROCHA, J. V.; LEAL, M. R. L. V.; MAIRE, G. L. 2021. Empirical model for forecasting sugarcane yield on a local scale in Brazil using Landsat imagery and random forest algorithm. **Computers and Electronics in Agriculture**, 184: 106063. doi: 10.1016/j.compag.2021.106063.

LUO, S.; CHEN, J. M.; WANG, C.; XI, X.; ZENG, H.; PENG, D.; LI, D. 2016. Effects of LiDAR point density, sampling size and height threshold on estimation accuracy of crop biophysical parameters. **Optics Express**, 24(11): 11578-11593. doi: 10.1364/OE.24.011578.

MAES, W. H.; STEPPE, K. 2019. Perspectives for Remote Sensing with Unmanned Aerial Vehicles in Precision Agriculture. **Trends in Plant Science**, 24(2): 152-164. doi: 10.1016/j.tplants.2018.11.007.

MAIMAITIJIANG, M.; SAGAN, V.; SIDIKE, P.; HARTLING, S.; ESPOSITO, F.; FRITSCHI, F. B. 2020. Soybean yield prediction from UAV using multimodal data fusion and deep learning. **Remote Sensing of Environment**, 237. doi: 10.1016/j.rse.2019.111599.

MALDANER, L. F.; CANATA, T. F.; DIAS, C. T. S; MOLIN, J. P. 2021. A statistical approach to static and dynamic tests for Global Navigation Satellite Systems receivers used in agricultural operations. **Scientia Agricola**, 78(5):327-345. doi: 10.1590/1678-992x-2019-0252.

MESAS-CARRASCOSA, F. J.; CASTRO, A. I. de; TORRES-SÁNCHEZ, J.; TRIVIÑO-TARRADAS, P.; JIMÉNEZ-BRENES, F. M.; GARCÍA-FERRER, A.; LÓPEZ-GRANADOS, F. 2020. Classification of 3D Point Clouds Using Color Vegetation Indices for Precision Viticulture and Digitizing Applications. **Remote Sensing**, 12, 317. doi: 10.3390/rs12020317.

MIELCAREK, M.; KAMIŃSKA, A.; STEREŃCZAK, K. 2020. Digital Aerial Photogrammetry (DAP) and Airborne Laser Scanning (ALS) as Sources of Information about Tree Height: Comparisons of the Accuracy of Remote Sensing Methods for Tree Height Estimation. **Remote Sensing**, 12(11): 1808. doi: 10.3390/rs12111808.

MIELCAREK, M.; STEREŃCZAK, K.; KHOSRAVIPOUR, A. 2018. Testing and evaluating different LiDAR-derived canopy height model generation methods for tree height estimation. **International Journal of Applied Earth Observation and Geoinformation**, 71, 132-143. doi: 10.1016/j.jag.2018.05.002.

MOLIN, J. P.; COLAÇO, A. F.; AMARAL, L. R. do. **Agricultura de Precisão**. 1 ed. Piracicaba: Oficina de Textos, 224 p., 2015.

MOLIJN, R. A.; IANNINI. L.; ROCHA, J. V.; HANSSEN, R. F. 2018. Ground reference data for sugarcane biomass estimation in São Paulo state, Brazil. **Sci Data**, 5(180150): 1-18. doi: 10.1038/sdata.2018.150.

MURRAY, J.; FENNELI, J. T.; BLACKBURN, G. A.; WHYATT, J. D.; LI, B. 2020. The novel use of proximal photogrammetry and terrestrial LiDAR to quantify the structural complexity of orchard trees. **Precision Agriculture**, 21: 473–483. doi: 10.1007/s11119-019-09676-4.

NASCIMENTO, A. H. C. DE; PEREIRA, A. K. P.; BEZERRA, A. C.; SILVA, E. S.; OLIVEIRA, A. L. DE; CAMINHA, O. R. 2017. Comparison between altimetric survey methods for systematization of lands for irrigation and drainage**. Revista Brasileira de Agricultura Irrigada**, 11(5): 1685-1692. doi: 10.7127/RBAI.V11N500749.

OKHRIMENKO, M.; COBURN, C.; HOPKINSON, C. 2019. Multi-Spectral Lidar: Radiometric Calibration, Canopy Spectral Reflectance, and Vegetation Vertical SVI Profiles. **Remote Sensing**, 11(13): 1556. doi: 10.3390/rs11131556.

PAULUS, S.; BEHMANN, J.; MAHLEIN, A. K.; PLÜMER, L.; KUHLMANN, H. 2014. Low-cost 3D systems - well suited tools for plant phenotyping. **Sensors**, 14(2): 3001–3018. doi: 10.3390/s14020300.

PAULUS, S. 2019. Measuring crops in 3D: using geometry for plant phenotyping. **Plant Methods**, 15: 103. doi: 10.1186/s13007-019-0490-0.

POLEY, G. L.; McDERMID, G. J. 2020. A Systematic Review of the Factors Influencing the Estimation of Vegetation Aboveground Biomass Using Unmanned Aerial Systems. **Remote Sensing**, 12(7): 1052. doi: 10.3390/rs12071052.

PORTZ, G.; MOLIN, J. P.; JASPER, J. 2012. Active crop sensor to detect variability of nitrogen supply and biomass on sugarcane fields. **Precision Agriculture**, 13: 33-44. doi: 10.1007/s11119-011-9243-4.

QGIS Development Team. 2018. QGIS Geographic Information System. Open-Source Geospatial Foundation Project. http://qgis.osgeo.org.

RAHMAN, M. M., ROBSON, A. J. 2020. Integrating Landsat-8 and Sentinel-2 Time Series Data for Yield Prediction of Sugarcane Crops at the Block Level. **Remote Sensing**, 12(8): 1313. doi: 10.3390/rs12081313.

RIPLEY, B. D. 1981. **Spatial statistics**. John Wiley Sons, chapter 3, New York.

ROSS, F. N. 2013. How did we get here? An early history of forestry lidar. **Canadian Journal of Remote Sensing**, 39(1): 6-17. doi: 10.5589/m13-011.

ROUSSEL, J. R.; AUTY, D.; BOISSIEU, F. de; MEADOR, A. S. 2019. lidR: Airborne LiDAR Data Manipulation and Visualization for Forestry Applications – version 2.0.2.

SAIZ-RUBIO, V.; ROVIRA-MÁS, F. 2020. From smart farming towards agriculture 5.0: A review on crop data management. **Agronomy Journal**, 10(2): 207. doi: 10.3390/agronomy10020207.

SANCHES, G. M.; DUFT, D. G.; KÖLLN, O. T.; LUCIANO, A. C. DOS S.; CASTRO, S. G. Q. DE; OKUNO, F. M.; FRANCO, H. C. J. 2018. The potential for RGB images obtained using unmanned aerial vehicle to assess and predict yield in sugarcane fields. **International Journal of Remote Sensing**, 39:15-16, 5402-5414. doi: 10.1080/01431161.2018.1448484.

SCHIRRMANN, M.; GIEBEL, A.; GLEINIGER, F.; PFLANZ, M.; LENTSCHKE, J.; DAMMER, K. H. 2016. Monitoring Agronomic Parameters of Winter Wheat Crops with Low-Cost UAV Imagery. **Remote Sensing**, 8(9): 706. doi: 10.3390/rs8090706.

SHENDRYK, Y.; SOFONIA, J.; GARRARD, R.; RIST, Y.; SKOCAJ, D.; THORBURN, P. 2020. Fine-scale prediction of biomass and leaf nitrogen content in sugarcane using UAV LiDAR and multispectral imaging. **International Journal of Applied Earth Observation and Geoinformation**, 92, 102177. doi: 10.1016/j.jag.2020.102177.

SILVA, C. A; HUDAK, A.; KLAUBERG, C.; VIERLING, L. A.; GONZALEZ-BENECKE, C. A.; CARVALHO, S. P. C.; RODRIGUEZ, L.C.E.; CARDIL, A. 2017. Combined effect of pulse density and grid cell size on predicting and mapping aboveground carbon in fast-growing Eucalyptus forest plantation using airborne LiDAR data. **Carbon Balance and Management**, 12(13): 1-16. doi: 10.1186/s13021-017-0081-1.

SILVA, V. S.; SILVA, C. A.; MOHAN, M.; CARDIL, A.; REX, F. E.; LOUREIRO, G. H.; ALMEIDA, D. R. A.; BROADBENT, E. N.; GORGENS, E. B.; DALLA CORTE, A. P.; SILVA, E. A.; VALBUENA, R.; KLAUBERG, C. 2020. Combined Impact of Sample Size and Modeling Approaches for Predicting Stem Volume in Eucalyptus spp. Forest Plantations Using Field and LiDAR Data. **Remote Sensing**, 12(9): 1438. doi: 10.3390/rs12091438.

SUMESH, K. C.; NINSAWAT, S.; SOM-ARD, J. 2021. Integration of RGB-based vegetation index, crop surface model and object-based image analysis approach for sugarcane yield estimation using unmanned aerial vehicle. **Computers and Electronics in Agriculture**, 180: 105903. doi: 10.1016/j.compag.2020.105903.

SUN, S.; LI, C.; PATERSON, A. H.; JIANG, Y.; XU, R.; ROBERTSON, J. S.; SNIDER, J. L.; CHEE, P. W. 2018. In-field High Throughput Phenotyping and Cotton Plant Growth Analysis Using LiDAR. **Frontiers in Plant Science**, 9(16). doi: 10.3389/fpls.2018.00016.

TILLY, N.; AASEN, H.; BARETH, G. 2015. Fusion of plant height and vegetation indices for the estimation of barley biomass. **Remote Sensing**, 7(12): 11449–11480. doi: 10.3390/rs70911449.

TILLY, N.; HOFFMEISTER, D.; CAO, Q.; HUANG, S.; LENZ-WIEDEMANN, V.; MIAO, Y.; BARETH, G. 2014. Multitemporal crop surface models: accurate plant height measurement and biomass estimation with terrestrial laser scanning in paddy rice. **Journal of Applied Remote Sensing**, 8(1): 083671. doi: 10.1117/1.JRS.8.083671.

VEGA, A.; CÓRDOBA, M.; CASTRO-FRANCO, M.; BALZARINI, M. 2019. Protocol for automating error removal from yield maps. **Precision Agriculture**, 20:1030–1044. doi: 10.1007/s11119-018-09632-8.

VISSER, H.; NIJS, T. de. 2006. The Map Comparison Kit. **Environmental Modeling & Software** 21, 346-358.

WALTER, J. D. C.; EDWARDS, J.; MCDONALD, G.; KUCHEL, H. 2019. Estimating biomass and canopy height with LiDAR for field crop breeding. **Frontiers in Plant Science**, 10(1145). doi: 10.3389/fpls.2019.01145.

WANG, M.; LIU, Z.; BAIG, M. H. A.; WANG, Y.; LI, Y.; CHEN, Y. 2019. Mapping sugarcane in complex landscapes by integrating multi-temporal Sentinel-2 images and machine learning algorithms. **Land Use Policy**, 88: 104190. doi: 10.1016/j.landusepol.2019.104190.

ZHANG, W.; QI, J.; WAN, P.; WANG, H.; XIE, D.; WANG, X.; YAN, G. 2016. An Easy-to-Use Airborne LiDAR Data Filtering Method Based on Cloth Simulation. **Remote Sensing**, 8(6): 501. doi: 10.3390/rs8060501.

# 4. INTEGRATING IMAGERY DATA AND MACHINE LEARNING TECHNIQUE FOR SUGARCANE YIELD MAPPING

**Part of this section was published in Remote Sensing Journal (CANATA, T. F.; WEI, M. C. F.; MALDANER, L. F.; MOLIN, J. P. 2021. Sugarcane yield mapping using high-resolution imagery data and machine learning technique. Remote Sensing, 13 (2): 232. doi: 10.3390/rs13020232)**

## ABSTRACT

Yield maps provide essential information to guide precision agriculture (PA) practices. Yet, on-board yield monitoring for sugarcane can be challenging. At the same time, orbital images have been widely used for indirect crop yield estimation for many crops like wheat, corn, and rice, but not for sugarcane. Aware of this, the objective of this study is to explore the potential of multi-temporal imagery data as an alternative for sugarcane yield mapping. The study was based on developing predictive sugarcane yield models integrating time-series orbital imaging and machine learning technique. A commercial sugarcane site was selected, and Sentinel-2 images were acquired from the beginning of the ratoon sprouting until harvesting of three consecutive cropping seasons. The predictive yield models based on RF (Random forest) and MLR (Multiple Linear Regression) were developed using orbital images and yield maps generated by a commercial sensor-system on harvesting. Original yield data were filtered and interpolated with the same spatial resolution of the orbital images. The entire dataset was divided into training and testing dataset for the predictor's variables of each crop stage. The spectral bands were more effective in estimating sugarcane yield for both models. But RF regression demonstrated lower RMSE (about 7.0 Mg $ha^{-1}$) compared with MLR method for the same predictor's variable. The integration of imagery data and machine learning demonstrated potential for modeling sugarcane yield at the field level.

## 4.1. Introduction

Remote sensing (RS) is a potential source of data for crop monitoring, providing spatial and temporal information. Orbital images are commonly used in agriculture to identify spectral variations resulting from soil and crop characteristics at a large-scale, supporting diagnostics for agronomic crop parameters and helping farmers to make better management decisions. The main limitations related to orbital images are the lack of ground truth data (calibration) and the measurement accuracy of the agronomical variables (LOBELL et al., 2015). Furthermore, the empirical models to predict agronomical parameters based on spectral information may have spatial and temporal restrictions for application across different fields and seasons (JEFFRIES et al., 2020; COLAÇO and BRAMLEY, 2019; SCHWALBERT et al., 2018; LOBELL, 2013).

For the sugarcane crop, the assessment of the spatial variability is challenging due to the limited adapted solutions, mainly for yield mapping. Yield maps are essential to better understand the within-field variability, to delimit management zones and improve site-specific management strategies (JEFFRIES et al., 2020; BRAMLEY et al., 2019; MOMIN et al., 2019). Sugarcane yield maps are usually obtained from data collected directly by monitors on harvesters that present some limitations, such as the required calibration, accessibility of data processing for farmers or users, and a lack of knowledge to manage data from more than one harvester (FULTON and PORT, 2018). One additional challenge for sugarcane yield mapping based on yield monitors compared to grains, is the high-resolution data (due to slow traveling speed of the harvester and narrow row spacing) combined with high biomass variability and noise from the yield monitor system. These limitations have guided the interest in RS techniques to monitor sugarcane yield.

Several studies reported the strength of linear correlation between the image-based vegetation indices (VIs) and sugarcane yield forecast (LUCIANO et al., 2021; RAHMAN and ROBSON, 2016; MULIANGA et al.,

2013; BÉGUÉ et al., 2010), but none of these were applied using yield data generated by harvesters at the field level. No technique is widely adopted yet for generating yield maps in sugarcane from imagery information and the current practice to relate biomass estimated by VIs and stalk yield is not consistent regarding spatial and temporal resolutions. Other strategies for sugarcane yield estimation have relied on mathematical models for regional scales that consider the meteorological and crop management variables at a low spatial resolution (HAMMER et al., 2019), which is insufficient for PA purposes. Sugarcane crop has an important economic role for Brazilian agribusiness with about 9 M ha, especially for São Paulo state that corresponds to 54% of national sugarcane production (Agricultural Economics Institute – IEA, 2019), where this study was developed.

An initial research regarding spectral patterns of reflectance for sugarcane was conducted by Simões et al. (2005) that found strong correlations until the end of the vegetative stage between the red spectral band (648 nm) and production parameters (leaf area index – LAI and total sugarcane biomass). Abdel-Rahman et al. (2008) listed different applications of RS techniques for sugarcane, such as disease detection, crop health status, and nutrition scouting, via identification of patterns in spectral data throughout its phenological stages and orbital images. Lisboa et al. (2018) found a relationship among the NDVI (Normalized Difference Vegetation Index) and the concentration of leaf-tissue nutrients when monitoring sugarcane yield, and they observed changes in light canopy reflectance according to the concentration of leaf-tissue nutrients. Rahman and Robson (2020) developed a time-series approach through orbital images from Sentinel-2 to estimate sugarcane yield at the individual block level. Results showed that the maximum Green Normalized Difference Vegetation Index (GNDVI) values across the block were most correlated ($r = 0.93$) with the average actual yield, reported by the sugar mill. Abdel-Rahman et al. (2012) investigated RF (Random Forest) predictive models considering VIs from Landsat constellation to study sugarcane yield under rainfed and irrigated conditions for two sugarcane varieties. The results suggested a strong relationship for predicting sugarcane yield, mainly, under irrigated conditions. Despite the satisfactory prediction accuracy, the field data collection was performed using manual harvesting (average yield values per plot), as such, the site-specific yield estimation is still a gap to bridge in research.

Another common feature of previous research is the reliance on a single image at a given crop stage to investigate the relationship among spectral VIs and yield. Given the relatively higher temporal resolution of available imagery (for example, Sentinel-2 constellation has a revisit frequency of 5 days), and the potential of novel analytic tools to handle many variable predictors, a time series approach for sugarcane yield prediction is worthwhile investigating. Machine Learning (ML) techniques have been shown to provide higher prediction accuracy compared to the traditional statistical analyses, as well as to identify dataset patterns (HUNT et al., 2019; JEONG et al., 2016; HOCHACHKA et al., 2007). These models are commonly subjected to testing and training processes, depending on the complexity of the dataset. The potential of ML techniques, such as RF and ANN (Artificial Neural Network), for agronomic data, was verified by Yuan et al. (2017) to estimate LAI of soybean. The authors concluded that RF, a non-parametric method, is more accurate to estimate it when sample plots and variation are relatively large. Yue et al. (2018) and Han et al. (2019) also reported the application of RF and ANN to assess the above-ground biomass of wheat and maize, respectively. These studies verified that the RF algorithm provided better results than other ML techniques. Schwalbert et al. (2020) evaluated the contribution of weather variables to estimate corn yield based on RS data and RF algorithm, which resulted in a mean absolute error (MAE) of about 0.89 Mg $ha^{-1}$. Thus, considering the previous experiences, the purpose of this investigation was to assess spectral bands and derived-VIs from orbital images to develop predictive sugarcane yield models based on RF and MLR algorithms. The specific objectives were

i) to develop yield prediction models based on time-series analysis of Sentinel-2 images; ii) to compare the accuracy of RF regression and MLR methods to predict sugarcane yield at the field level.

## 4.2. Material and Methods

### 4.2.1. Study area

The study was conducted in a commercial site of 56.40 ha (Figure 1), composed of four fields, located in the municipality of Botucatu, São Paulo, Brazil (22°41'42.8" S; 48°16'54.0" W; 480 m) during the 2017/2018, 2019/2020, and 2020/2021 sugarcane growing seasons. The climate in the study region is mesothermal, Cwa - humid subtropical (Köppen climate classification), which includes drought in the winter from June to September and wet conditions from November to April. The average annual rainfall in the municipality is 1433 mm. The air relative humidity is 71% with an annual average temperature of 23ºC. All fields of the study site were cultivated with SP83-2847 sugarcane variety (4th ratoon – 2017/2018 season) with a row spacing of 1.50 m in Argisol (EMBRAPA, 2013), and it was mechanically harvested in the late season (wet time of the year – October and November). The previous harvesting dates (10/14/2017, 11/11/2018, and 11/16/2019) were considered as a reference to determine the days after cutting (DAC) associated with the date of the orbital images and related to the phenological crop stage. Figure 2 presents the air temperature and precipitation values from the study site for all crop seasons.

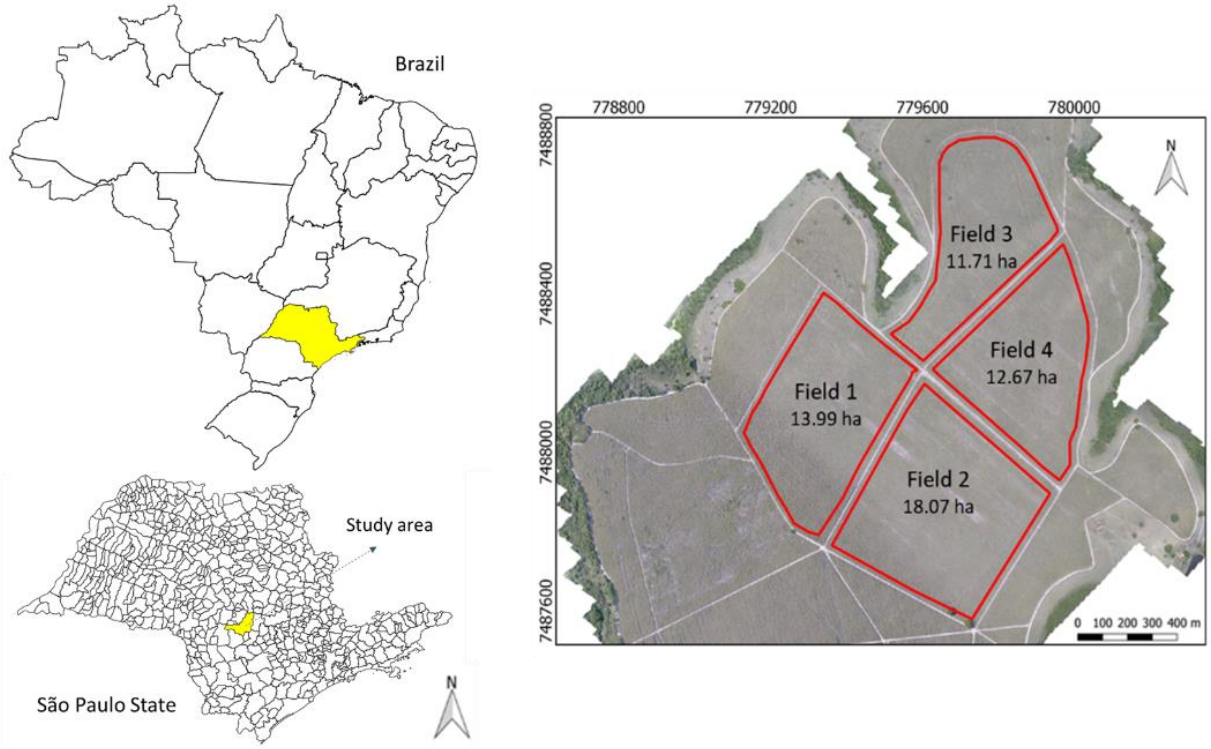


**Figure 1.** Location of sugarcane study site

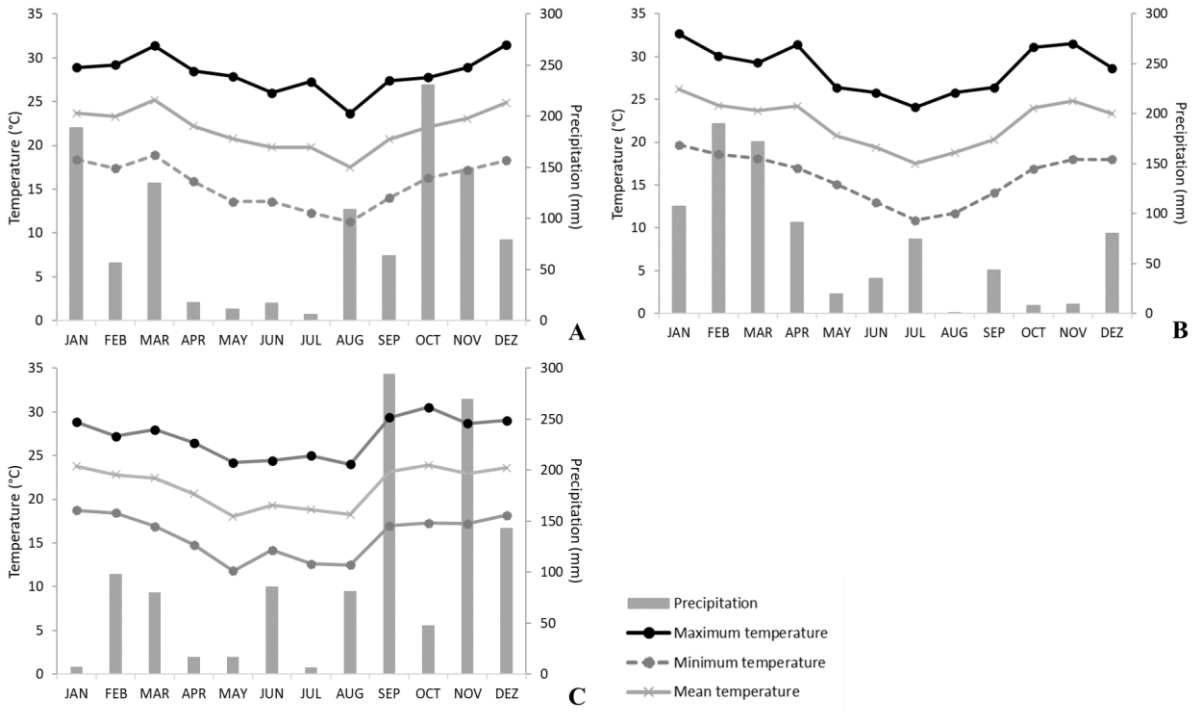


**Figure 2.** Air temperature and precipitation values from the region of study site for the 2018/2019 growing season (A) 2019/2020 season (B); 2020/2021 season (C). Source: CIIAGRO (2021)

### 4.2.2. Imagery data

The orbital images from Sentinel-2 were used for this study. This satellite constellation uses a multi-spectral instrument with 13 spectral channels with a 290 km swath width. All images were downloaded without charge from the United States Geological Survey (USGS) via Earth Explorer website. The images were selected with low cloud cover (<1%) and clipped to the region of interest. All images were projected on the WGS/UTM zone 22S. An internal buffer of 5 m was applied to each field boundary using Quantum Geographic Information System (QGIS 2.18.26, 2018) to ensure that the spectral data corresponded to the sugarcane plants. The original orbital images were submitted to atmospheric correction before each VIs calculation using a free open-source plugin Semi-Automatic Classification 5.4.2 (CONGEDO, 2016) on QGIS 2.18.26 (2018). This procedure was done to convert the digital numbers to reflectance data, considering the DOS1 (Dark Object Subtraction) atmospheric correction methodology (CHAVEZ, 1996). Five spectral bands from Sentinel-2 were considered in this study (Table 1). The most common VIs cited in the literature for crop yield monitoring were calculated. Four VIs were evaluated (Table 2) throughout the sugarcane development cycle, which included the NDVI (ROUSE et al., 1974), Normalized Difference Red-Edge Index (NDRE) (BARNES et al., 2000), GNDVI (GITELSON et al., 1996), and Wide Dynamic Range Vegetation Index (WDRVI) (GITELSON, 2004). As suggested by Abrahão et al. (2009) and Maresma et al. (2018) the value 0.10 was adopted for the weighting coefficient (a) of WDRVI.

**Table 1.** Specifications of the spectral bands from Sentinel-2

| Spectral bands | Central wavelength (nm) | Resolution | | |
|---|---|---|---|---|
| | | Spatial (m) | Temporal (days) | Radiometric (bits) |
| B2 Blue | 490 | 10 | 5 | 12 |
| B3 Green | 560 | | | |
| B4 Red | 665 | | | |
| B8 NIR | 842 | | | |
| B5 Red-Edge | 705 | 20 | | |

NIR: *Near-infrared*

**Table 2.** Vegetation indexes considered in the study

| Vegetation indexes | Equation | Authors |
|---|---|---|
| Normalized Difference Vegetation Index | NDVI = (NIR – Red) / (NIR + Red) | Rouse et al. (1974) |
| Normalized Difference Red-Edge Index | NDRE = (NIR – Red-edge) / (NIR + Red-edge) | Barnes et al. (2000) |
| Green Normalized Difference Vegetation Index | GNDVI = (NIR – Green) / (NIR + Green) | Gitelson et al. (1996) |
| Wide Dynamic Range Vegetation Index | WDRVI = (a x NIR - Red)/(a x NIR + Red) | Gitelson (2004) |

Red: reflectance in the red region (630 nm - 685 nm); red-edge: reflectance in the transition region (690 nm - 730 nm); NIR: reflectance in the near-infrared region (760 nm - 1500 nm); Green: reflectance in the green region (542 nm - 578 nm); a: weighting coefficient (0.10)

Table 3 summarizes the dates of orbital images taken and the respective phenological stage of sugarcane according to Matsuoka and Stolf (2012). Each phenological stage was identified according to the DAC to standardize the variables for data processing of all seasons. No images for the initial and maturation crop stages were found without cloud cover.

**Table 3.** Dates of the orbital images and respective phenological stages of sugarcane

| ID | DAC | Orbital images (month/day) | | | Phenological stage |
|---|---|---|---|---|---|
| | | 2018 | 2019 | 2020 | |
| T1 | 90 | 02/04; 02/09; 02/24 | 02/09 | 02/14; 03/05 | Tillering |
| T2 | 120 | 03/06; 03/11; 03/16; 03/21 | 03/06; 03/26; 03/31 | 03/15; 03/25 | Tillering |
| T3 | 150 | 04/05; 04/20; 04/25; 04/30 | 04/20; 04/25 | 04/04; 04/19; 04/29 | Tillering |
| D1 | 180 | 05/20; 05/30 | 05/05; 05/30 | 05/09; 05/19; 05/29 | Development |
| D2 | 210 | 06/19; 06/29 | 06/09; 06/14; 06/24; 06/29 | 06/13; 06/18 | Development |
| D3 | 240 | 07/04; 07/09; 07/14; 07/19; 07/24; 07/29 | 07/09; 07/14; 07/24 | 07/13; 07/23 | Development |
| R1 | 270 | 08/13; 08/18; 08/23; 08/28 | 08/08; 08/18; 08/23; 08/28 | 08/02; 08/12; 08/27 | Ripening |
| R2 | 300 | 09/07; 09/22 | 09/07; 09/12; 09/17 | 09/06; 09/26 | Ripening |
| R3 | 330 | 10/12; 10/22 | 10/02; 10/12; 10/17 | 10/11 | Ripening |

ID: identification; DAC: days after cutting

### 4.2.3. Development of predictive models

The methodology for generating the sugarcane yield maps used as reference for modeling is described in 3.2.4 subsection. The main difference was the spatial resolution adopted (10 m x 10 m) for the semivariogram calculation. Aware of the uneven availability of orbital images from year to year, it was used the average value of the orbital imagery data that composed each phenological stage. For example, in season 2017/2018, the value set to the ripening stage 1 (R1) was the average spectral value of the images from "08/13", "08/18", "08/23" and "08/28". Thus, as the four fields present the same variable predictors (imagery data), the dataset from all seasons were grouped. Two approaches were carried out to predict sugarcane yield at the field level based on MLR and RF regression. Approach I: the developed yield prediction model from the dataset of 2018/2019 and 2019/2020 seasons (CANATA et al., 2021) was applied on dataset of 2020/2021 season; Approach II: developing a unique yield prediction model considering the three consecutive crop seasons for the same fields. In this case, the number of observations from the entire dataset was randomly divided into the training (2/3) and testing (1/3). All statistical analyses and yield prediction models were performed using the R 3.5.5 software (2018) with the built-in function *lm* for the MLR model, and *randomForest* from the random forest package (LIAW and WIENER, 2002) for RF regression. As it is required that the results are reproducible, the function *set.seed* was used with the value 123 before fitting the predictive models.

The predictive yield model based on MLR was fitted for each type of predictor variables (spectral bands, GNDVI, NDVI, NDRE, and WDRVI). Aiming to improve MLR prediction accuracy, the variable selection was carried out relying on the p-value < 0.05, and that process was conducted until all the predictor variables that had a p-value > 0.05 were eliminated. To find the p-value, the built-in function *summary* from R 3.5.5 software (2018) was used. An additional exploratory analysis was the spatial correlation between the VIs for each period of the sugarcane development cycle and yield data using Pearson's correlation coefficient (r). The synthesis of the methodology is shown in Figure 3. For both models (RF and MLR), the independent variables were the reflectance values of the spectral bands (totaling 45 spectral band variables; 5 bands times 9 dates) and derived VIs (totaling 36 VIs variables; 4 VIs times 9 dates). The observed sugarcane yield (measured by the on-board sensor-system) was the dependent variable to be predicted. For RF regression predictions, it was necessary to fine-tune two parameters: (a) *ntree*, the average result of many trees; and (b) *mtry*, predictor subset value. To find the best *ntree* value, the prediction error rate

for a range of 0 to 500 was calculated, and the one that presented the lowest error before stabilization was selected (*elbow rule*) (TRACY et al., 2016). In both cases, the *mtry* selection was based on the lowest RMSE. All models were compared considering the $R^2$, RMSE, and MAE.

## 4.3. Results and discussion

### 4.3.1. Statistical analysis

The descriptive statistics of the original and filtered yield data are presented in Table 4. The filtered yield data ranged from 43 to 82 Mg $ha^{-1}$ for the 2018/2019 crop season, from 44 to 108 Mg $ha^{-1}$ for the 2019/2020 crop season, and from 40 to 139 Mg $ha^{-1}$ for the 2020/2021 crop season. The coefficient of variation (CV) of the filtered data was 9% for the 2018/2019 crop season, 13% for the 2019/2020 crop season, and 20% for the subsequent season. The results highlighted that there is a requirement to exclude discrepant values from the original data to better understand the actual spatial variability of the fields, for that, the data filtering was carried out to decrease values of the standard deviation (SD) and the average sugarcane yield. For the 2019/2020 season, the mean yield increased about 11% compared with the previous season, which was not expected because of the decreased yield values over the number of ratoons. But the highest precipitation during the tillering crop stage may have benefited the increase in production.

**Table 4.** Descriptive statistics of the sugarcane yield data considering all fields

| Season | Dataset | n | Minimum | Median | Mean | Maximum | SD | CV (%) |
|---|---|---|---|---|---|---|---|---|
| | | | Mg $ha^{-1}$ | | | | | |
| 2018/2019 | Original | 53,759 | 0.86 | 70.85 | 71.20 | 501.23 | 23.53 | 33.04 |
| | Filtered | 16,202 | 42.74 | 64.28 | 63.98 | 81.97 | 5.75 | 8.99 |
| 2019/2020 | Original | 67,716 | 10.39 | 72.52 | 112.90 | 498.21 | 81.96 | 72.60 |
| | Filtered | 28,247 | 43.54 | 70.88 | 70.97 | 107.90 | 9.12 | 12.85 |
| 2020/2021 | Original | 62,811 | 0.01 | 76.28 | 85.08 | 555.84 | 26.22 | 40.29 |
| | Filtered | 21,199 | 40.01 | 73.56 | 73.70 | 139.17 | 14.85 | 20.15 |

n: number of samples; SD: standard deviation; CV: coefficient of variation

Despite the exclusion of more than 50% of the original data, which was expected due to the local and global filtering (MALDANER and MOLIN, 2020), the number of points per hectare was, at least, 16 samples $ha^{-1}$ according to the calculated grid (RIPLEY, 1981). Table 5 summarizes the best-adjusted variogram model used for interpolating yield data with an RMSE of 0.53 Mg $ha^{-1}$ for the 2018/2019 season, 1.41 Mg $ha^{-1}$ for the 2019/2020 season, and 1.49 Mg $ha^{-1}$ for the 2020/2021 season.

**Table 5.** Fitted model and semi-variogram variables used to interpolate sugarcane yield data

| Season | Model | Range (m) | Sill | Nugget | RMSE (Mg ha$^{-1}$) | Calc. grid (samples ha$^{-1}$) |
|---|---|---|---|---|---|---|
| 2018/2019 | Exponential | 42.04 | 33.79 | 12.95 | 0.53 | 23 |
| 2019/2020 | Exponential | 49.30 | 23.54 | 5.19 | 1.41 | 16 |
| 2020/2021 | Exponential | 41.04 | 32.53 | 11.18 | 1.49 | 24 |

RMSE: root mean squared error; Calc. grid: calculated grid (= 10,000/(0.5 Range))$^2$

The sugarcane yield maps for each crop season are presented in Figure 3 as a data layer to assess the spatio-temporal variability of the sugarcane fields considering all seasons. An exploratory analysis of the dataset indicated that the linear correlation between the VIs and sugarcane yield maps did not present values greater than 0.50. Such results will negatively influence the MLR prediction accuracy since there is no strong linear relationship among dependent and independent variables. The same condition was pointed out by Pissolito et al. (2020). That is the main reason for combining multiple imagery data (time-series) and RF regression as an alternative technique to perform yield prediction. The temporal variability of the sugarcane fields did not demonstrate consistency over the years, considering that it was not found the same spots of yield for the same field. This result can influence the performance of the predictive yield models when applying one established model to another dataset, such as the subsequent season.

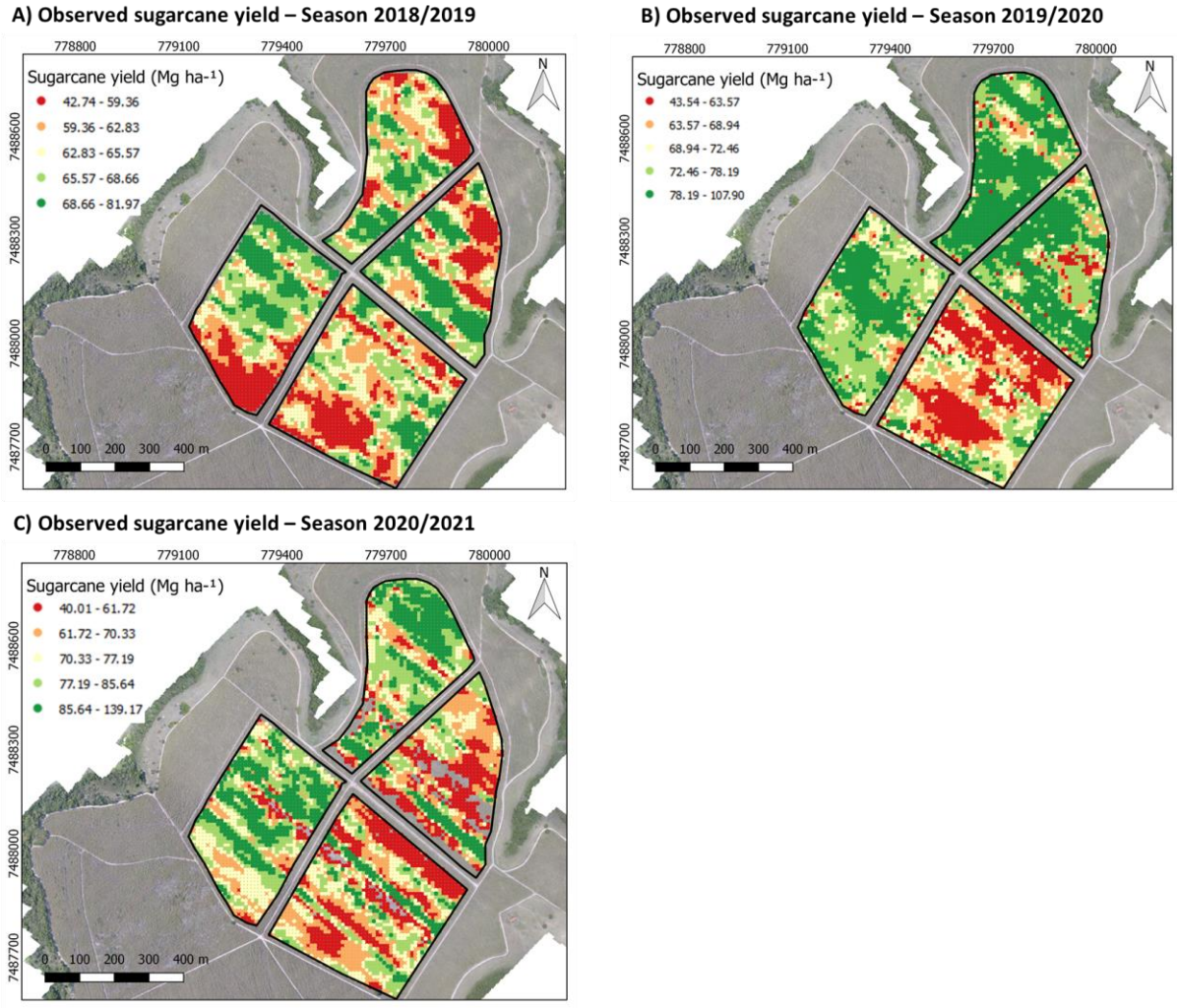


**Figure 3.** Sugarcane yield maps of 2018/2019 season (A); 2019/2020 season (B); 2020/2021 season (C)

Figure 4 demonstrates the crop vigor mapping based on NDRE for the transition from tillering to development crop stage, as indicated in Canata et al. (2021), as a potential data source for assessing the spatio-temporal variability of the sugarcane fields based on local spots of crop vigor variation over the seasons (Figure 4A – 2018/2019 season; Figure 4B - 2019/2020 season; Figure 4C – 2020/2021 season). The cause of the crop vigor variation can be associated with the consequences of phenotypic changes, such as water stress, nutritional limitations, incidence of disease and pests, that reduce crop yield. Thus, the identification of the spectral response of the crop through satellite imagery supports the decision-making for local recommendations along the development crop cycle. Other studies also suggested the use of the red-edge spectral band as an alternative to reduce the influence of soil background at the early stages of wheat, as well as saturation for later phenological stages of the crop (LI et al., 2019). A similar approach was proposed by Cui et al. (2018) and Sun et al. (2019) for estimating LAI of canopy trees. Rocha et al. (2019) applied RF regression to estimate sugarcane biomass in the early stages of crop development, considering the association between the biometrics characteristics of the crop, such as number and height of stalks, and the reflectance data from active crop canopy sensors. The relative error considering NDRE as a predictor variable of sugarcane biomass was about 7.0 Mg $ha^{-1}$.

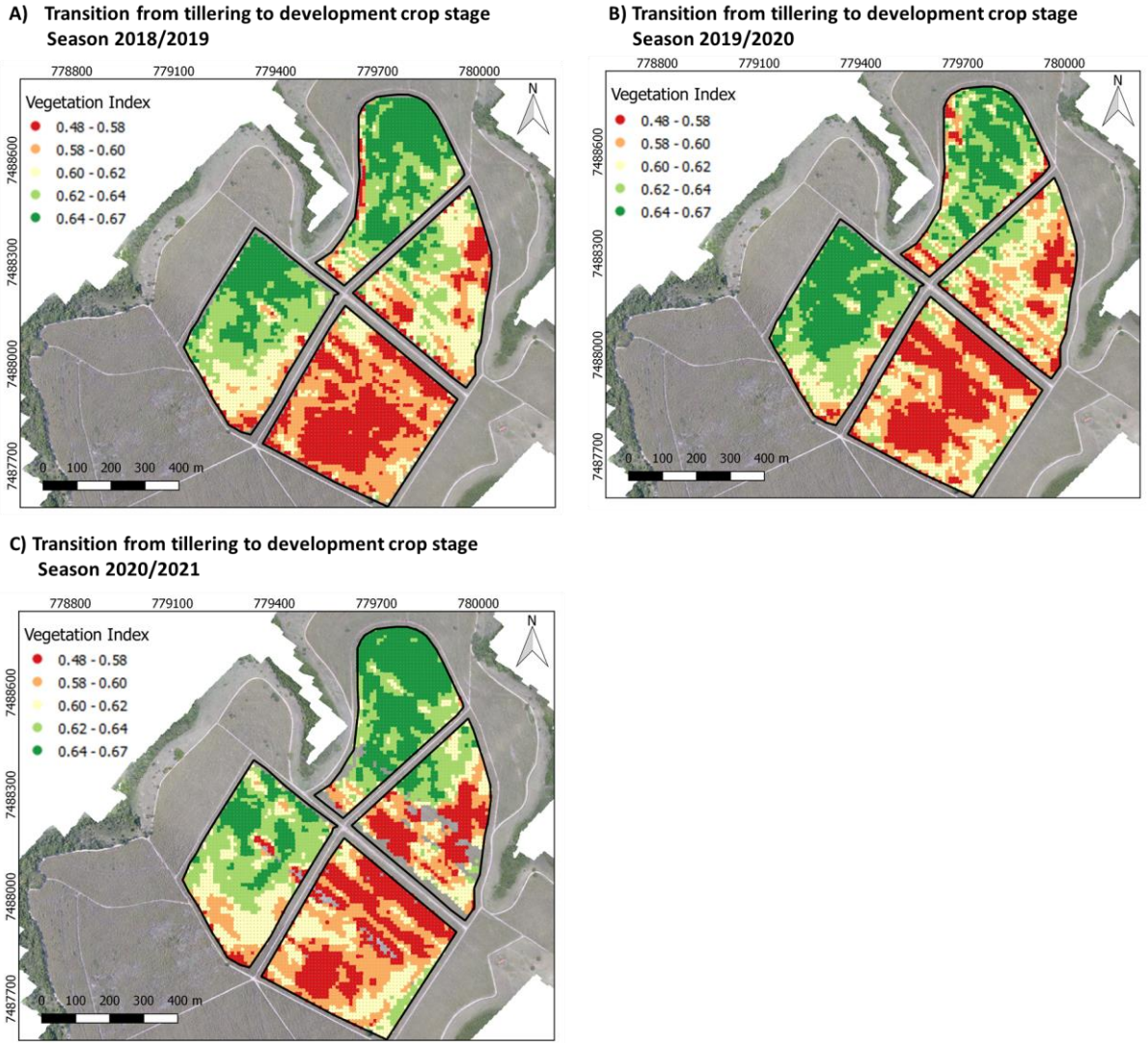


**Figure 4.** Crop vigor mapping based on Normalized Difference Red Edge Index - NDRE considering the transition from tillering to development crop stage for 2018/2019 season (A); 2019/2020 season (B); 2020/2021 season (C)

### 4.3.2. Accuracy assessment of yield modeling

For RF regression the parameter *ntree* was equal to 100 for both spectral bands and derived-VIs models. For *mtry*, values from 2 to 45 (maximum number of predictors variables, excluding those were variance was close to zero) were applied for the spectral bands, with 26 being used. For the VIs models, values from 2 to 9 were tested, with 2 being selected. Table 6 demonstrates the accuracy metrics used to compare the performance of the proposed approaches based on MLR and RF regression for testing dataset. Approach I did not present a greater accuracy considering the variables from spectral bands and VIs, mainly due to the limited performance of modeling applied across different seasons (JEFFRIES et al., 2020; COLAÇO and BRAMLEY, 2019). In this case, the RMSE obtained for RF regression was about 15 Mg $ha^{-1}$. Approach II presented better performance regarding RMSE, $R^2$, and MAE values for RF regression, compared with Approach I, considering the spectral bands variables (RMSE of 7.0 Mg $ha^{-1}$ and $R^2$=0.61). Comparing NDVI, GNDVI, NDRE, and WDRVI, they all presented similar accuracy results for estimating sugarcane yield. These results, except for NDRE, corroborate the results presented in Zhao et al. (2016) that reported no significant difference among the use of GNDVI, NDVI, and WDRVI for predicting sugarcane crop

growth and yield. However, their approach based on linear regression models was different from the one in this study that tested both linear and non-linear models, as it was noted that the non-linear (RF regression) model performed better, independent of the type of predictor variables. For modeling based on MLR, the results of Approach II demonstrated lower $R^2$ (about 0.40) and higher RMSE (about 9.0 Mg $ha^{-1}$), compared to the RF regression. Other studies also reported RF prediction as more accurate than MLR method (LUCIANO et al., 2021; WEI et al., 2020; KAYAD et al., 2019). More details regarding the accuracy of the predictive yield models for different predictor variables considering 2018/2019 and 2019/2020 sugarcane seasons are described in Canata et al. (2021). A refinement of the model should include environmental variables and agricultural management practices because they influence on crop production can potentially improve the accuracy of predictive yield models. Also, this study considered a single site study, while the ideal condition to refine the modeling should involve multiple seasons and several commercial fields.

**Table 6.** Accuracy of the predictive yield models for testing dataset

| | | **RMSE (Mg $ha^{-1}$)** | | **$R^2$** | | **MAE (Mg $ha^{-1}$)** | |
|---|---|---|---|---|---|---|---|
| **Variables** | **Models** | Approach I | Approach II | Approach I | Approach II | Approach I | Approach II |
| Spectral bands | MLR | 19.23 | 8.51 | 0.07 | 0.44 | 7.76 | 6.03 |
| | RF | 13.98 | 7.08 | 0.26 | 0.61 | 10.53 | 4.72 |
| GNDVI | MLR | 35.42 | 8.74 | 0.09 | 0.41 | 25.86 | 6.25 |
| | RF | 13.98 | 7.92 | 0.25 | 0.51 | 10.57 | 5.48 |
| NDRE | MLR | 31.60 | 8.88 | 0.10 | 0.39 | 22.93 | 6.37 |
| | RF | 13.15 | 7.79 | 0.26 | 0.53 | 9.79 | 5.35 |
| NDVI | MLR | 68.87 | 8.78 | 0.08 | 0.40 | 45.99 | 6.25 |
| | RF | 14.05 | 7.83 | 0.21 | 0.54 | 10.59 | 5.38 |
| WDRVI | MLR | 58.68 | 8.77 | 0.04 | 0.40 | 39.03 | 6.25 |
| | RF | 17.75 | 7.89 | 0.03 | 0.51 | 13.73 | 5.43 |

MLR: Multiple Linear Regression; RF: Random Forest; RMSE: root-mean-square error; MAE: mean absolute error

The spectral bands were more effective (the highest $R^2$ and the lowest RMSE) in estimating sugarcane yield for both models. In other words, better results were found using the spectral bands directly rather than calculating Vis. This result should influence the computational processing of orbital images because it is less time-consuming to analyze spectral bands when compared to the normalization of the reflectance values. Also, once associated with the crop vigor, the amount of biomass has a high degree of correlation with the spectral behavior of the plants. So, a relationship can be used in the process of remotely estimating or predicting harvests (VARELLA et al., 2015). It was expected that linear approaches, such as MLR, that predict yield based on VIs would present worse accuracy performance than non-linear models like RF regression. Zhao et al. (2016) applied MLR with spectral bands and simple linear regression with NDVI to predict sugarcane yield and found that MLR did not improve accuracy when compared to the simple linear regression. Thus, they proceeded using the simple linear regression and found $R^2$ values ranging from 0.22 to 0.41. Despite the higher $R^2$ found in the MLR model, the RF regression is the model that outperformed the linear approach, highlighting its suitability to be used to support yield prediction models based on orbital images. Dubey et al. (2018) developed a time-series analysis for VIs to forecast sugarcane yield based on empirical models with RMSE values ranging from 7.0 to 17.0 Mg $ha^{-1}$, but such analysis was conducted at the district level. Considering the Approach II as the best modeling for sugarcane yield prediction, the predicted values based on RF regression for each variable are shown in Figure 5 for the 2018/2019 season (Figure 5A – spectral bands; Figure 5B – GNDVI; Figure 5C – NDRE; Figure 5D – NDVI; Figure 5E – WDRVI). Which supports the similarity with

the spatial patterns found in observed sugarcane yield maps at the field level (Figure 3A). The predicted yield maps based on RF regression using the same Approach for 2019/2020 and 2020/2021 seasons are shown in Figure 6 and Figure 7, respectively. The predicted yield maps based on MLR and Approach II for all seasons are shown in Appendices from D to F.

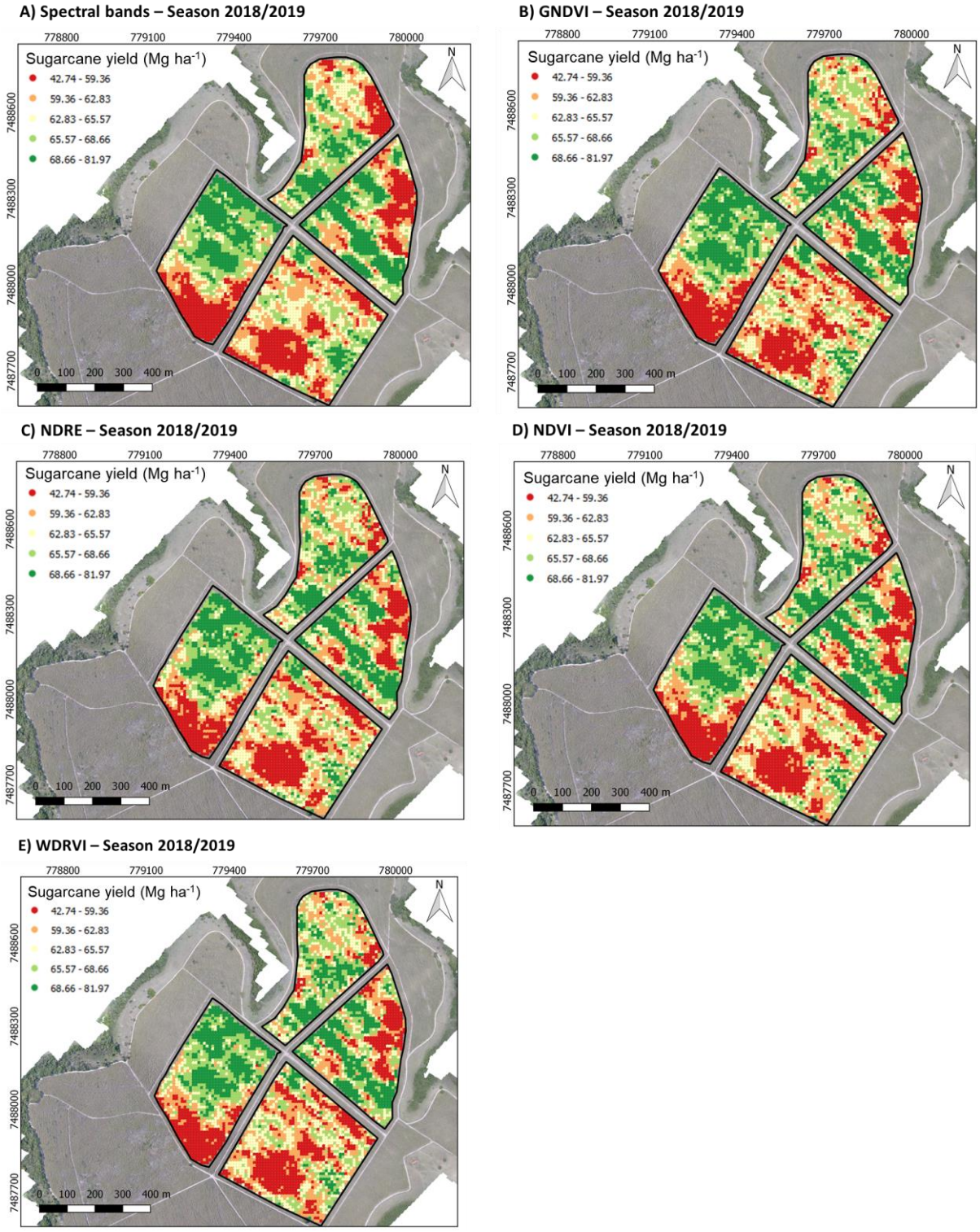


**Figure 5.** Predicted sugarcane yield maps based on Random Forest regression for the 2018/2019 season using Spectral Bands (A); Green Normalized Difference Vegetation Index - GNDVI (B); Normalized Difference Red Edge Index - NDRE (C); Normalized Difference Vegetation Index - NDVI (D); Wide Dynamic Range Vegetation Index - WDRVI (E)

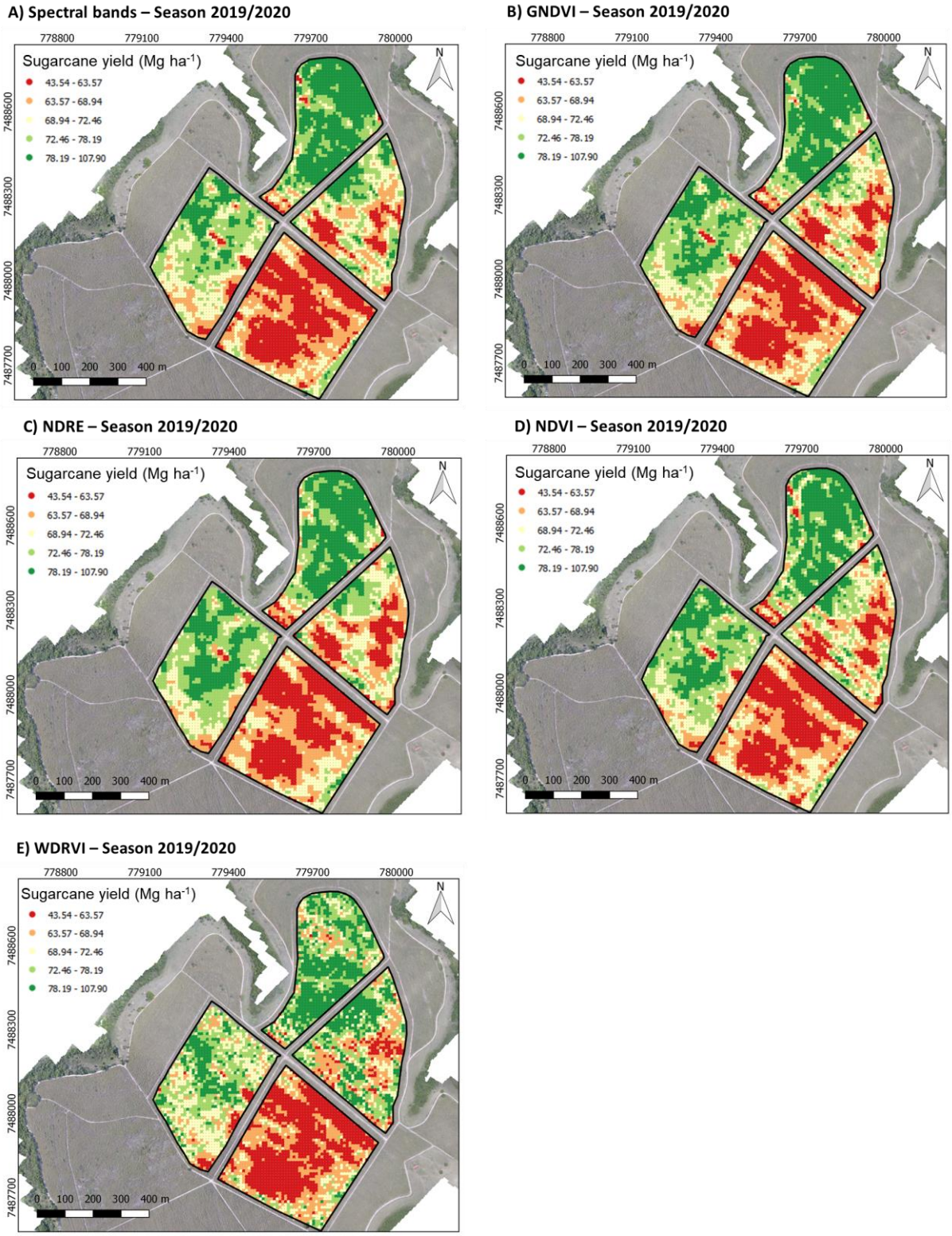


**Figure 6.** Predicted sugarcane yield maps based on Random Forest regression for the 2019/2020 season using Spectral Bands (A); Green Normalized Difference Vegetation Index - GNDVI (B); Normalized Difference Red Edge Index - NDRE (C); Normalized Difference Vegetation Index - NDVI (D); Wide Dynamic Range Vegetation Index - WDRVI (E)

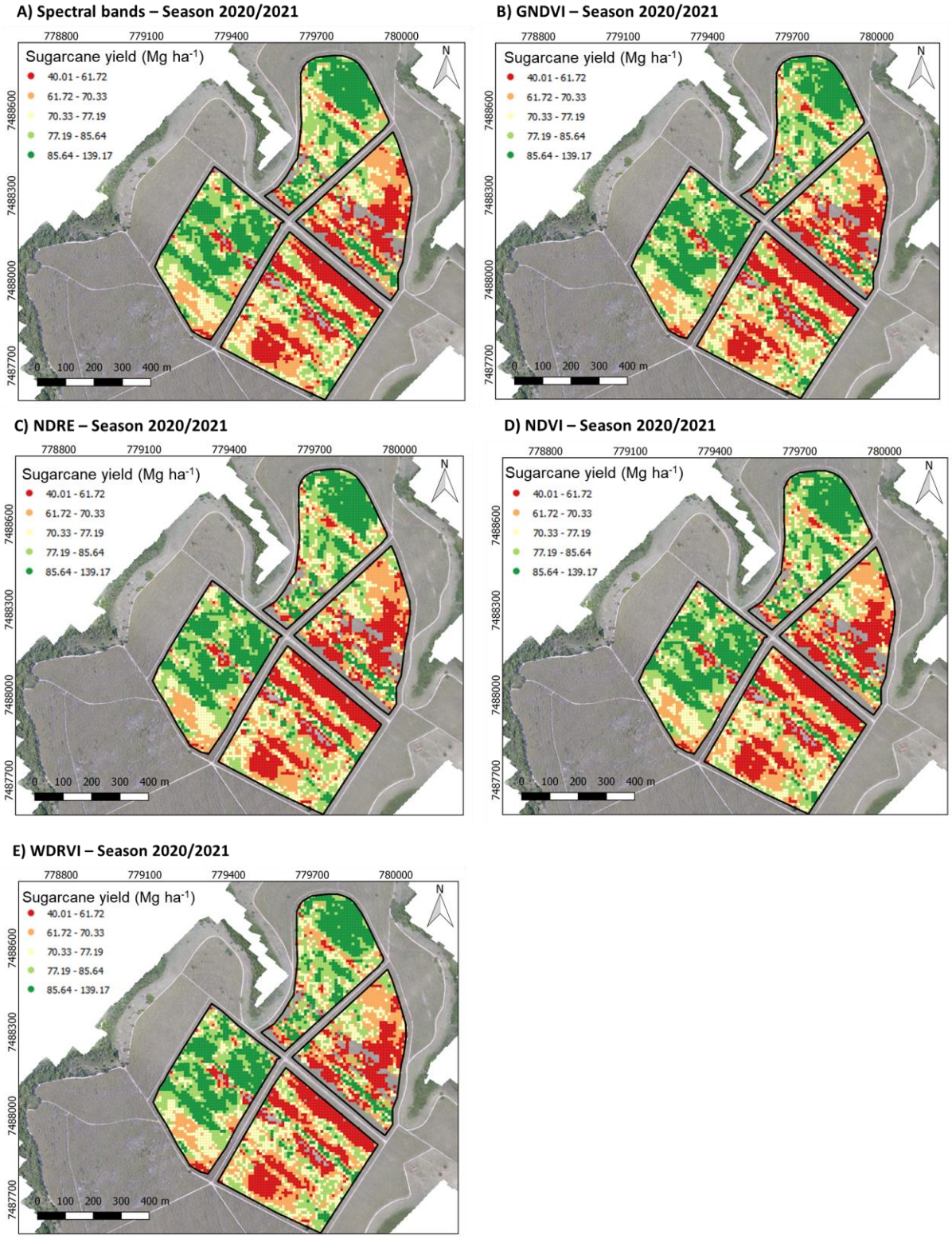


**Figure 7.** Predicted sugarcane yield maps based on Random Forest regression for the 2020/2021 season using Spectral Bands (A); Green Normalized Difference Vegetation Index - GNDVI (B); Normalized Difference Red Edge Index - NDRE (C); Normalized Difference Vegetation Index - NDVI (D); Wide Dynamic Range Vegetation Index - WDRVI (E)

This study presents a first approach to explore the multi-temporal satellite-based method to determine sugarcane yield at the field level. The predictor variables from 74 orbital images for each phenological crop stage

included, individually, values of five spectral bands and four VIs with a spatial resolution of 10 m x 10 m assigned to compose the data used to infer the potential of MLR and RF regression methods to estimate sugarcane yield. Also, the type of input predictors for both models were evaluated to fit the predictive models using high-resolution data. The study demonstrates the potential of using spectral bands as an alternative approach to the common crop yield forecast based on VIs (LUCIANO et al., 2021; DUBEY et al., 2018; LISBOA et al., 2018; MOREL et al., 2014). The spatial variability of the sugarcane fields was mapped for the range of yield data values across all fields over the three consecutive seasons. The association of high-resolution imagery data and ML technique showed satisfactory results for estimating and mapping sugarcane yield, which can be applied for supporting PA practices and, also, to provide a better understanding of the spatial variability within-field over the seasons. The time-series analysis of orbital images enabled the development of a methodology based on ML technique to advance on understanding the spatio-temporal variability of sugarcane fields. It helps to improve the decision-making process, as imagery data can provide relevant information regarding the potential of production over the season and locally. Future research on RS techniques for crop monitoring should also aim at near real-time diagnostics of crop status to support local interventions and optimize agricultural production. The advantages of RS applications for agricultural systems involve advancing on integrating machinery operation according to the field conditions, which can be assessed with greater accuracy than traditional methods that usually involve low-scale and labor-intensive.

## 4.4. Conclusion

Integrating multi-temporal imagery data from Sentinel-2 and Random Forest regression enabled the development of predictive yield models at the field level. The use of spectral bands outperformed derived-VIs, mainly considering the reflectance data of transition from tillering to development crop stage. The approach using a unique yield prediction model considering the three consecutive crop seasons for the same fields demonstrated greater accuracy than the model applied for an individual season. Also, Random Forest regression showed greater accuracy (lowest RMSE and higher $R^2$) when compared with the Multiple Linear Regression for both approaches. Overall, spatial patterns were mapped using time-series analysis of imagery data along the crop cycle, mainly based on NDRE, demonstrating different potential levels of production at the field level before harvesting.

## References

ABDEL-RAHMAN, E. M.; AHMED, F. B. 2008. The application of remote sensing techniques to sugarcane (*Saccharum* spp. hybrid) production: a review of the literature, **International Journal of Remote Sensing**, 29(13): 3753-3767. doi: 10.1080/01431160701874603.

ABDEL-RAHMAN, E.; AHMED, F. B.; RIYAD, I. 2012. Random forest regression for sugarcane yield prediction based on Landsat TM derived spectral parameters. In: Sugarcane: Production, Cultivation and Uses. Chapter 10.

ABRAHÃO, S. A.; PINTO, F. de A. de C.; QUEIROZ, D. M. de; SANTOS, N. T.; GLERIANI, J. M.; ALVES, E. A. 2009. Índices de vegetação de base espectral para discriminar doses de nitrogênio em capim-tanzânia. **Revista Brasileira de Zootecnia**, 38(9): 1637-1644. doi: 10.1590/S1516-35982009000900001.

BAIO, F. H. R.; NEVES, D. C.; CAMPOS, C. N. S.; TEODORO, P. E. 2018. Relationship between cotton productivity and variability of NDVI obtained by Landsat images. **Bioscience Journal**, 34(6): 197–205. doi: 10.14393/BJ-v34n6a2018-39583.

BARBOSA, A.; TREVISAN, R.; HOVAKIMYAN, N.; MARTIN, N. F. 2020. Modeling yield response to crop management using convolutional neural networks. **Computers and Electronics in Agriculture**, 170: 105197. doi: 10.1016/j.compag.2019.105197.

BARNES, E. M.; CLARKE, T. R.; RICHARDS, S. E.; COLAIZZI, P. D.; HABERLAND, J.; KOSTRZEWSKI, M.; WALLER, P.; CHOI, C.; RILEY, E.; THOMPSON, T.; LASCANO, R. J.; LI, H.; MORAN, M. S. 2000. Coincident detection of crop water stress, nitrogen status and canopy density using ground-based multispectral data. In: 5th International Conference on Precision Agriculture**. Proceedings**... 2000.

BÉGUÉ, A.; LEBOURGEOIS, V.; BAPPEL, E.; TODOROFF, P.; PELLEGRINO, A.; BAILLARIN, F.; SIEGMUND, B. 2010. Spatio-temporal variability of sugarcane fields and recommendations for yield forecast using NDVI. **International Journal of Remote Sensing**, 31(20): 5391-5407. doi: 10.1080/01431160903349057.

BRAMLEY, R. G. V.; OUZMAN, J.; GOBBETT, D. L. 2019. Regional scale application of the precision agriculture thought process to promote improved fertilizer management in the Australian sugar industry. **Precision Agriculture**, 20: 362-378. doi: 10.1007/s11119-018-9571-8.

CANATA, T. F.; WEI, M. C. F.; MALDANER, L. F.; MOLIN, J. P. 2021. Sugarcane Yield Mapping Using High-Resolution Imagery Data and Machine Learning Technique. **Remote Sensing**, 13(2): 232. doi: 10.3390/rs13020232.

CHAVEZ, P. Jr. 1996. Image-Based Atmospheric Corrections - Revisited and Improved. **Photogrammetric Engineering and Remote Sensing**, 62(9): 1025-1036.

CONGEDO, L. 2016. Semi-Automatic Classification Plugin Documentation. doi: http://dx.doi.org/10.13140/RG.2.2.29474.02242/1.

CISNEROS, A.; FIORIO, P.; MENEZES, P.; PASQUALOTTO, N.; VAN WITTENBERGHE, S.; BAYMA, G.; FURLAN NOGUEIRA, S. 2020. Mapping Productivity and Essential Biophysical Parameters of Cultivated Tropical Grasslands from Sentinel-2 Imagery. **Agronomy**, 10(5): 711. doi: 10.3390/agronomy10050711.

COLAÇO, A. F.; BRAMLEY, R. 2019. Site–Year Characteristics Have a Critical Impact on Crop Sensor Calibrations for Nitrogen Recommendations. **Agronomy Journal**, 111(4):2047-2059. doi: 10.2134/agronj2018.11.0726.

CUI, Z.; KEREKES, J. P. 2018. Potential of Red Edge Spectral Bands in Future Landsat Satellites on Agroecosystem Canopy Green Leaf Area Index Retrieval. **Remote Sensing**, 10(9): 1458. doi: 10.3390/rs10091458.

DUBEY, S. K.; GAVLI, A. S.; YADAV, S. K.; SEHGAL, S.; RAY, S. S. 2018. Remote Sensing-Based Yield Forecasting for Sugarcane (*Saccharum officinarum* L.) Crop in India. **Journal of the Indian Society of Remote Sensing**, 46: 1823–1833. doi: 10.1007/s12524-018-0839-2.

EMBRAPA - Empresa Brasileira de Pesquisa Agropecuária. 2013. Sistema Brasileiro de Classificação de Solos (3rd ed. Rev. ampl., p. 353). Brasília, DF: Empresa Brasileira de Pesquisa Agropecuária (Embrapa).

FULTON, J. P.; PORT, K. 2018. Precision agriculture data management. In: D.K. Shannon; D.E. Clay; N.R. Kitchen. Precision Agriculture Basics. ASA, CSSA, SSSA, Madison, WI.

GITELSON, A. A.; KAUFMAN, Y. J.; MERZLYAK, M. N. 1996. Use of a green channel in remote sensing of global vegetation from EOS- MODIS. **Remote Sensing of Environment**, 58(3): 289-298.

GITELSON, A. A. 2004. Wide Dynamic Range Vegetation Index for Remote Quantification of Crop Biophysical Characteristics. **Journal of Plant Physiology**, 161(2): 165–173. doi: 10.1078/0176-1617-01176.

JEFFRIES, G. R.; GRIFFIN, T. S.; FLEISHER, D. H.; NAUMOVA, E. N.; KOCH, M.; WARDLOW, B. D. 2020. Mapping sub-field maize yields in Nebraska, USA by combining remote sensing imagery, crop simulation models, and machine learning. **Precision Agriculture**, 21: 678–694. doi: 10.1007/s11119-019-09689-z.

HAN, L.; YANG, G.; DAI, H.; XU, B.; YANG, H.; FENG, H.; LI, Z.; YANG, X. 2019. Modeling maize above-ground biomass based on machine learning approaches using UAV remote-sensing data. **Plant Methods** 15(10): 1–19. doi: 10.1186/s13007-019-0394-z.

HAMMER, R. G.; SENTELHAS, P. C.; MARIANO, J. C. Q. 2019. Sugarcane yield prediction through data mining and crop simulation models. **Sugar Tech**, 22: 216-225. doi: 10.1007/s12355-019-00776-z.

HOCHACHKA, W. M.; CARUANA, R.; FINK, D.; MUNSON, A.; RIEDEWALD, D.; SOROKINA, D.; KELLING, S. 2007. Data-mining discovery of pattern and process in ecological systems. **Journal of Wildlife Management**, 71(7): 2427–2437. doi: 10.2193/2006-503.

HUNT, M. L.; BLACKBURN, G. A.; CARRASCO, L.; REDHEAD, J. W.; ROWLAND, C. S. 2019. High resolution wheat yield mapping using Sentinel-2. **Remote Sensing of Environment**, 233: 111410. doi: 10.1016/j.rse.2019.111410.

KAYAD, A.; SOZZI, M.; GATTO, S.; MARINELLO, F.; PIROTTI, F. 2019. Monitoring within-field variability of corn yield using Sentinel-2 and machine learning techniques. **Remote Sensing**, 11(23): 2873. doi: 10.3390/rs11232873.

KHALIQ, A.; COMBA, L.; BIGLIA, A.; AIMONINO, D. R.; CHIABERGE, M.; GAY, P. 2019. Comparison of satellite and UAV-based multispectral imagery for vineyard variability assessment. **Remote Sensing**, 11(4): 436. doi:10.3390/rs11040436.

JEONG, J. H.; RESOP, J. P.; MUELLER, N. D.; FLEISHER, D. H.; YUN, K.; BUTLER, E. E.; TIMLIN, D. J.; SHIM, K. M.; GERBER, J. S.; REDDY, V. R.; KIM, S. H. 2016. Random forests for global and regional crop yield predictions. **PLoS ONE**, 11, e0156571. doi: 10.1371/journal.pone.0156571.

LEVITAN, N.; GROSS, B. 2018. Utilizing collocated crop growth model simulations to train agronomic satellite retrieval algorithms. **Remote Sensing**, 10(12): 1968. doi: 10.3390/rs10121968.

LI, W.; JIANG, J.; GUO, T.; ZHOU, M.; TANG, Y.; WANG, Y.; ZHANG, Y.; CHENG, T.; ZHU, Y.; CAO, W.; YAO, X. 2019. Generating Red-Edge Images at 3 M Spatial Resolution by Fusing Sentinel-2 and Planet Satellite Products. **Remote Sensing**, 11(12): 1422. doi: 10.3390/rs11121422.

LIAW, A.; WIENER, M. 2002. Classification and Regression by randomForest. R News 2/3:18–22.

LISBOA, I. P.; DAMIAN, J. M.; CHERUBIN, M. R.; BARROS, P. P. S.; FIORIO, P. R.; CERRI, C. C.; CERRI, C. E. P. 2018. Prediction of sugarcane yield based on NDVI and concentration of leaf-tissue nutrients in fields managed with straw removal. **Agronomy**, 8(9): 196. doi: 10.3390/agronomy8090196.

LOBELL, D. B. 2013. The use of satellite data for crop yield gap analysis. **Field Crops Research**, 143: 56–64. doi: 10.1016/j.fcr.2012.08.008.

LOBELL, D. B.; THAU, D.; SEIFERT, C.; ENGLE, E.; LITTLE, B. 2015. A scalable satellite-based crop yield mapper. **Remote Sensing of Environment**, 164: 324–333. doi: 10.1016/j.rse.2015.04.021.

LUCIANO, A. C. S. dos; PICOLI, M. C. A.; DUFT, D. G.; ROCHA, J. V.; LEAL, M. R. L. V.; MAIRE, G. L. 2021. Empirical model for forecasting sugarcane yield on a local scale in Brazil using Landsat imagery and random forest algorithm. **Computers and Electronics in Agriculture**, 184: 106063. doi: 10.1016/j.compag.2021.106063.

MALDANER, L. F.; MOLIN, J. P. 2020. Data processing within rows for sugarcane yield mapping. **Scientia Agricola**, 77(5): e20180391. doi: 10.1590/1678-992x-2018-0391.

MARESMA, Á.; ARIZA, M.; MARTÍNEZ, E.; LLOVERAS, J.; MARTÍNEZ-CASASNOVAS, J. A. 2018. Analysis of Vegetation Indices to Determine Nitrogen Application and Yield Prediction in Maize (*Zea mays* L.) from a Standard UAV Service. **Remote Sensing**, 10(3): 368. doi: 10.3390/rs10030368.

MATSUOKA, S.; STOLF, R. 2012. Sugarcane tillering and ratooning: key factors for a profitable cropping. In: Sugarcane: Production, Cultivation and Uses. Editors: Gonçalves, J. F.; Correia, K. D. Nova Science Publishers, 5(2): 137-157.

MOMIN, M. A.; GRIFT, T. E.; VALENTE, D. S.; HANSEN, A. C. 2019. Sugarcane yield mapping based on vehicle tracking. **Precision Agriculture**, 20: 896–910. doi: 10.1007/s11119-018-9621-2.

MOREL, J.; BÉGUÉ, A.; TODOROFF, P.; MARTINÉ, J. F.; LEBOURGEOIS, V.; PETIT, M. 2014. Coupling a sugarcane crop model with the remotely sensed time series of fIPAR to optimise the yield estimation. **European Journal of Agronomy**, 61: 60-68. doi: 10.1016/j.eja.2014.08.004.

MULIANGA, B.; BÉGUÉ, A.; SIMOES, M.; TODOROFF, P. 2013. Forecasting Regional Sugarcane Yield Based on Time Integral and Spatial Aggregation of MODIS NDVI. **Remote Sensing,** 5(5): 2184-2199. doi: 10.3390/rs5052184.

MUTANGA, S.; SCHOOR, C.; OLORUNJU, P.; GONAH, T.; RAMOELO, A. 2013. Determining the Best Optimum Time for Predicting Sugarcane Yield Using Hyper-Temporal Satellite Imagery. **Advances in Remote Sensing**, 2(3): 269-275. doi: 10.4236/ars.2013.23029.

PISSOLITO, J.; BERSANI, V.; CANATA, T. F.; MALDANER, L. F.; MOLIN, J. P. 2020. High-resolution imagery data to assess the spatial variability of sugarcane fields. **Brazilian Journal of Development**, 6(12): 100266-100280. doi: 10.34117/bjdv6n12-500.

QGIS Development Team, 2018. QGIS Geographic Information System. Open-Source Geospatial Foundation Project. http://qgis.osgeo.org.

R Core Team. R: A Language and Environment for Statistical Computing; R Foundation for Statistical Computing: Vienna, Austria, 2018.

RAHMAN, M. M.; ROBSON, A. J. 2016. A Novel Approach for Sugarcane Yield Prediction Using Landsat Time Series Imagery: A Case Study on Bundaberg Region. **Advances in Remote Sensing**, 5(2): 93-102. doi: 10.4236/ars.2016.52008.

RAHMAN, M. M.; ROBSON, A. J. 2020. Integrating Landsat-8 and Sentinel-2 Time Series Data for Yield Prediction of Sugarcane Crops at the Block Level. **Remote Sensing**, 12(8): 1313. doi: 10.3390/rs12081313.

RIPLEY, B. D. 1981. **Spatial statistics**. John Wiley Sons. Chapter 3, New York.

ROCHA, M. G. da; BARROS, F. M. M. de; OLIVEIRA, S. R. M. de; AMARAL, L. R. do. 2019. Biometric characteristics and canopy reflectance association for early-stage sugarcane biomass prediction. **Scientia Agricola**, 76(4): 274-280. doi: 10.1590/1678-992X-2017-0301.

ROUSE, J. W.; HAAS, R. H.; SCHELL, J. A.; DEERING, D. W. 1974. Monitoring vegetation systems in the great plains with ERTS. In: Earth Resourses Technology Satellite – 1 Symposium. **Proceedings**... 1974. p. 309-317.

SCHWALBERT, R. A.; AMADO, T. J. C.; NIETO, L.; VARELA, S.; CORASSA, G. M.; HORBE, T. A. N.; RICE, C. W.; PERALTA, N. R.; CIAMPITTI, I. A. 2018. Forecasting maize yield at field scale based on high-resolution satellite imagery. **Biosystems Engineering**, 171: 179–192. doi: 10.1016/j.biosystemseng.2018.04.020.

SCHWALBERT, R. A.; AMADO, T. J. C.; NIETO, L.; CORASSA, G. M.; RICE, C. W.; PERALTA, N. R.; SCHAUBERGER, B.; GORNOTT, C.; CIAMPITTI, I. A. 2020. Mid-season county-level corn yield forecast for US Corn Belt integrating satellite imagery and weather variables. **Crop Science**, 60. doi: 10.1002/csc2.20053.

SHANAHAN, J. F.; SCHEPERS, J. S.; FRANCIS, D. D.; VARVEL, G. E.; WHILHELM, W. W.; TRINGE, J. M.; SCHLEMMER, M. R.; MAJOR, D. J. 2001. Use of remote-sensing imagery to estimate corn grain yield. **Agronomy Journal**, 93(3): 583-589. doi: 10.2134/agronj2001.933583x.

SIBANDA, M.; MUTANGA, O.; ROUGET, M. 2015. Examining the potential of Sentinel-2 MSI spectral resolution in quantifying above ground biomass across different fertilizer treatments. **ISPRS Journal of Photogrammetry and Remote Sensing**, 110:55-65. doi: 10.1016/j.isprsjprs.2015.10.005.

SIMÕES, M. S. dos; ROCHA, J. V.; LAMPARELLI, R. A. C. 2005. Spectral variables, growth analysis and yield of sugarcane. **Scientia Agricola**, 62 (3): 199-207. doi: 10.1590/S0103-90162005000300001.

SUN, Y.; QIN, Q.; REN, H.; ZHANG, T.; CHEN, S. 2019. Red-Edge Band Vegetation Indices for Leaf Area Index Estimation from Sentinel-2/MSI Imagery**. IEEE Transactions on Geoscience and Remote Sensing**, 58(2): 826-840. doi: 10.1109/TGRS.2019.2940826.

TRACY, T.; FU, Y.; ROY, I.; JONAS, E.; GLENDENNING, P. 2016. Towards Machine Learning on the Automata Processor. In High Performance Computing; Kunkel, J., Balaji, P., Dongarra, J., Eds.; Springer: Cham, Switzerland, 9697: 200–218. doi: 10.1007/978-3-319-41321-1_11.

VARELLA, C. A. A.; GLERIANI, J. M.; SANTOS, R. M. dos. 2015. Chapter 9 - Precision Agriculture and Remote Sensing. **Sugarcane**, 185-203. doi: 10.1016/B978-0-12-802239-9.00009-8.

WEI, M. C. F.; MALDANER, L. F.; OTTONI, P. M. N.; MOLIN, J. P. 2020. Carrot Yield Mapping: A Precision Agriculture Approach Based on Machine Learning. **Artificial Intelligence**, 1(2): 229-241. doi: 10.3390/ai1020015.

YUAN, H.; YANG, G.; LI, C.; WANG, Y.; LIU, J.; YU, H.; FENG, H.; XU, B.; ZHAO, X.; YANG, X. 2017. Retrieving soybean leaf area index from unmanned aerial vehicle hyperspectral remote sensing: Analysis of RF, ANN, and SVM regression models. **Remote Sensing**, 9(4): 309. doi: 10.3390/rs9040309.

YUE, J.; FENG, H.; YANG, G.; LI, Z. 2018. A comparison of regression techniques for estimation of above-ground winter wheat biomass using near-surface spectroscopy. **Remote Sensing**, 10(1): 66. doi: 10.3390/rs10010066.

ZHAO, D.; GORDON, V. S.; COMSTOCK, J. C.; GLYNN, N. C.; JOHNSON, R. M. 2016. Assessment of Sugarcane Yield Potential across Large Numbers of Genotypes using Canopy Reflectance Measurements. **Crop Science**, 56: 1747 – 1759. doi: 10.2135/cropsci2015.12.0747.

ZHOU, Z.; HUANG, J.; WANG, J.; ZHANG, W.; KUANG, Z.; ZHONG, S.; SONG, X. 2015. Object-Oriented Classification of Sugarcane Using Time-Series Middle-Resolution Remote Sensing Data Based on AdaBoost. **PLoS ONE**, 10(11): e0142069. doi: 10.1371/journal.pone.0142069.

## 5. FINAL CONSIDERATIONS

Precision agriculture adoption consider yield maps as essential for an initial investigation of the spatial variability of the fields. As sensors have advanced in agricultural tasks the most recent technologies to support it are integrated with artificial intelligence to provide robust solutions for accurate diagnostics of crop status, recommendations, and local interventions in a minimum interval of time. 3D sensing data in agriculture provides geometrical attributes of the crop, such as plant height, which it was demonstrated in this study spatially associated with the variation of sugarcane yield. The parameters for data acquisition and the workflow of data processing were described to enable the application of LiDAR technology for other sugarcane field conditions, as an alternative solution to spatialize more effectively an agronomical variable. The maps generated through the high-resolution data can support the decision-making process for site-specific crop management, since it demonstrates the conditions of the plant height over the seasons at the field level.

Satellite imagery in agriculture is intensively adopted as a remote sensing tool to infer about the potential production of agricultural areas based on the variation of spectral response of the vegetation. There is a diversity of applications and sources of orbital images for research and commercial purpose in agriculture with perspectives of enhancing spatial and temporal resolutions to provide more details of the target (vegetation). In this study, a modeling for sugarcane yield mapping was developed using reflectance data and yield data with a greater number of samples than commonly found in literature. Also, the investigation allows to determine the most correlated period of crop stage for estimating sugarcane yield, the transition from tillering to development crop stage. The research should continuously optimize the data acquisition for multiple sugarcane fields over different seasons and adding different predictor's variables that influence on yield response. As the computational performance tends to improve and larger database would be accessible, it should be reasonable to consider the data fusion of multiple layers, such as 3D sensing data, reflectance data, weather data, modeling of crop growth data, and yield data, as a manner to offer more accurate information for the decision-making process in agricultural systems.

# APPENDICES

**APPENDIX A.** LiDAR-derived metrics from canopy height model (CHM) for 2018/2019 sugarcane growing season – percentiles: P99th (A); P98th (B); P97th (C); P96th (D); P95th (E); P94th (F); P93th (G); P92th (H); P91th (I); P90th (J); P50th (K)

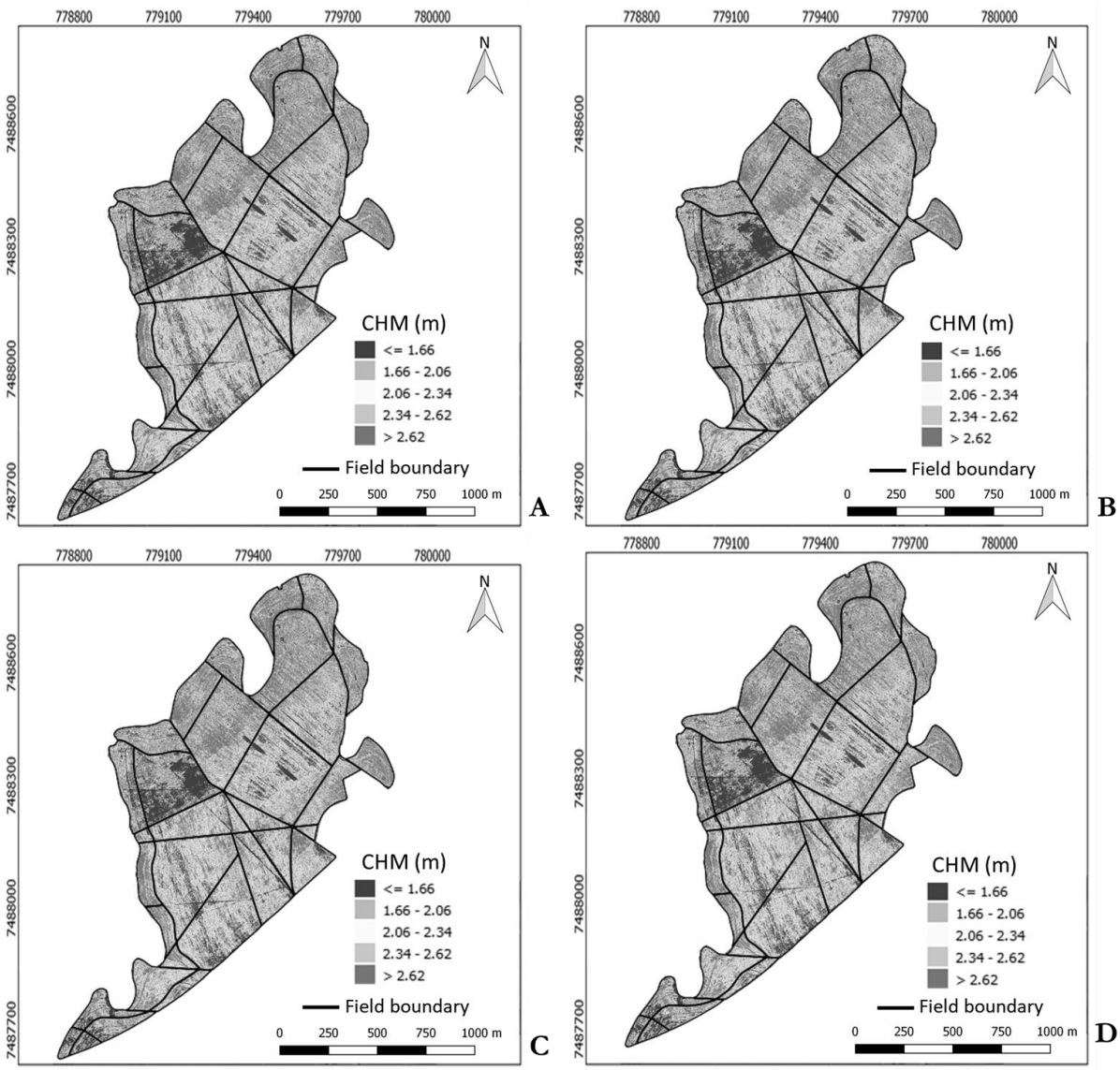

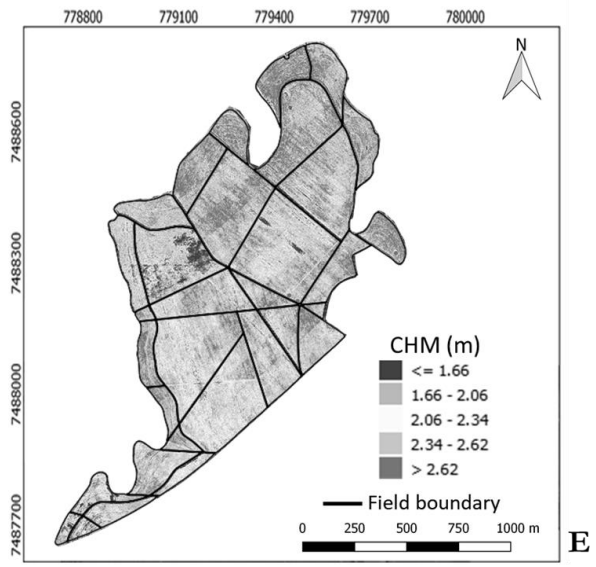
778800
779100
779400
779700
780000
7488600
7488300
7488000
7487700
N
CHM (m)
<= 1.66
1.66 - 2.06
2.06 - 2.34
2.34 - 2.62
> 2.62
Field boundary
0 250 500 750 1000 m

E

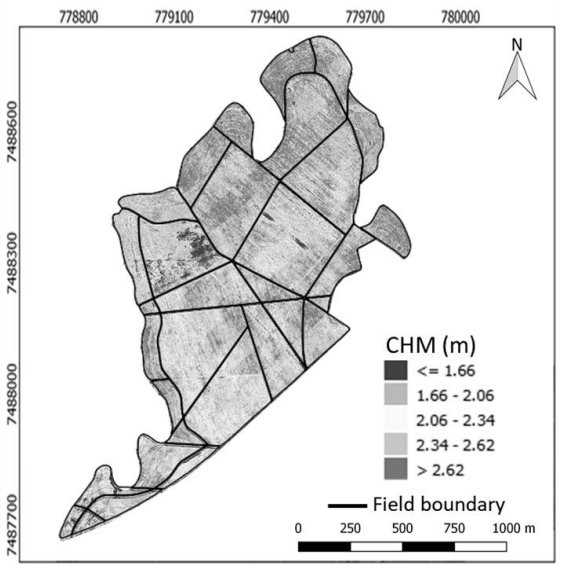
778800
779100
779400
779700
780000
7488600
7488300
7488000
7487700
N
CHM (m)
<= 1.66
1.66 - 2.06
2.06 - 2.34
2.34 - 2.62
> 2.62
Field boundary
0 250 500 750 1000 m

F

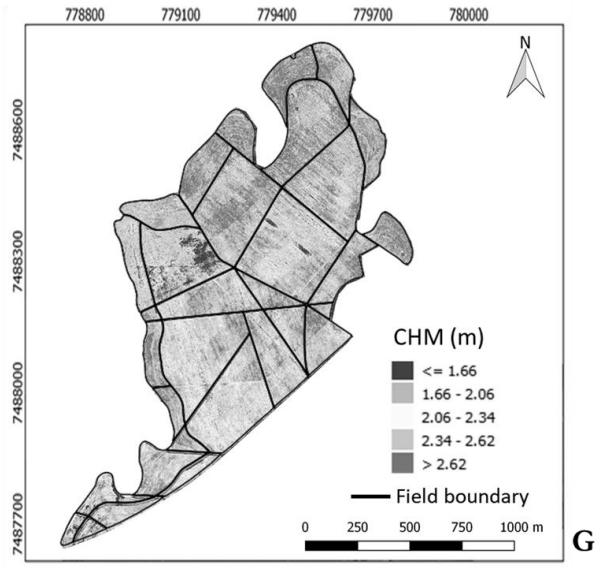
778800
779100
779400
779700
780000
7488600
7488300
7488000
7487700
N
CHM (m)
<= 1.66
1.66 - 2.06
2.06 - 2.34
2.34 - 2.62
> 2.62
Field boundary
0 250 500 750 1000 m

G

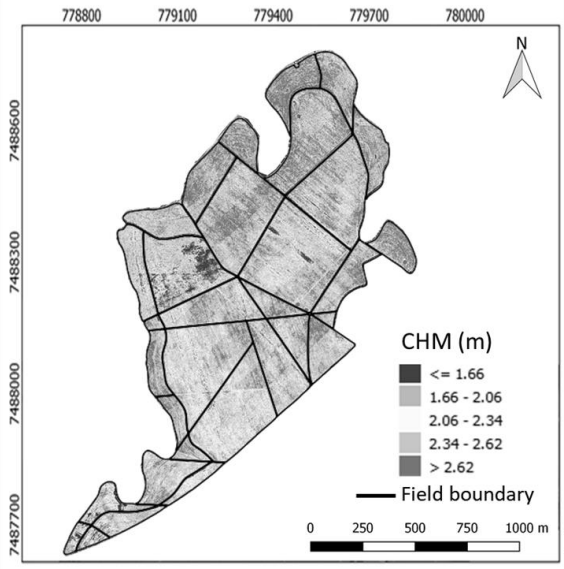
778800
779100
779400
779700
780000
7488600
7488300
7488000
7487700
N
CHM (m)
<= 1.66
1.66 - 2.06
2.06 - 2.34
2.34 - 2.62
> 2.62
Field boundary
0 250 500 750 1000 m

H

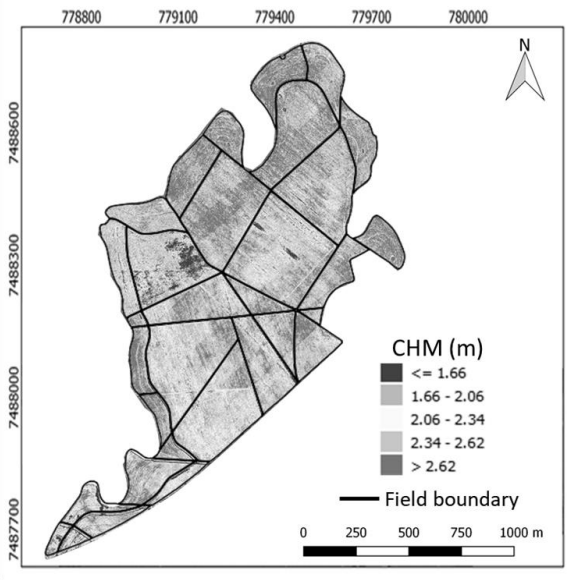
778800
779100
779400
779700
780000
7488600
7488300
7488000
7487700
N
CHM (m)
<= 1.66
1.66 - 2.06
2.06 - 2.34
2.34 - 2.62
> 2.62
Field boundary
0 250 500 750 1000 m

I

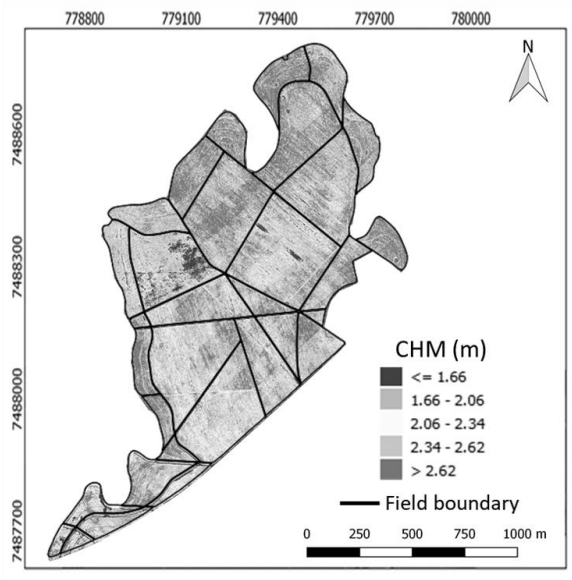
778800
779100
779400
779700
780000
7488600
7488300
7488000
7487700
N
CHM (m)
<= 1.66
1.66 - 2.06
2.06 - 2.34
2.34 - 2.62
> 2.62
Field boundary
0 250 500 750 1000 m

J

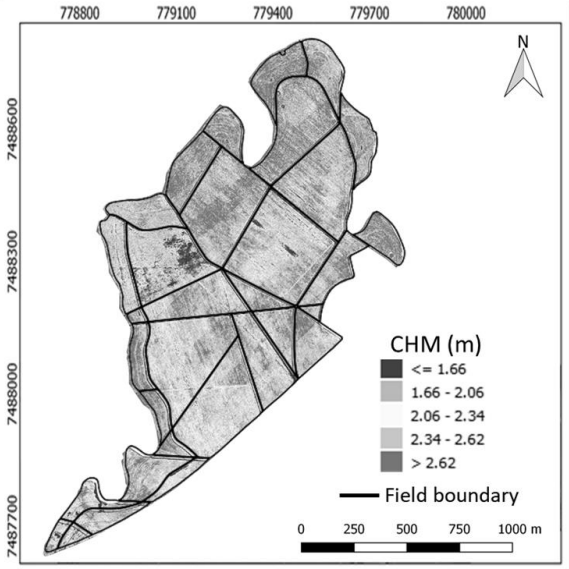
778800
779100
779400
779700
780000
7488600
7488300
7488000
7487700
N
CHM (m)
<= 1.66
1.66 - 2.06
2.06 - 2.34
2.34 - 2.62
> 2.62
Field boundary
0 250 500 750 1000 m

K

**APPENDIX B.** LiDAR-derived metrics from canopy height model (CHM) for 2019/2020 sugarcane growing season – percentiles: P99th (A); P98th (B); P97th (C); P96th (D); P95th (E); P94th (F); P93th (G); P92th (H); P91th (I); P90th (J); P50th (K).

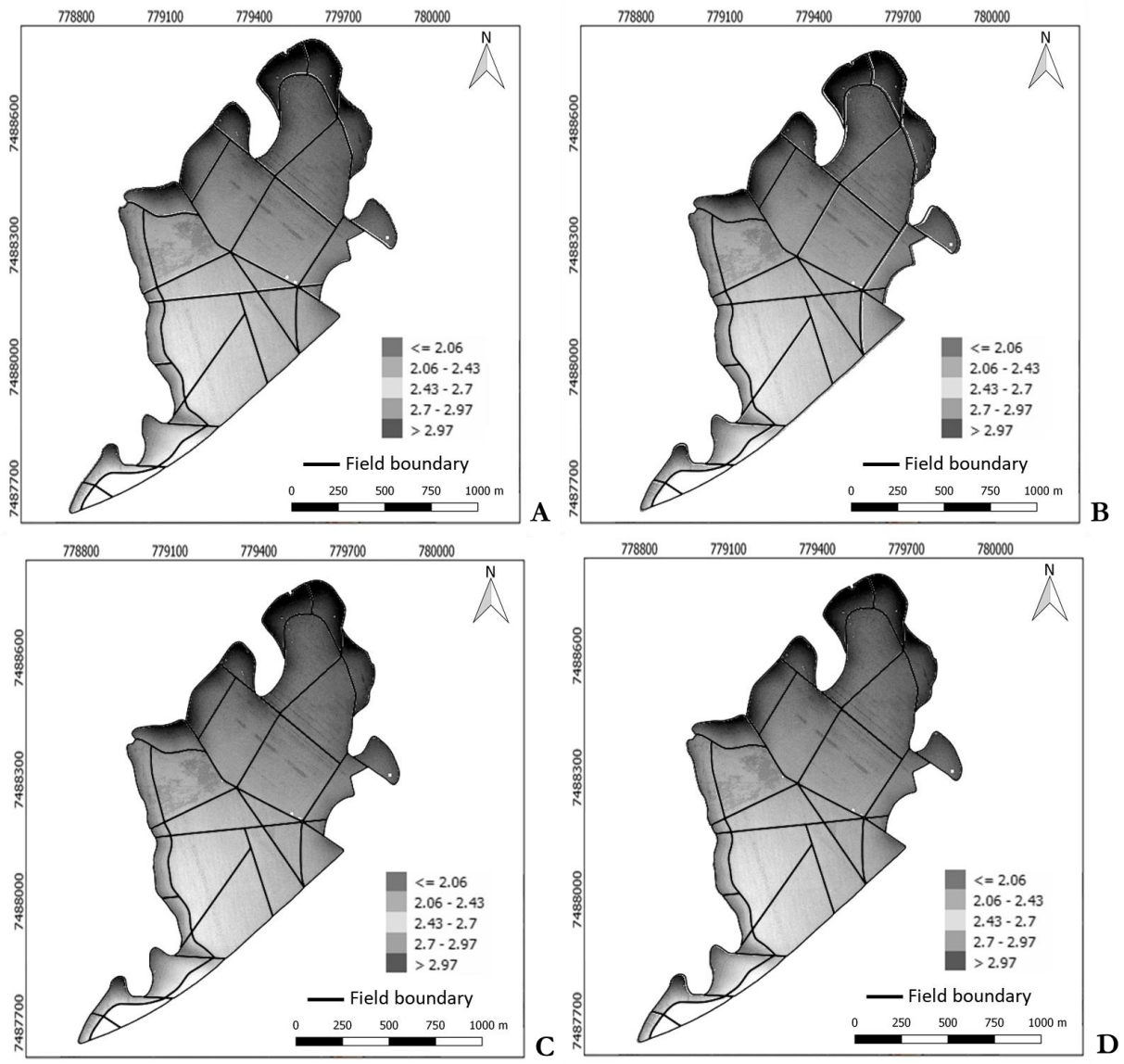

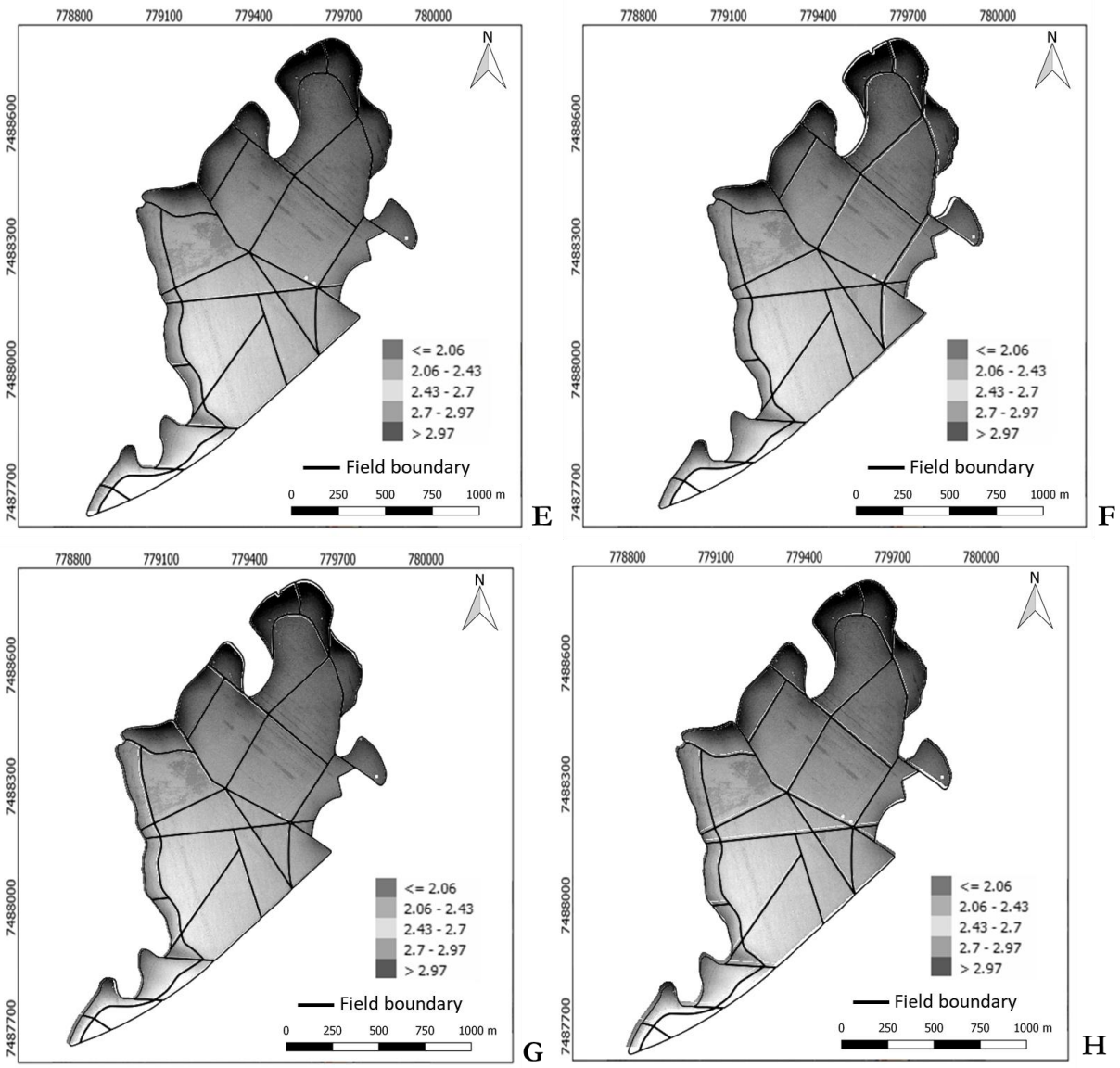
778800
779100
779400
779700
780000
7488600
7488300
7488000
7487700
N
<= 2.06
2.06 - 2.43
2.43 - 2.7
2.7 - 2.97
> 2.97
Field boundary
0 250 500 750 1000 m
E
F
G
H

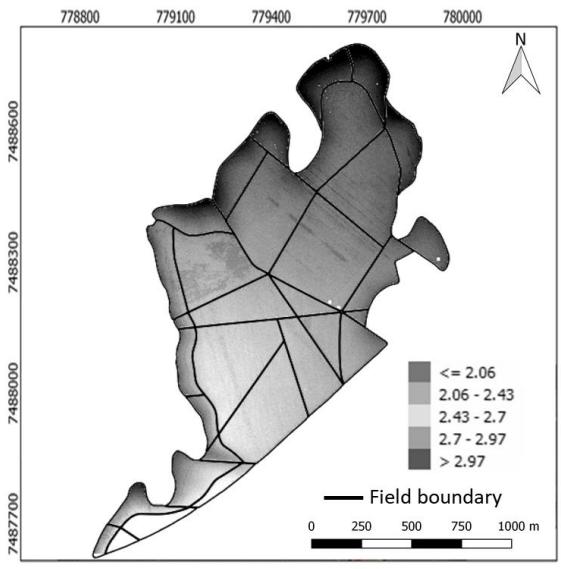
778800
779100
779400
779700
780000
N
7488600
7488300
7488000
7487700
<= 2.06
2.06 - 2.43
2.43 - 2.7
2.7 - 2.97
> 2.97
Field boundary
0 250 500 750 1000 m

I

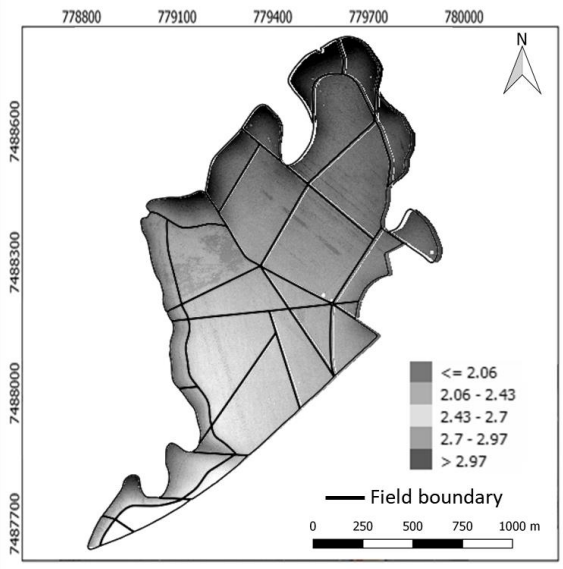
778800
779100
779400
779700
780000
N
7488600
7488300
7488000
7487700
<= 2.06
2.06 - 2.43
2.43 - 2.7
2.7 - 2.97
> 2.97
Field boundary
0 250 500 750 1000 m

J

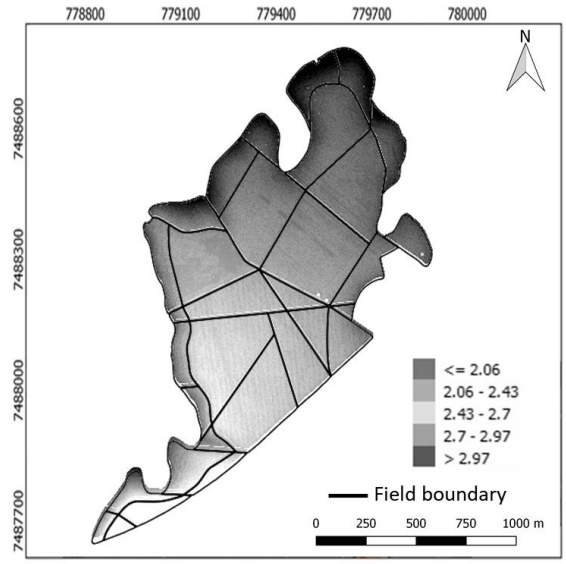
778800
779100
779400
779700
780000
N
7488600
7488300
7488000
7487700
<= 2.06
2.06 - 2.43
2.43 - 2.7
2.7 - 2.97
> 2.97
Field boundary
0 250 500 750 1000 m

K

**APPENDIX C.** The submitted paper regarding the accuracy of the sensor-system for sugarcane yield mapping

IEEE Access

# An approach to sugarcane yield estimation using sensors in the harvester and ZigBee technology

| | |
|---|---|
| Journal: | *IEEE Access* |
| Manuscript ID | Access-2021-14633 |
| Manuscript Type: | Regular Manuscript |
| Date Submitted by the Author: | 19-Apr-2021 |
| Complete List of Authors: | Maldaner, Leonardo Felipe; Universidade de São Paulo, Department of Biosystems Engineering<br>Canata, Tatiana; Universidade de São Paulo, Department of Biosystems Engineering<br>Molin, José Paulo; University of Sao Paulo, Biosysytems Engineering Department |
| Keywords: Please choose keywords carefully as they help us find the most suitable Editor to review: | Agriculture, Wireless sensor networks, Agricultural machinery |
| Subject Category<br>Please select at least two subject categories that best reflect the scope of your manuscript: | Geoscience and remote sensing, Instrumentation and measurement, Sensors |
| Additional Manuscript Keywords: | |
| | |

**APPENDIX D.** Predicted sugarcane yield maps based on Multiple Linear Regression for the 2018/2019 season using Spectral Bands (A); Green Normalized Difference Vegetation Index - GNDVI (B); Normalized Difference Red Edge Index - NDRE (C); Normalized Difference Vegetation Index - NDVI (D); Wide Dynamic Range Vegetation Index - WDRVI (E)

**A) Spectral bands – Season 2018/2019**

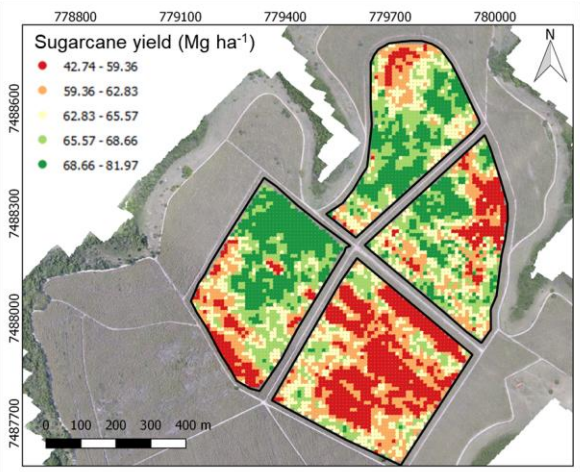


**B) GNDVI – Season 2018/2019**

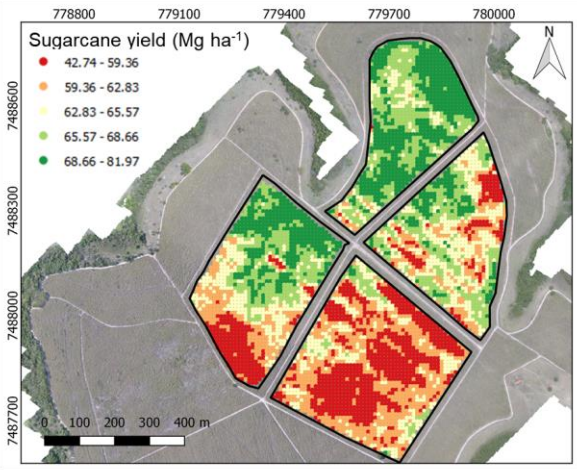


**C) NDRE – Season 2018/2019**

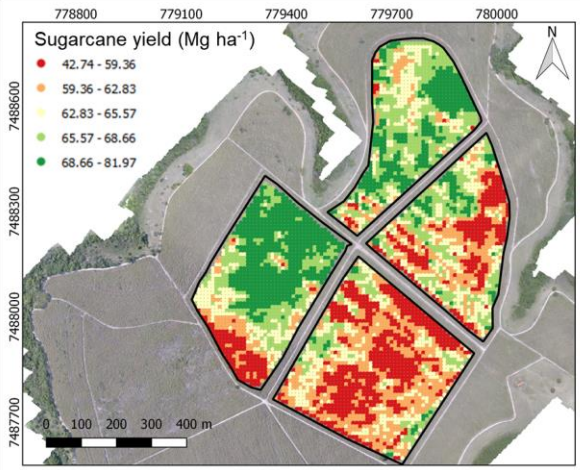


**D) NDVI – Season 2018/2019**

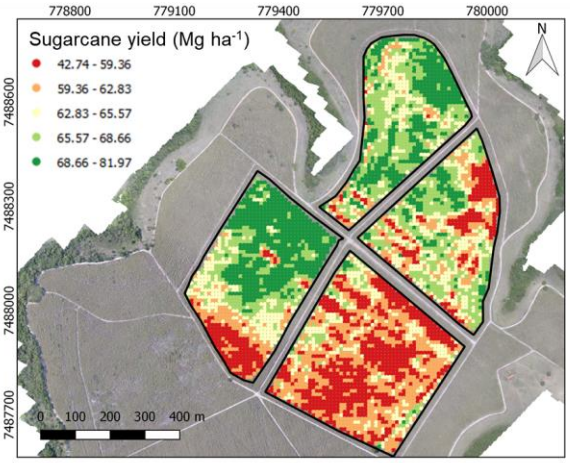


**E) WDRVI – Season 2018/2019**

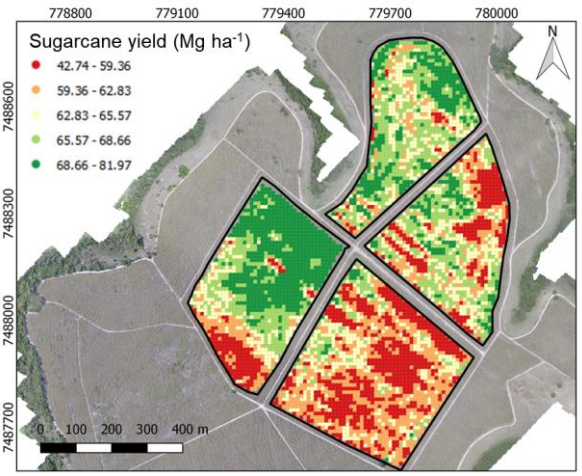

**APPENDIX E.** Predicted sugarcane yield maps based on Multiple Linear Regression for the 2019/2020 season using Spectral Bands (A); Green Normalized Difference Vegetation Index - GNDVI (B); Normalized Difference Red Edge Index - NDRE (C); Normalized Difference Vegetation Index - NDVI (D); Wide Dynamic Range Vegetation Index - WDRVI (E)

**A) Spectral bands – Season 2019/2020**

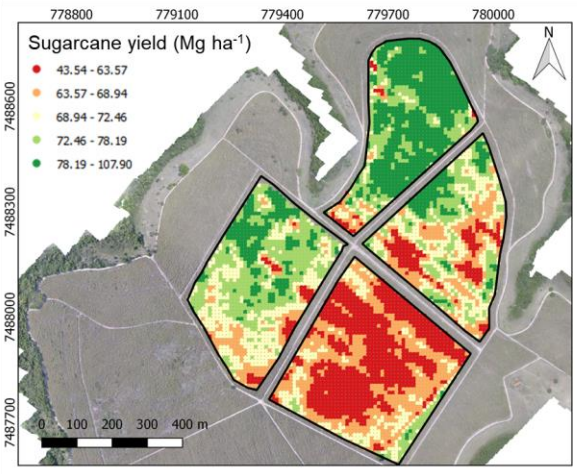


**B) GNDVI – Season 2019/2020**

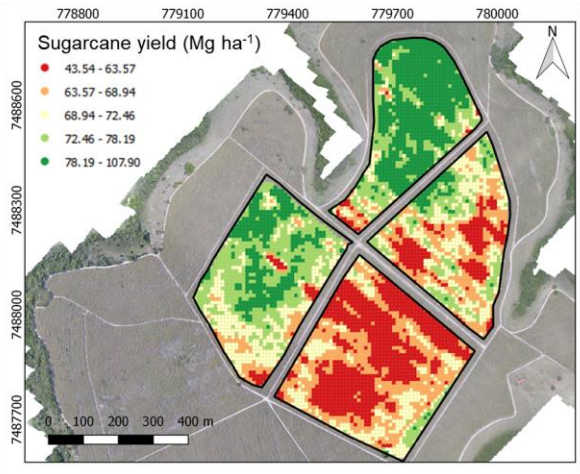


**C) NDRE – Season 2019/2020**

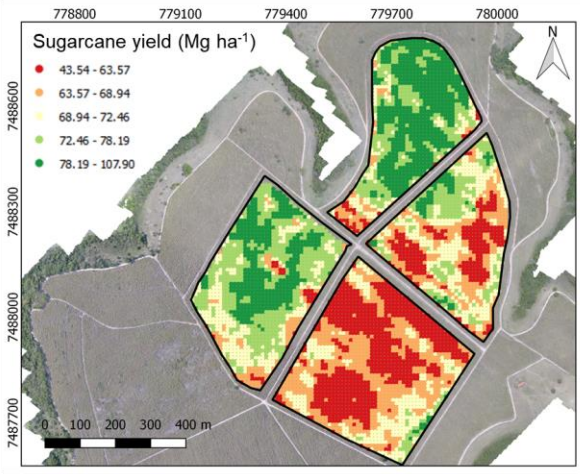


**D) NDVI – Season 2019/2020**

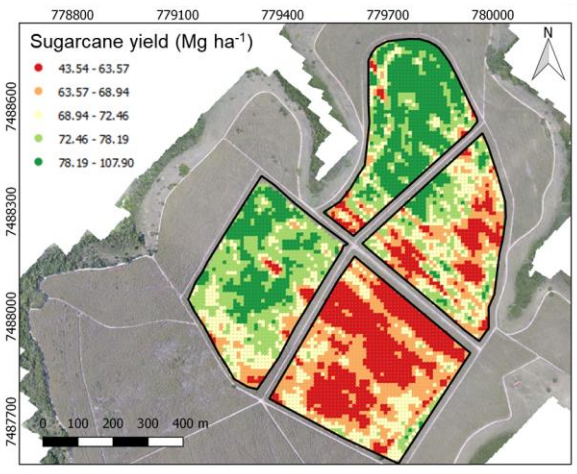


**E) WDRVI – Season 2019/2020**

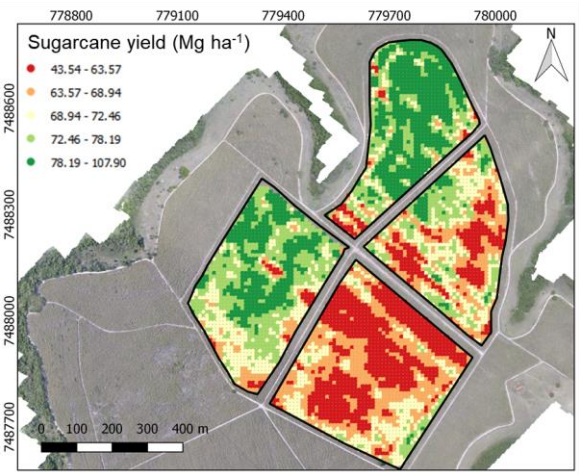

**APPENDIX F.** Predicted sugarcane yield maps based on Multiple Linear Regression for the 2020/2021 season using Spectral Bands (A); Green Normalized Difference Vegetation Index - GNDVI (B); Normalized Difference Red Edge Index - NDRE (C); Normalized Difference Vegetation Index - NDVI (D); Wide Dynamic Range Vegetation Index - WDRVI (E)

**A) Spectral bands – Season 2020/2021**

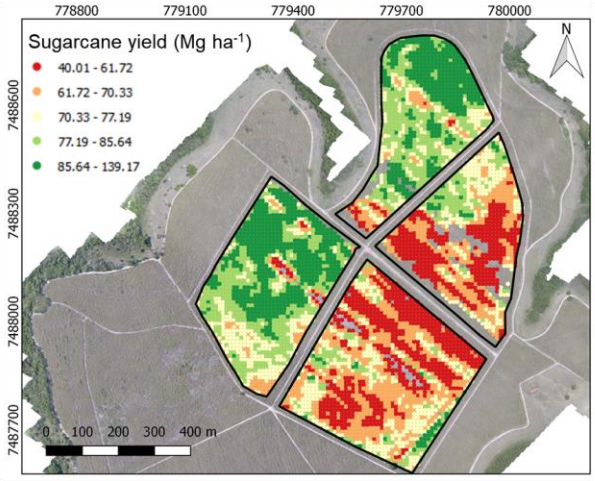


**B) GNDVI – Season 2020/2021**

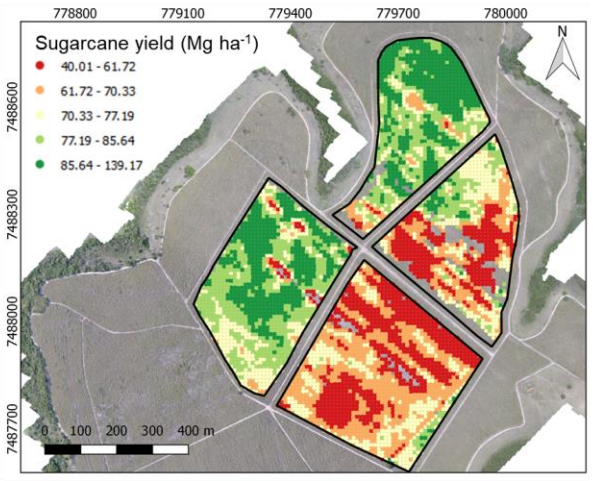


**C) NDRE – Season 2020/2021**

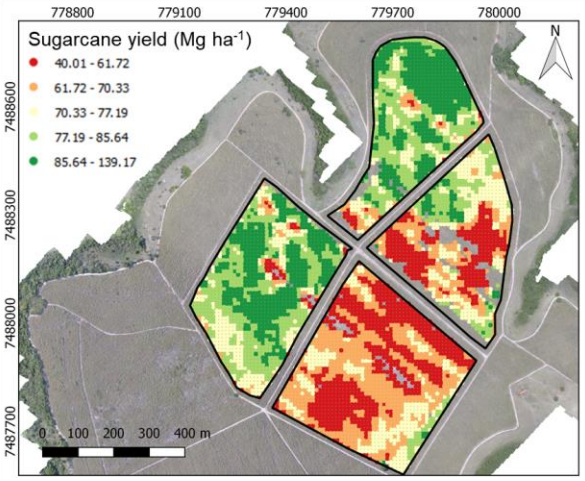


**D) NDVI – Season 2020/2021**

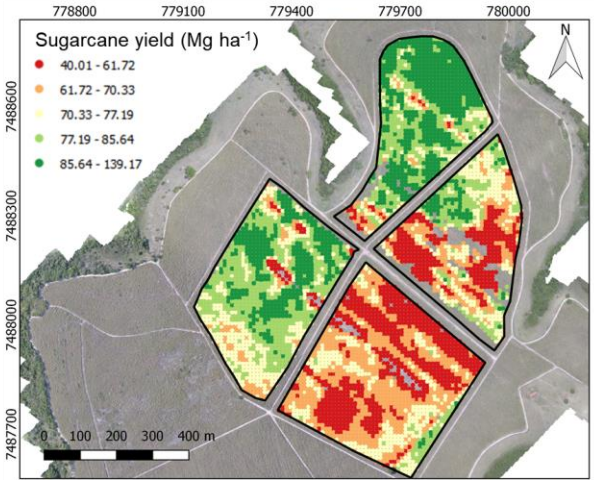


**E) WDRVI – Season 2020/2021**